

CHARACTERIZATION AND MOLECULAR MOTION IN  
UNILAMELLAR LIPID VESICLES

By

Heather Pillman

A DISSERTATION

Submitted to  
Michigan State University  
In partial fulfillment of the requirements  
for the degree of

DOCTOR OF PHILOSOPHY

CHEMISTRY

2011

## ABSTRACT

### CHARACTERIZATION OF MOLECULAR MOTION AND ORGANIZATION IN UNILAMELLAR LIPID VESICLES

By

Heather Pillman

Membrane proteins in biological cells are involved in nearly every function of cell life. For these reasons, there is great interest in incorporating chemically selective biomolecules, such as transmembrane proteins and enzymes, into membrane-based biosensors. Proteins must be reconstituted into environments that mimic the behavior of natural plasma membranes in order for them to retain their biological specificity and activity. Synthetic lipid bilayers are compositionally simple systems that approximate the dynamic fluid nature of the cell membrane, making them attractive systems for the incorporation of biomolecules.

As an initial step toward understanding bilayer systems, we have focused our research on investigating the dynamic behavior and fluidity of phospholipid vesicles lacking incorporated proteins. We have interrogated specific regions of our lipid vesicles using fluorescent “reporter” molecules to determine the dynamic behavior and molecular-scale organization of unilamellar lipid vesicles using time-resolved fluorescence spectroscopy techniques. We have used the polar chromophore nitro-2-1,3-benzoxadiazol-4-yl (NBD) tethered to the headgroups of phosphoethanolamine (PE)

lipids to study the dependence of headgroup functionality on inter-lipid hydrogen bonding interactions. We gauged these interactions using a time-correlated single photon counting (TCSPC) instrument to measure rotational diffusion dynamics in lipid vesicles and fluorescence recovery after pattern photobleaching (FRAPP) to determine translational diffusion dynamics in supported lipid bilayers. We have also used the untethered chromophores pyrene and perylene, imbedded in the acyl chain regions of phosphocholine (PC) lipid vesicles to determine the local viscosity and phase of the lipid bilayers as a function of bulk ethanol concentration. We have observed a structural perturbation in the acyl chain regions of the bilayer at ethanol concentrations of *ca.* 0.6 M, which points to the influence of controlled amounts of impurities on lipid order and phase. Lastly, we have used imbedded perylene to study the effects of excess excitation energy dissipation on the molecular-scale organization of phospholipid vesicles, and cholesterol-containing phospholipid vesicles. In both vesicle systems, we concluded that the order of the local environment of the chromophore determines the efficiency of energy transfer, and the extent of local heating. Taken collectively, the results of these experiments have provided valuable insight into the chemical and structural factors that influence lipid bilayer fluidity.

## ACKNOWLEDGEMENTS

I first and foremost have to thank my advisor, Dr. Gary J. Blanchard, for helping me at every stage of my graduate career. For giving me advice on everything from my research projects to job offers, and for never letting me give up or get too overwhelmed when the laser was uncooperative. In short, thank you for always being inspiring, patient, and positive-thinking in all things chemistry related, and teaching me everything I know about research and lasers. I am so grateful for the opportunity I've had to work with you and with the Blanchard group. Joining your group was the best decision I have ever made.

I would also like to thank all of the teachers and professors I have had the great pleasure of working with and learning from over the years. Thank you to my fifth-grade teacher, Mrs. Burnett, for helping me to discover my love for science at an early age. I also would not be here today if not for Mrs. Laura Lutz—not only my high school chemistry teacher, but my favorite teacher—who taught me on my very first day of class that fire alarms were fun, and that chemistry was my destiny. Thank you also to all of my professors at MSU for encouraging me to work hard and to always strive to be a better scientist, especially the members of my Guidance Committee. In particular, I would like to thank Doctors Greg Swain, Gavin Reid, David Weliky, Merlin Bruening, Dana Spence, Kathy Severin, and Robert Ofoli.

I also owe a huge debt of gratitude to the scientists who've been my mentors over the years, in particular Dr. Dwella Moton Nelson and Dr. Saadia Eltayeb. You, more than anyone else, helped me find my way on the path to making chemistry my career.

In addition, I must also thank every member of the Blanchard Group (past and present) for being both my co-workers and friends, supporting me in innumerable ways, and keeping me sane when the road was very rough. In particular, Monika Dominska, Benjamin Oberts, Margaretta Dimos, Douglas Gornowich, Christine Hay, and Iwan Setiawan. I would not have succeeded in graduate school without all of you. I will miss you.

Most importantly, I thank God for giving me the strength and courage to achieve my dreams, and I can never thank my family and friends enough for their unflinching confidence in me, and their constant outpourings of encouragement, love, and prayers. Thank you to my wonderful extended family: aunts, uncles, cousins, and grandparents. In particular, thank you to my very best friend, Joshua Nasrollahi, for always being in my corner and refusing to ever let me give up. I love you with all my heart. Special thanks to Nicholas and Andrew, for being great brothers and for giving me some serious competition over the years. And lastly, immeasurable thanks to my parents, John and Annemarie Pillman, for always believing in me and never doubting for a second that I would succeed. Without your love and support, I would not be where I am today. I love you both more than I can say, and I dedicate this dissertation to you.

# TABLE OF CONTENTS

List of Tables .....	viii
List of Figures .....	ix
Chapter 1: Introduction .....	1
Chapter 2: Rotational and Translational Dynamics of Headgroup-Tethered Chromophores in Lipid Vesicles .....	17
Introduction.....	17
Experimental Section.....	23
Results and Discussion .....	27
Conclusions.....	41
Chapter 3: Investigating Membrane Fluidity of Phospholipid Bilayers Using Steady-State Fluorescence Measurements .....	42
Introduction.....	42
Experimental Section.....	49
Results and Discussion .....	51
Conclusions.....	59
Chapter 4: Interrogating the Effects of Ethanol on the Organization of Lipid Vesicles Using Time-Resolved Fluorescence Measurements .....	60
Introduction.....	60
Experimental Section.....	65
Results and Discussion .....	68
Conclusions.....	83
Chapter 5: Effects of Localized Energy Dissipation on the Motional Dynamics of Unilamellar Vesicles .....	84
Introduction.....	84
Experimental Section.....	89
Results and Discussion .....	92
Conclusion .....	110

Chapter 6: Consequences of Transient Heating on the Motional Dynamics of Cholesterol-Containing Phospholipid Vesicles .....	111
Introduction.....	111
Experimental Section.....	114
Results and Discussion .....	117
Conclusions.....	138
Chapter 7: Conclusions .....	139
Literature Cited .....	145

## LIST OF TABLES

Table 2.1. Fluorescence lifetimes ( $\tau_1$ and $\tau_2$ ) and reorientation times ( $\tau_{OR1}$ and $\tau_{OR2}$ ) of NBD-PE in bilayer lipid vesicles, determined by TCSPC.....	29
Table 2.2. Cartesian components of the rotational diffusion constant (MHz) of NBD-PE chromophores in bilayer lipid vesicles .....	34
Table 2.3. Mobilities and diffusion coefficients of NBD-PE in supported lipid bilayers on fused silica. FRAPP data represent average values for three bilayers. At least five different areas were interrogated for each bilayer. ....	38
Table 4.1. Cartesian components of the rotational diffusion constant and aspect ratio $D_z/D_x$ as a function of solution phase ethanol concentration at 289 K and 303 K. Errors are $\pm 1\sigma$ for at least four individual determinations at each ethanol concentration.....	75
Table 5.1. The rotational diffusion constant, aspect ratio $D_z/D_x$ , and calculated local viscosity as a function of temperature .....	99
Table 5.2. Experimental reorientation times and calculated changes in local viscosity and temperature associated with internal conversion of perylene .....	106
Table 6.1. Measured reorientation times as a function of system temperature.....	129
Table 6.2. The rotational diffusion constant, aspect ratio $D_{major}/D_{minor}$ , and calculated local viscosity as a function of temperature.....	131
Table 6.3. Experimental reorientation times and calculated changes in local viscosity and temperature associated with internal conversion of perylene .....	136

## LIST OF FIGURES

Figure 1.1. Structures of (a) gel phase lipid bilayer and (b) fluid phase lipid bilayer .....	5
Figure 1.2. Structures of chromophores used in this project and excitation and emission spectra. (a) Free pyrene for the steady-state behavior of phospholipid vesicles, (b) free perylene for dynamics measurements of the acyl chain region of phospholipid vesicles, and (c) nitro-2-1,3-benzoxadiazol-4-yl tethered to the headgroup of phosphoethanolamine lipids for studying the effects of headgroup hydrogen bonding on lipid vesicle dynamics. ....	9
Figure 1.3. (a) Time-resolved emission intensities for polarizations collected parallel ( $I_{\parallel}(t)$ ) and perpendicular ( $I_{\perp}(t)$ ) to the vertically polarized excitation pulse. (b) The functional form of the orientational anisotropy decay obtained from transients in (a). Residuals are distributed along the y-intercept and the solid line is the fit of the data.....	12
Figure 2.1. Excitation and emission spectra of 1e-6 M NBD-phosphatidylethanolamine (NBD-PE) in chloroform. ....	19
Figure 2.2. Molecular structures of lipids used in this study: dioleoylphosphatidylcholine (DOPC), dioleoylphosphatidylglycerol (DOPG), and the chromophore NBD-phosphatidylethanolamine (NBD-PE) .....	20
Figure 2.3. (a) Fluorescence lifetime and (b) induced orientational anisotropy data for NBD-PE in a DOPG/DOPC mixed lipid vesicle. The residuals for a fitted two-component exponential decay function are shown for both panels .....	28
Figure 2.4. A typical FRAPP recovery curve for a DOPC/NBD-PE supported bilayer membrane (above) along with residuals (below). Total photobleaching time was 300 ms.....	37
Figure 3.1. Structures of 14:0 DMPC, pyrene, and absorbance and emission spectra of 1e-5 M pyrene in chloroform.....	46

Figure 3.2. Emission spectra of pyrene demonstrating the relationship between concentration and excimer band intensity in 3e-6 M pyrene in DMPC vesicles (dotted line) and 3e-5 M pyrene in DMPC vesicles (solid line). ..... 47

Figure 3.3. Pyrene excimer band intensity for the chromophore incorporated into 100 nm diameter DMPC vesicles, as a function of ethanol concentration. Error bars are  $\pm 1\sigma$  for three individual determinations at each ethanol concentration. The dashed line is a linear regression fit to the data ..... 54

Figure 3.4. Dynamic light scattering data on vesicle size as a function of solution ethanol concentration. Uncertainties reported are  $\pm 1\sigma$  for at least three determinations ..... 57

Figure 4.1. Structures of 14:0 DMPC and perylene, and normalized absorption and emission spectra of perylene in DMPC vesicles ..... 69

Figure 4.2. (a) Experimental data for perylene reorientation in a 100 nm diameter DMPC vesicle, with 0.25 M ethanol concentration at 289 K. (b) Induced orientational anisotropy decay function for the data shown in panel (a), along with the best-fit function to the data. For this fit the function is  $f(t) = (0.11 \pm 0.004)\exp(-t/(339\pm 24 \text{ ps})) + (0.04 \pm 0.003)\exp(-t/(2483\pm 185 \text{ ps}))$  ..... 73

Figure 4.3. (a) Dependence of perylene  $D_x$  and  $D_z$  on ethanol concentration for 100 nm diameter DMPC vesicles at 289 K. (b) Dependence of perylene  $D_x$  and  $D_z$  on ethanol concentration for 100 nm diameter DMPC vesicles at 303 K. Errors are  $\pm 1\sigma$  for at least four individual determinations at each ethanol concentration. .... 76

Figure 5.1. Structures of 14:0 DMPC and perylene, and normalized excitation and emission spectra of perylene in DMPC vesicles ..... 96

Figure 5.2. (a) Experimental data for perylene reorientation in 100 nm diameter DMPC vesicles at 292 K, excited at 435 nm ( $S_1 \leftarrow S_0$ ). (b) Induced orientational anisotropy de-cay function for the data shown in panel (a), along with the best-fit function to the data ..... 98

Figure 5.3. (a) Experimental data for perylene reorientation in 100 nm diameter DMPC vesicles at 292 K, and excited at 260 nm ( $S_2 \leftarrow S_0$ ). (b) Induced orientational anisotropy decay function for the data shown in panel (a), along with the best-fit function to the data.....	101
Figure 5.4. Dependence of reorientation time on temperature for 100 nm diameter DMPC vesicles, for excitation of the $S_1 \leftarrow S_0$ transition ( $\circ$ ) and the $S_2 \leftarrow S_0$ transition ( $\bullet$ ). Errors are $\pm 1\sigma$ for at least four individual determinations at each temperature .....	104
Figure 6.1. Structures of 14:0 DMPC, perylene, cholesterol, and normalized excitation and emission spectra of perylene in DMPC vesicles .....	119
Figure 6.2. (a) Experimental data for perylene reorientation in 100 nm diameter DMPC vesicles at 270.5 K, excited at 430 nm ( $S_1 \leftarrow S_0$ ). (b) Induced orientational anisotropy decay function for the data shown in panel (a), along with the best-fit function to the data.....	122
Figure 6.3. (a) Experimental data for perylene reorientation in 100 nm diameter DMPC vesicles at 273 K, excited at 260 nm ( $S_2 \leftarrow S_0$ ). (b) Induced orientational anisotropy decay function for the data shown in panel (a), along with the best-fit function to the data.....	123
Figure 6.4. (a) Experimental data for perylene reorientation in 100 nm diameter DMPC vesicles at 283 K, excited at 260 nm ( $S_2 \leftarrow S_0$ ). (b) Induced orientational anisotropy decay function for the data shown in panel (a), along with the best-fit function to the data.....	124

## CHAPTER 1

### INTRODUCTION

The development of novel, chemically robust sensing devices that mimic the behavior and functionality of biological cells are in increasingly high demand in a variety of markets. These biologically-based sensors have various applications in areas such as medical diagnostics<sup>2</sup> (*i.e.* blood glucose monitors) and the detection of biological warfare agents and toxins<sup>3-4</sup>. Biosensors, which borrow design elements from biological components, consist of three main parts: an analyte of interest, a bioreceptor, and a transducer. A bioreceptor is a biologically-derived molecule, such as an enzyme or a transmembrane protein that is chemically selective for a specific analyte. The interaction of the analyte with the bioreceptor results in the production of a chemical signal, which the transducer then converts into a new type of signal by electrochemical or optical means, for example. This new signal is detected with the aid of electronics, allowing for interpretation by the user. In this way, an analyte of interest can be measured and quantified.

Biological cell membranes are the regulators of cell life; they mediate the influx of nutrients and the release of waste, and are extremely complex and dynamic in nature. Cell membrane structure and fluidity play critical roles in regulating the life of the cell.<sup>5-6</sup> The physical properties of the cell membrane are vital to cell function, including protein activity and membrane permeability. A biological cell membrane typically consists of approximately 100 – 500 different chemical constituents, depending on the

location and function of the cell in the organism. The cell membrane is composed of various lipids, including phospholipids, glycerophospholipids, and sphingolipids, which make up a bilayer leaflet structure in which other components are imbedded. Some other membrane constituents are carbohydrates, cholesterol, sphingomyelin, and peripheral and transmembrane proteins. All of these constituents work cooperatively to regulate the cell and, for this reason, the cell membrane is often touted as being the ideal platform for biosensor technology.<sup>7-9</sup>

Proposed membrane-based biosensors consist of a phospholipid bilayer with imbedded transmembrane proteins fused directly to a solid substrate, such as gold or quartz, which would act as a chemical or optical transducer.<sup>10-12</sup> Then using electrochemical means, for example, the flow of charged analytes could be detected and measured. However, there are several issues that need to be addressed before a functional membrane-based biosensor could be constructed. The first obstacle to overcome is the insertion of a functional transmembrane protein. Transmembrane proteins lose their biological activity when they are removed from the fluid environment of the plasma membrane of the cell; therefore, the surface of the transducer must be modified in such a way that it will support a fluid environment similar to that of a biological membrane, in order to promote protein reconstitution. In order for a transmembrane protein to function properly in a lipid bilayer, both ends of the protein must have access to the surrounding aqueous environment. If a lipid bilayer is in direct contact with a solid substrate, there will be very little space for a protein to imbed, and if a protein does imbed, it will most likely denature and become biologically inactive.

Several methods have been proposed for rectifying this issue; one promising approach is achieved by the formation of a hydrophilic spacer between the substrate surface and the lipid bilayer. The hydrophilic spacer is prepared by conjugating lipids with a short chain polymer, such as polyethylene glycol (PEG), terminated with a thiol group, and fusing the functionalized lipids to a gold substrate, thus tethering the bottom lipid leaflet to the substrate.<sup>13-16</sup> This method supports the formation of an aqueous layer between the substrate and the bottom lipid leaflet, which helps the bilayer to maintain some of its fluid properties and protein bioactivity by shielding the protein from direct contact with the substrate.

It was the goal of this project to investigate the molecular motion and organizational properties of simple lipid bilayer systems under a variety of conditions to provide a foundation for the development of membrane-based biosensors. For our experiments we considered two lipid bilayer systems: the planar lipid bilayer and the lipid vesicle or liposome. As was outlined above, planar lipid bilayers or solid-supported lipid bilayers appear to be the ideal platform for the development of biomimetic sensors, and can be prepared in a step-wise manner, such as the transfer of individual lipid monolayers from an air-water interface to a solid substrate using Langmuir—Blodgett<sup>17</sup> (lower leaflet) and Langmuir—Schaefer<sup>18</sup> (upper leaflet) techniques. These methods of lipid bilayer deposition produce chemically robust and stable solid-supported bilayer systems. However, the incorporation of transmembrane proteins into solid-supported lipid bilayers prepared using the Langmuir—Blodgett and Langmuir—Schaefer techniques presents a challenge because a requirement of monolayer deposition is that the

proteins are located at the air-water interface, which causes them to denature. Another method for the preparation of solid-supported lipid bilayers that is more conducive to the incorporation of transmembrane proteins is the adsorption and fusion of unilamellar lipid vesicles onto the substrate surface.<sup>19-21</sup>

Phospholipids are a major component in biological cell membranes and are amphipathic molecules that consist of a polar headgroup region and two nonpolar acyl chains. In aqueous solution phospholipids aggregate and self-assemble into spherical lipid vesicle structures, where the polar headgroups make up the interior and exterior surface area of the vesicle in direct contact with the aqueous environment, and the acyl chain moieties are directed toward one another creating a hydrophobic inner leaflet region.<sup>4</sup> Lipid vesicles not only make excellent model cell membrane systems, but they are relatively simple to prepare and manipulate, and their structure promotes the incorporation of transmembrane proteins. For these reasons, lipid vesicle fusion is an extremely appealing method for the formation of solid-supported lipid bilayers, and ultimately for the development of membrane-based biosensors. However, before attempting to incorporate functional transmembrane proteins into lipid vesicles, it is necessary to first investigate the behavior and dynamic properties of simple lipid vesicle systems.

The interactions between neighboring lipids, as well as the interactions between lipids and non-lipid constituents influence the dynamic properties of the bilayer membrane.<sup>22</sup> One way a biological cell can regulate itself is by manipulating the fluidity of the membrane.<sup>5</sup> In this way, the cell is able to control the permeability of the

membrane, and selectively activate proteins. Membrane fluidity is a concept that describes a number of intricate molecular motions, and can be thought of as a measure of the viscous drag effects between individual membrane constituents. Some of the molecular motions that comprise membrane fluidity are lipid rotational, translational, and lateral diffusion, as well as protrusion in and out of the bilayer, and the formation of trans-gauche isomers or kinks.<sup>23</sup>

The concept of membrane fluidity is also related to the phase of the lipids. All lipids have a characteristic gel-to-fluid phase transition temperature,  $T_m$ . The  $T_m$  can be thought of as the lipid melting point. At temperatures below  $T_m$ , lipids exist in a highly ordered “gel” phase characterized by fully extended acyl chains, tilted at an angle slightly away from the bilayer normal. In gel phase lipid bilayers, the close-packed structure of the bilayer, strong van der Waals interactions between acyl chain moieties, and hydrogen bonding interactions between the polar headgroups and the surrounding aqueous medium all contribute to the bilayer exhibiting very little motional freedom. At temperatures above  $T_m$ , lipid acyl chains become disordered as the structure of the hydrocarbon tails becomes increasingly disrupted by the formation of trans-gauche conformers.<sup>24</sup> These kinks in the formerly trans-configured lipid acyl chains disrupt both the lipid order and the inter-lipid interactions, resulting in an increase in the motional freedom of the lipids and the formation of the “fluid” phase. The gel-to-fluid phase transition is demonstrated in Figure 1.1. The phase and fluidity of the lipid bilayer are influenced by a number of factors, including the length of the acyl chains, the existence of any unsaturations in the

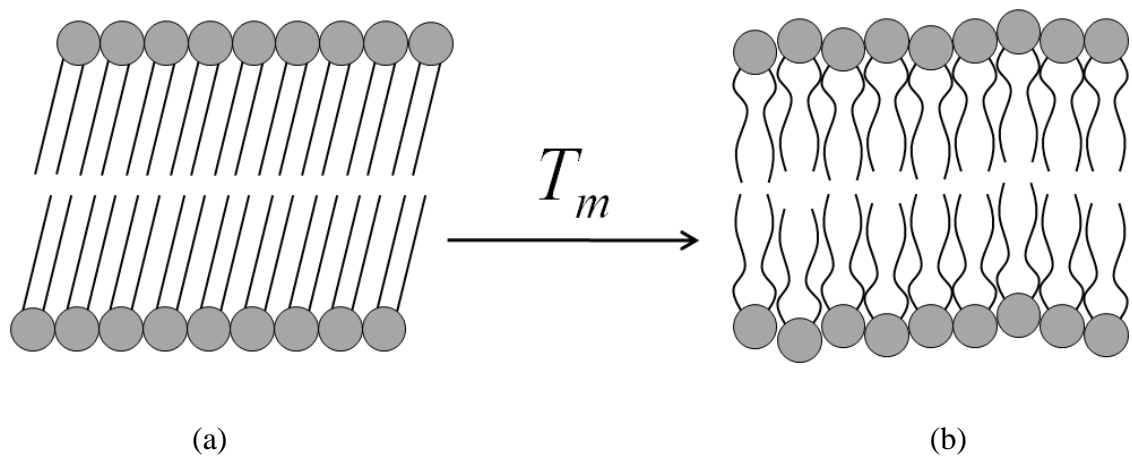


Figure 1.1. Structures of (a) gel phase lipid bilayer and (b) fluid phase lipid bilayer.

chains, the presence of non-lipid constituents in the bilayer, and the temperature of the system.<sup>25</sup> The effect of lipid phase on the fluidity and dynamic properties of the membrane must be better understood in compositionally simple systems if there is to be hope of constructing a membrane-based biosensor.

Fluorescence techniques are especially appealing in biological applications because they are non-destructive and highly sensitive.<sup>26</sup> To study the effects various chemical “impurities” and temperature-induced perturbations have on the dynamic behavior of lipid vesicle systems, we utilized a fluorescent molecular probe or chromophore, which acts as a reporter molecule, to investigate these effects. In order to study the consequences of various chemical and physical perturbations on the fluidity of the lipid bilayer, we need to exploit the fluorescent properties of the chromophore. Fluorescence is the emission of energy in the form of photons from an electronically excited species.<sup>27</sup> Fluorescent molecules are first excited by the selective absorption of photons at a specific wavelength. The excited molecules can then emit photons at a longer wavelength than that required for excitation, and by this radiative relaxation mechanism, return to the ground state. Although molecules may be excited to an electronic state, Kasha’s rule<sup>28</sup> states that emission occurs *only* from the transition from the lowest vibrational level of the lowest energy excited state to the ground state. The average amount of time electronically excited molecules remain in the excited state before emission is the fluorescence lifetime. The interaction of excited state molecules with their local environment can affect the molecules’ fluorescence spectrum and

lifetime, so by monitoring the optical response of a population of fluorescent probes, we are able to derive information about the local medium of the chromophores.<sup>29-33</sup>

Chromophores provide detailed information about the structure, behavior, and polarity of their local environments, and can be chosen to interrogate a selected region of the bilayer. For example, a small nonpolar probe preferentially resides in the acyl chain region of the bilayer while a polar chromophore will associate with the headgroup region of the bilayer, or the aqueous surroundings. By selectively exciting the chromophore sequestered in its local environment, and measuring the resulting fluorescence signal, one is able to collect both steady-state and dynamic information on the probe, and acquire information about the surrounding molecules as well. Time-domain fluorescence measurements are typically in the form of fluorescence lifetime or anisotropy,<sup>26</sup> and are related to the rotational and translational diffusion of the chromophores in their environment, as well as the motion of the molecules surrounding the probe. These data can then be used to elucidate information about the membrane permeability, fluidity, local viscosity, and lipid phase.

To begin investigation of vesicle systems, a chromophore was initially chosen to interrogate either the acyl chain region of the bilayer or the lipid headgroup region, selectively. The aromatic hydrocarbon pyrene (Fig. 1.2a) was chosen to interrogate the acyl chain region of the lipid bilayer. Due to pyrene's nonpolar, planar structure, it preferentially imbeds in the nonpolar region of the bilayer.<sup>29-33</sup> Pyrene is also useful as a molecular probe because of its sensitivity to solvent polarity and its ability to form excimers.<sup>34</sup> An excimer, (MM)\*, is formed when an electronically excited molecule of

pyrene ( $M^*$ ) collides and reacts with a ground state molecule of pyrene ( $M$ ). The process can be thought of as dynamic fluorescence quenching of the pyrene monomers.<sup>35</sup> When a pyrene excimer is formed, its characteristic emission band is broad, structureless, and red shifted from the emission bands of pyrene monomer. The formation of excimers is concentration- dependent, therefore the higher the concentration of pyrene monomer in solution prior to excitation, the higher the probability of a collision between an excited state and ground state monomer during the lifetime of the excited state.<sup>27</sup> Because of the concentration dependence of excimer formation, the intensity of the excimer emission band scales with pyrene concentration. Excimer formation is also a diffusion-limited process, meaning the temperature and viscosity of the medium affect the intensity of the excimer emission band centered at *ca.* 472 nm. We exploited pyrene's ability to form excimers to study the effects of ethanol perturbation on phospholipid vesicle systems, and we discuss these experiments in Chapter 3.

To interrogate the rotational diffusion dynamics of our lipid vesicle systems, we used time-resolved fluorescence spectroscopy techniques to measure the fluorescence anisotropy of either headgroup-tethered nitro-2-1,3-benzoxadiazol-4-yl (NBD, Figure 1.2c) or the polycyclic aromatic hydrocarbon perylene (Figure 1.2b), which selectively localizes in the nonpolar aliphatic chain region of the bilayer. Chromophores with absorption transition moments oriented in a specific direction will preferentially absorb light that is polarized along this same axis. So, if a short, intense pulse of vertically polarized light is directed into a sample of randomly oriented chromophores, the molecules with transition moments oriented nominally parallel to the incident pulse will

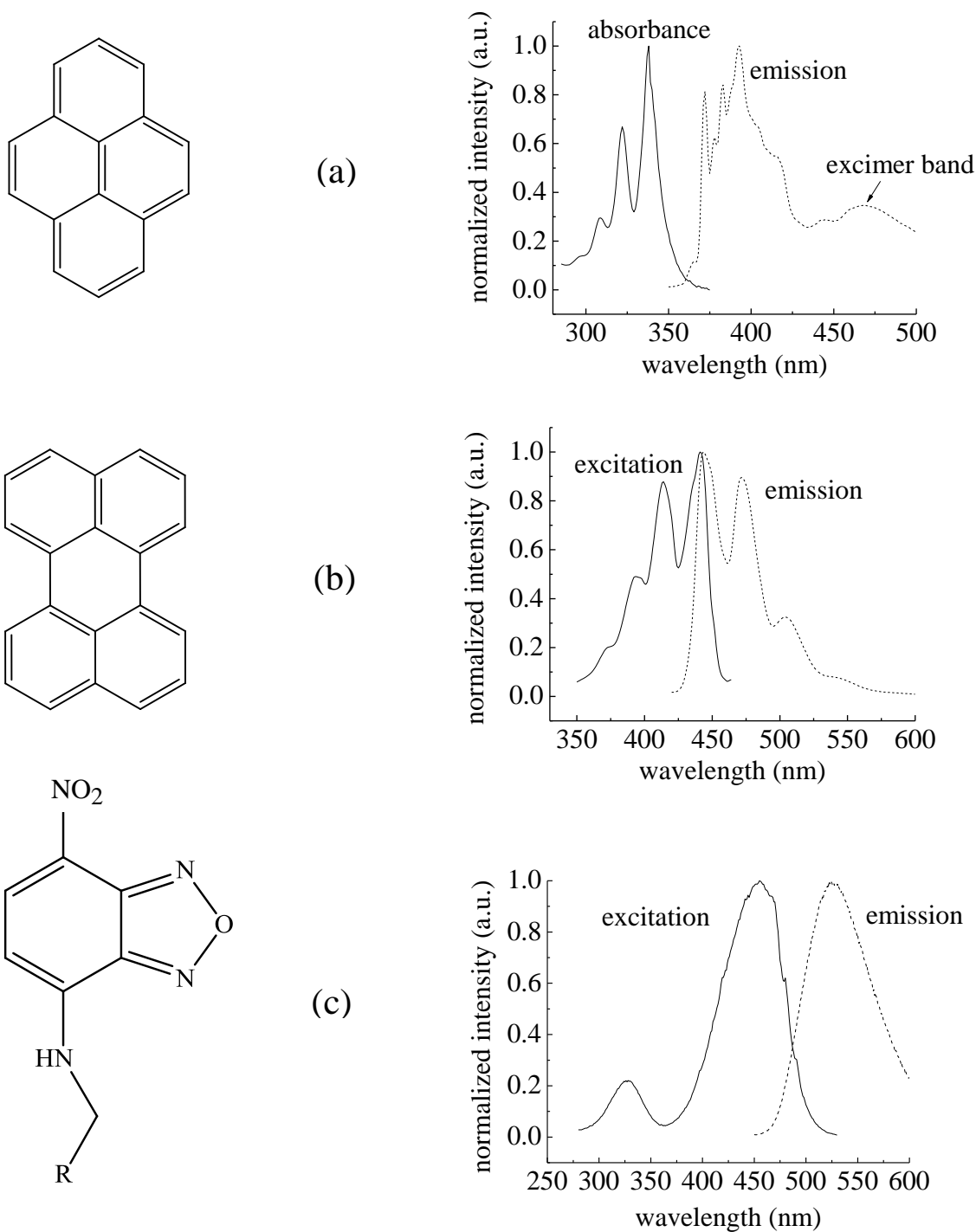


Figure 1.2. Structures of chromophores used in this project and excitation and emission spectra. (a) Free pyrene for the steady-state behavior of phospholipid vesicles, (b) free perylene for dynamics measurements of the acyl chain region of phospholipid vesicles, and (c) nitro-2-1,3-benzoxadiazol-4-yl tethered to the headgroup of phosphoethanolamine lipids for studying the effects of headgroup hydrogen bonding on lipid vesicle dynamics.

be preferentially excited. This non-random population of excited molecules then produces a fluorescence emission transient with polarization determined by the distribution of emission transition dipole moments. The fluorescence emission from the excited chromophores decays over the lifetime of the excited state as the polarizations of the transition dipole moments re-randomize or depolarize. The total intensity of light,  $I$ , emitted from a random distribution of chromophore molecules is the sum of its Cartesian components:

$$I = I_x + I_y + I_z \quad (1.1)$$

For a vertically ( $z$ -axis) polarized excitation pulse propagating along the  $x$ -axis, the components of the fluorescence intensity oriented parallel and perpendicular to the incident beam are defined as  $I_z = I_{||}$  and  $I_x = I_y = I_{\perp}$ . Therefore, observing the polarized transients,  $I_y$  and  $I_x$ , along the  $z$ -axis as a function of time yields a total intensity defined by Equation 1.2.

$$I(t) = I_{||}(t) + 2I_{\perp}(t) \quad (1.2)$$

For fluorescence anisotropy measurements, the polarized emission transients from the sample,  $I_{||}(t)$  and  $I_{\perp}(t)$ , are combined to produce the induced orientational anisotropy function,  $R(t)$ :

$$R(t) = \frac{I_{||}(t) - I_{\perp}(t)}{I_{||}(t) + 2I_{\perp}(t)} \quad (1.3)$$

where the denominator represents the total intensity of the system (Fig. 1.3, Eq. 1.2). Chromophores that are in a completely unrestricted environment, such as a continuum solution, are able to access every directional orientation as they re-randomize over the lifetime of the fluorescence. So, as the unhindered excited chromophores emit and re-randomize, the anisotropy decays over time to zero, at which point the orientations of the molecules are randomly oriented. The amount of time measured from the point when a non-random orientational distribution of excited state chromophores first begins emitting fluorescence, until fluorescently decaying to the ground state and re-randomizing is called the reorientation time constant ( $\tau_{OR}$ ). This value provides information about the motion of the chromophore while re-randomizing, as well as the “restrictiveness” of the local environment of the probe.<sup>36</sup> If the anisotropy function is determined according to Eq. 1.3, and plotted as a function of time (Figure 1.3b), it produces an exponential decay described by:

$$R(t) = R(0)\exp(-t / \tau_{OR}) \quad (1.4)$$

where  $R(0)$  is the initial orientational anisotropy. For one photon excitation,  $R(0)$  usually ranges in value from -0.2 to 0.4, depending on the angle between the absorption and emission transition moments. The reorientation time constant for spherical solute molecules in a continuous solvent is related to the rotational diffusion constant,  $D$ , and to the local viscosity,  $\eta$ , of the surrounding environment according to the Debye-Stokes-Einstein equation:<sup>37-39</sup>

$$\tau_{OR} = \frac{1}{6D} = \frac{\eta Vf}{k_B T S} \quad (1.5)$$

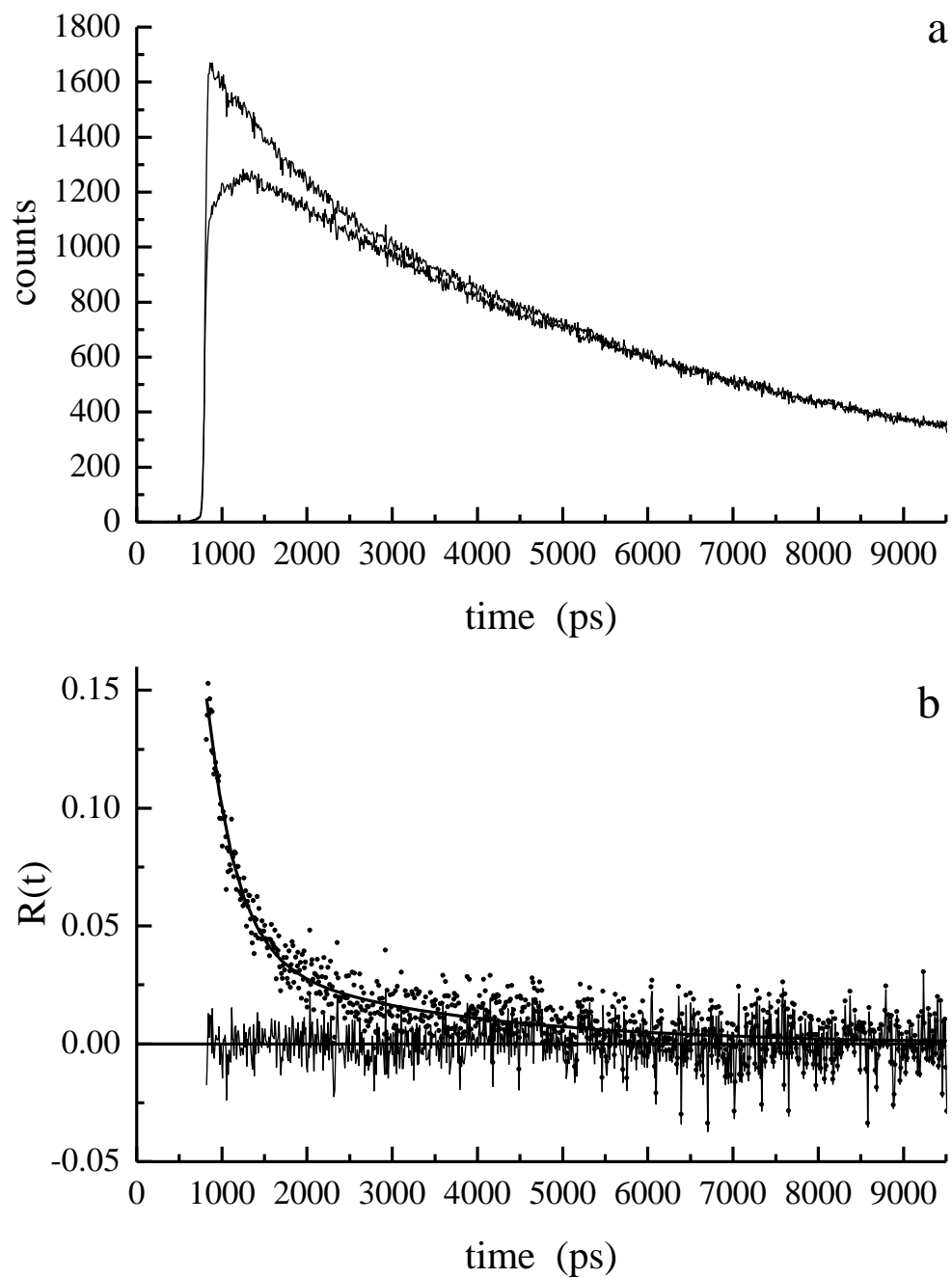


Figure 1.3. (a) Time-resolved emission intensities for polarizations collected parallel ( $I_{\parallel}(t)$ ) and perpendicular ( $I_{\perp}(t)$ ) to the vertically polarized excitation pulse. (b) The functional form of the orientational anisotropy decay obtained from transients in (a). Residuals are distributed along the  $y$ -intercept and the solid line is the fit of the data.<sup>1</sup>

where  $V$  is the hydrodynamic volume of the chromophore,  $f$  is a frictional term to compensate for the interactions between the solute and solvent,  $k_B$  is the Boltzmann constant,  $T$  is the absolute temperature, and  $S$  is a shape factor that accounts for the shape of the chromophore. Therefore, time-resolved fluorescence anisotropy measurements of chromophores incorporated into either the acyl chain or headgroup region of the lipid bilayer provide detailed information on the molecular motion of the probe molecules in their local environment.

Typically, fluorescent probes sweep out a non-spherical volume while reorienting, and can therefore be thought of as ellipsoidal rotors. The recovered anisotropy decay describes the shape of the volume swept out by the reorienting chromophore, and is related to the Cartesian components of the diffusion constant ( $D_x$ ,  $D_y$ , and  $D_z$ ), according to a treatment by Chuang and Eisenthal,<sup>40</sup> where

$$D = \frac{1}{3}(D_x + D_y + D_z) \tag{1.6}$$

Theoretically the time-resolved anisotropy can produce up to five exponential decays, but typically no more than two exponentials are observed experimentally. According to Chuang and Eisenthal, the ellipsoid shape of the reorienting probe depends on the orientation of its absorbing and emitting transition moments. Assuming that both the absorption and emission transition moments are aligned along the same axis, in the  $\pi$ -plane system of the chromophore, two assumptions can be made. The first is that the molecule is a prolate rotor rotating predominantly about its long in-plane axis, where

$D_x > D_y = D_z$ , and the recovered orientational anisotropy function takes the form of a single-exponential decay:

$$R(t) = 0.4 \exp(-6D_z t) \quad (1.7)$$

The second assumption is that the chromophore is behaving as an oblate rotor, with its dominant rotation about the out-of-plane axis, perpendicular to the chromophore's  $\pi$ -plane, where  $D_z > D_x = D_y$ , and the anisotropy function produces a two-component exponential decay:

$$R(t) = 0.1 \exp(-(2D_x + 4D_z)t) + 0.3 \exp(-6D_x t) \quad (1.8)$$

Another set of empirical expressions for prolate and oblate rotors is produced if it is assumed that the absorption and emission transition moments are polarized along the chromophore short in-plane axis

$$\text{Prolate: } R(t) = 0.1 \exp(-(4D_x + 2D_z)t) + 0.3 \exp(-6D_x t) \quad (1.9)$$

$$\text{Oblate: } R(t) = 0.4 \exp(-(4D_x + 2D_z)t) \quad (1.10)$$

Fitting the experimentally-obtained anisotropy decay function according to assumptions regarding the orientation of the absorption and emission transition moment of the chromophore provides information on the diffusion constant of the molecule based on the assumption of a rotor shape (Eqs. 1.7 – 1.10). Then using the Debye-Stokes-Einstein equation (Eq. 1.5), the viscosity of the local environment of the chromophore can be determined, and conclusions can be made as to the dynamic behavior and fluidity of the local environment.

In the course of this project, we have used three different chromophore molecules to investigate the molecular motion and organization of lipid bilayer systems in the form of unilamellar vesicles. In Chapter 2 we used a nitro-2-1,3-benzoxadiazol-4-yl (NBD) (Figure 1.2c) chromophore tethered to the headgroup of a phosphoethanolamine lipid (18:0 NBD-PE) to investigate the hydrogen bonding interactions between the headgroup moieties of the NBD-PE lipids and systems consisting of either phosphocholine (18:0 PC) or phosphoglycerol (18:0 PG) lipids. In Chapter 3 we discuss using the polycyclic aromatic hydrocarbon (PAH) pyrene (Figure 1.2a) to investigate the lateral diffusion and fluid properties of acyl chain regions of 14:0 PC lipid vesicles. In Chapter 4 we used the PAH perylene (Figure 1.2b) to investigate the organizational and fluid properties of the acyl chain regions of 14:0 PC lipid vesicles. In Chapters 5 and 6, we again used perylene to study the effects of thermal energy dissipation on the motional dynamics of 14:0 PC lipid vesicle acyl chain regions. The conclusions of all of these experiments are discussed in Chapter 7.

## CHAPTER 2

# Rotational and Translational Dynamics of Headgroup-Tethered Chromophores in Lipid Vesicles

### Introduction

A vital concept in the regulation of biological cell life is membrane fluidity, which encompasses the translational, rotational and trans-leaflet diffusion of constituent lipids,<sup>41</sup> and influences cellular functions such as signaling, protein activity and response to stimuli.<sup>42</sup> In order to study the molecular-scale behavior of cell membranes, simple model membrane systems composed of pure lipids can be employed. Some typical model lipid bilayer systems which can be used to mimic the physical properties and dynamics of cell membranes<sup>43-44</sup> are unilamellar vesicles in solution,<sup>45</sup> solid or substrate-supported lipid bilayers,<sup>46</sup> and lipid bilayers or monolayers tethered to polymer cushions.<sup>47-48</sup> Changes in membrane fluidity also affect the permeability of the membrane to nutrients and waste by altering the rate of transbilayer diffusion. For example, the rate of transbilayer diffusion of an important signaling molecule that transmits information between mammalian cells, nitric oxide, has been shown to decrease with decreasing membrane fluidity.<sup>49</sup>

One way in which biological cells control fluidity is by adjusting the composition of membrane constituents. For example, incorporation of lysophosphatidylcholine lipids into egg-phosphatidylcholine solid-supported lipid bilayers increases the rate of

translational diffusion by disrupting the van der Waals interactions between hydrophobic acyl chains, making the bilayers more fluid. On the other hand, the addition of egg-phosphatidylethanolamine into solid-supported egg-phosphatidylcholine lipid bilayers results in pronounced headgroup hydrogen bonding, which enhances van der Waals interactions due to tighter packing and lowers the rate of translational diffusion.<sup>50</sup>

In the present study, we have investigated the effects of phospholipid headgroup hydrogen bonding on the translational and rotational dynamics of 1,2-dioleoyl-*sn*-glycero-3-phosphoethanolamine-N-7-nitro-2-1,3-benzoxadiazol-4-yl (18:1 NBD-PE, Fig. 2.1) in lipid bilayers comprised of 1,2-dioleoyl-*sn*-glycero-3-phosphocholine (DOPC) and 1,2-dioleoyl-*sn*-glycero-3-[phospho-*rac*-(1-glycerol)] (DOPG). The molecular structures of these lipids are shown in Figure 2.2. Although zwitterionic phosphatidylcholine (PC) lipids such as DOPC comprise the majority of lipids found in biological membranes, anionic lipids such as DOPG also play significant roles in regulating membrane function.<sup>51</sup> Phosphatidylglycerol (PG) lipids are believed to be responsible for maintaining membrane lipid surface charge density, a property that not only affects membrane permeability to ions and charged metabolites, but also the activity of certain membrane proteins.<sup>52</sup>

Based on the structure of PC lipid bilayers, it is theorized that hydrogen bonding is possible between the oxygen atoms in the phosphate functionalities of neighboring lipid headgroups, and that there are electrostatic interactions between the negatively

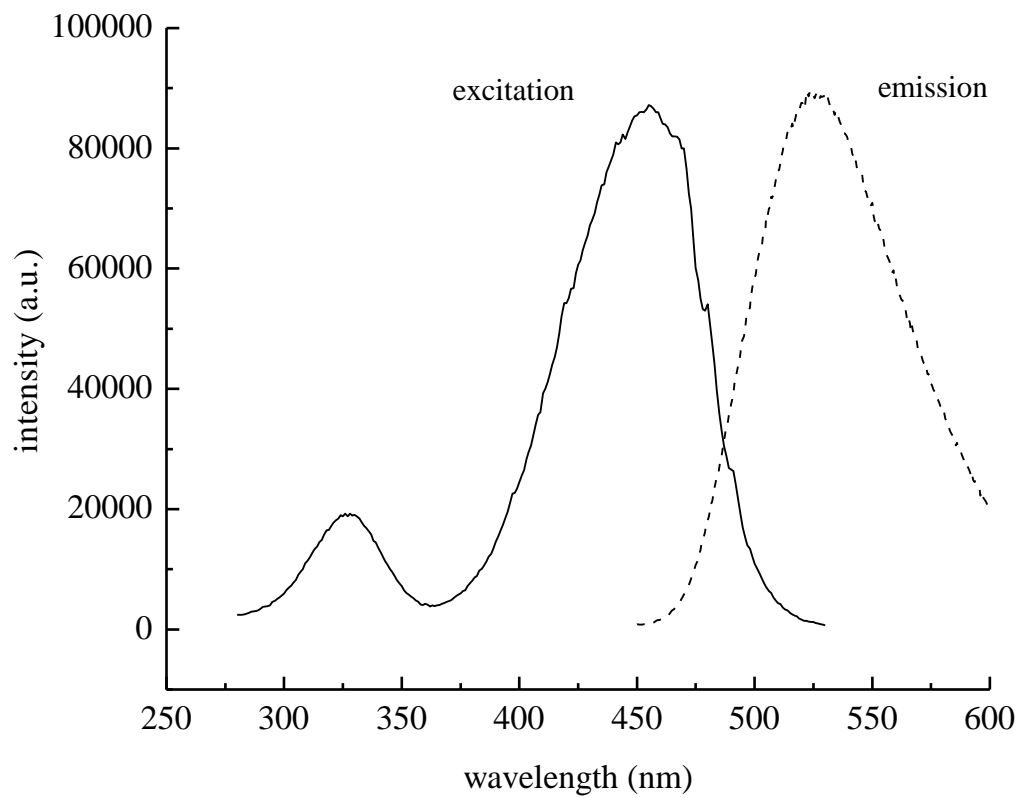


Figure 2.1. Excitation and emission spectra of  $1\text{e-}6$  M NBD-phosphatidylethanolamine (NBD-PE) in chloroform.

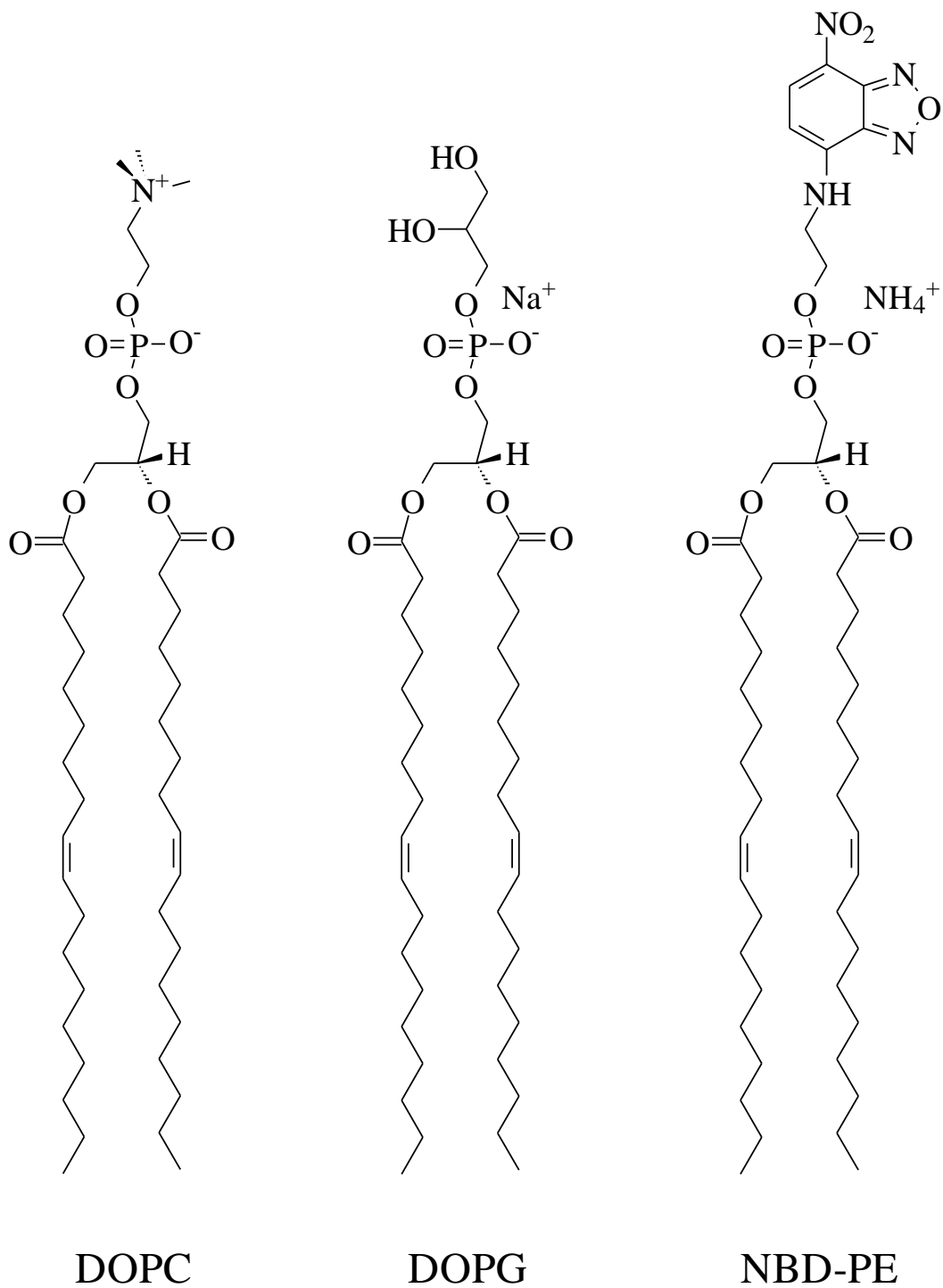


Figure 2.2. Molecular structures of lipids used in this study: dioleoylphosphatidylcholine (DOPC), dioleoylphosphatidylglycerol (DOPG), and the chromophore NBD-phosphatidylethanolamine (NBD-PE).

charged phosphate oxygen and the positively charged choline nitrogen.<sup>53-56</sup> PG lipids, in contrast, are rich in headgroup functionalities that can form hydrogen bonds with other membrane constituents,<sup>57,58</sup> and they are also capable of forming hydrogen bonds between the glycerol moiety and phosphate oxygen of neighboring PG lipids.<sup>59-60</sup> The presence of hydrogen bonds can be measured directly using infrared spectroscopy<sup>61</sup> or indirectly using fluorescence spectroscopy to monitor the dynamics of fluorescently-tagged lipid headgroups in lipid bilayers. In this study, we investigated interactions between NBD-PE and headgroup regions of neighboring lipids in both vesicle and solid-supported lipid bilayer systems. We measured translational diffusion coefficients and mobile fractions using fluorescence recovery after pattern photobleaching (FRAPP), and fluorescence lifetimes and rotational diffusion times using time-correlated single photon counting (TCSPC).

In order to investigate lipid headgroup-headgroup interactions we chose the fluorescently-tagged lipid NBD-PE, which has an NBD chromophore tethered to its polar headgroup. In addition, two bulk lipids were used to form the lipid bilayer system, DOPC and DOPG, which have identical hydrophobic acyl chain structures, but differ in headgroup functionality. Therefore, using NBD-PE as the molecular probe of our lipid systems allowed us to examine molecular-scale issues related to lipid headgroup interactions while maintaining comparatively constant acyl chain interactions. We must note that we are able to form intact lipid vesicles comprised of 98% of the anionic lipid DOPG, however no direct comparison can be made in supported lipid structures because only a few concentrations of anionic lipids such as DOPG can produce fluid bilayer

structures.<sup>62</sup> Regardless of this limitation, it is possible to compare mixed lipid systems in both structural formats, and these data provide useful insight into the dynamical properties of the NBD-PE contained within them.

## Experimental Section

*Vesicle Preparation:* Phospholipids 1,2-dioleoyl-*sn*-glycero-3-phosphocholine (DOPC), 1,2-Dioleoyl-*sn*-Glycero-3-[Phospho-*rac*-(1-glycerol)] (DOPG), and 1,2-Dioleoyl-*sn* Glycero-3 Phosphoethanolamine-N-7-nitro-2-1,3-benzoxadiazol-4-yl (18:1 NBD-PE) were purchased from Avanti Polar Lipids Inc. (Alabaster, AL) and used without further purification. For fluorescence lifetime and anisotropy measurements 1 mM lipid solutions were made consisting of: 1) 98 mol% DOPC and 2 mol% of NBD-PE, 2) 98 mol% DOPG and 2 mol% NBD-PE, and 3) 59 mol% DOPC, 39 mol% DOPG, and 2 mol% NBD-PE were prepared. For FRAPP measurements 1 mM lipid solutions were made consisting of: 1) 98 mol% DOPC and 2 mol% NBD-PE, and 2) 59 mol% DOPC, 39 mol% DOPG, and 2 mol% NBD-PE. The chloroform solvent was then evaporated from the lipid mixture and the dry lipid film was hydrated with Tris<sup>®</sup>-HCl buffer (Sigma-Aldrich, St. Louis, MO) containing NaCl (FisherScientific, Fair Lawn, NJ) for 30 min. prior to extrusion. The buffer (10 mM Tris<sup>®</sup>, 150 mM NaCl, pH 8) was prepared using water from a Milli-Q Plus water purification system (Millipore, Bedford, MA). The mixtures were processed five times through a freeze-thaw-vortex cycle to ensure complete mixing of the sample constituents. Each cycle consisted of immersion in liquid nitrogen for 5 min., followed by immersion in a 60°C water bath for 5 min., and then vortexing the thawed sample for 2 min. The hydrated mixtures were extruded 11 times through a polycarbonate membrane with a nominal pore diameter of 100 nm (Avanti Polar Lipids Inc., Alabaster, AL). All extrusions were performed at room temperature.

*Time-Correlated Single Photon Counting (TCSPC):* Time-resolved fluorescence anisotropy and lifetime data were measured using a TCSPC instrument. The experimental setup has been described in detail elsewhere,<sup>63-64</sup> so only the essential features are given here. The light source is a CW mode-locked Nd:YAG laser (Coherent Antares 76-s, Santa Clara, CA) that produces 100 ps 1064 nm pulses at a 76 MHz repetition rate. The third harmonic of the Nd:YAG laser output was used to excite a cavity-dumped dye laser (Coherent 702-2, Santa Clara, CA) operated with Stilbene 420 dye (Exciton, Dayton, OH) at 460 nm. The average output power of this laser was ca. 25 mW, with 5 ps pulses at a 4 MHz repetition rate. The sample emission was detected with a microchannel plate photomultiplier tube (MCP-PMT, Hamamatsu R3809U-50, Bridgewater, NJ). The electronics used to temporally resolve the fluorescence transients included a constant fraction discriminator (CFD, Tennelec 454) and a time-to-amplitude converter/biased amplifier (TAC, Tennelec 864). The collection wavelength (545 nm, 10 nm detection bandwidth) and polarization were computer controlled using LabVIEW 7.1 code. The fluorescence lifetime data were collected at 54.7° with respect to the vertical excitation polarization, while the reorientation data were collected at polarizations parallel (0°) and perpendicular (90°) to the vertically polarized incident light pulse.

*Deposition of Supported Lipid Bilayers:* Fused silica microscope slides (75 mm x 25 mm x 1 mm) were purchased from Technical Glass Products, Inc. (Painesville, OH). The slides were cleaned by bath sonication (Branson 1510, Branson Ultrasonic Corporation, Danbury, CT) in detergent solution for 20 min., rinsed with DI water, baked at 160°C for 4 h, and plasma treated (Harrick Plasma, Ithaca, NY) with oxygen under vacuum (150 mTorr) for 10 min. immediately before bilayer deposition. Supported

bilayer lipid membranes were deposited by vesicle fusion in a custom-made flow cell as described elsewhere.<sup>65</sup> The flow cell was initially washed with buffer, followed by a 3-hour incubation with liposome solution and a final buffer wash to remove unadsorbed vesicles. All experiments were performed at room temperature.

*Fluorescence Recovery After Pattern Photobleaching (FRAPP):* FRAPP was used to measure the rate of translational diffusion of chromophores in supported bilayer membranes formed on silica microscope slides. The experimental setup has been described in detail elsewhere.<sup>65</sup> A double syringe pump system (Harvard Apparatus) was used to infuse and withdraw solutions simultaneously from a custom-made 1 mL flow cell. The 488 nm laser line from an argon ion laser (95, Lexel Laser, Fremont, CA) was directed through a 5x beam expander (Edmund Optics, Inc., Barrington, NJ), a filter cube (Ex: 450-490/DM: 510/Em: 515-565), and a pair of optical flats<sup>65</sup> that toggle between a low intensity (20 $\mu$ W) monitoring beam for continuous fluorescence emission measurements, and a high intensity (500 mW) beam for photobleaching chromophores. Light passing through the sample was collected by an inverted microscope (Zeiss Axiovert 135M, Carl Zeiss, Thornwood, NY) with a 32x objective lens (Carl Zeiss, Thornwood, NY). The light intensity was measured by a side-on photomultiplier tube (PMT, Hamamatsu R4632, Bridgewater, NJ) connected to a photon counter (SR400 Stanford Research Systems, Sunnyvale, CA) and a fast preamplifier (SR445 Stanford Research Systems, Sunnyvale, CA). A Ronchi ruling (50 lines per inch, Edmund Optics, Inc., Barrington, NJ) in the back image plane of the microscope created a fringe pattern on the sample. An aperture placed in the image plane in front of the PMT restricted the

observation area, resulting in an illuminated area of approximately 200  $\mu\text{m}$  in diameter and an observed area of 75  $\mu\text{m}$ . This was done to prevent unbleached fluorophores from diffusing from outside the bleached (patterned) area into the observation zone during fluorescence recovery measurements. Stripe periodicity in the sample plane was 25 $\mu\text{m}$ .

## Results and Discussion

The goal of this work was to investigate the interactions between neighboring lipid headgroups in a bilayer structure by examining the rotational and translational diffusion behavior of a tethered chromophore in lipid vesicles and supported lipid bilayers. DOPC and DOPG were chosen as the primary lipids in this study for two reasons. First, these lipids have low characteristic phase transition temperatures ( $T_m$ ) of 253K for DOPC<sup>66</sup> and 258K for DOPG,<sup>60</sup> ensuring that the bilayers will exist in a disordered, fluid phase at ambient temperature. Second, the two lipids have identical acyl chain lengths but different headgroup functionalities, so differences in chromophore dynamics can be attributed entirely to headgroup interactions. We consider the rotational diffusion and fluorescence lifetime data first.

*Fluorescence Lifetime and Anisotropy Data.* Fluorescence lifetime and anisotropy decay data provide information on the molecular environment(s) of the NBD chromophore in vesicles of the following compositions: 1) 98 mol% DOPC and 2 mol% NBD-PE, 2) 98 mol% DOPG and 2 mol% NBD-PE, and 3) 59 mol% DOPC, 39 mol% DOPG, and 2 mol% NBD-PE. Additionally, we examined vesicles 100 nm and 2000 nm in diameter to assess the influence of membrane curvature on rotational dynamics. For all measurements, there were no discernable differences in either the lifetime or the anisotropy data for the two vesicle sizes, suggesting that curvature is not an issue for these measurements.

A two-component exponential decay was observed for the fluorescence lifetime data for NBD-PE in each vesicle system (Figure 2.3a, Table 2.1). There are two possible

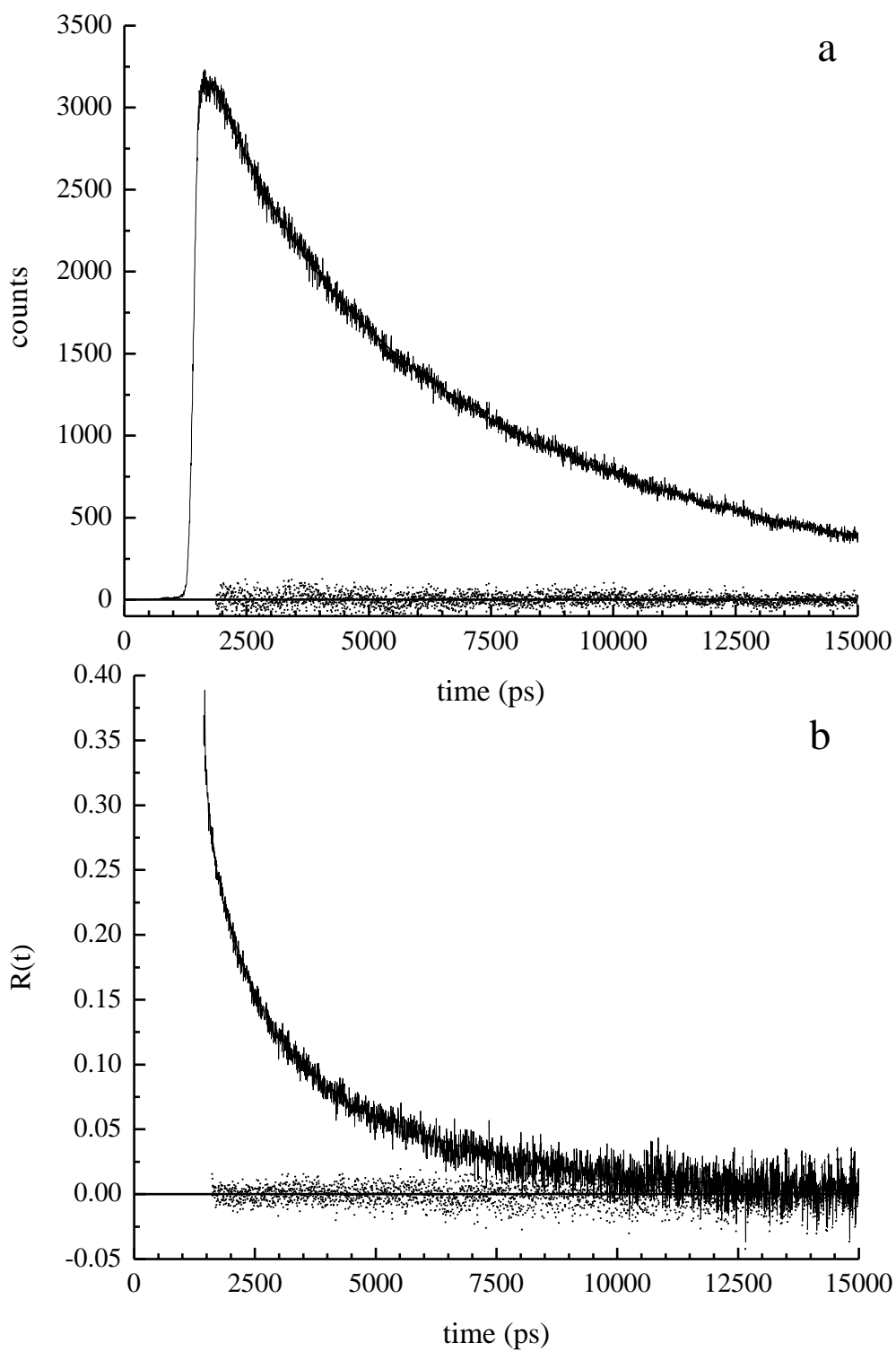


Figure 2.3. (a) Fluorescence lifetime and (b) induced orientational anisotropy data for NBD-PE in a DOPG/DOPC mixed lipid vesicle. The residuals for a fitted two-component exponential decay function are shown for both panels.

Table 2.1. Fluorescence lifetimes ( $\tau_1$  and  $\tau_2$ ) and reorientation times ( $\tau_{OR1}$  and  $\tau_{OR2}$ ) of NBD-PE in bilayer lipid vesicles, determined by TCSPC.

	$\tau_1$ (ns)	$\tau_2$ (ns)	$\tau_{OR1}$ (ns)	$\tau_{OR2}$ (ns)
DOPC	$1.92 \pm 0.12$	$7.83 \pm 0.21$	$0.65 \pm 0.05$	$3.67 \pm 0.10$
DOPG	$2.13 \pm 0.07$	$7.70 \pm 0.11$	$0.49 \pm 0.20$	$3.20 \pm 0.52$
DOPC/DOPG	$1.89 \pm 0.19$	$7.48 \pm 0.14$	$0.77 \pm 0.52$	$3.93 \pm 0.05$

explanations for this finding. Either the chromophore is sensing two unique environments with populations that do not exchange significantly on the timescale of the excited-state relaxation, or the chromophore exists in a dielectric gradient, where slight changes in the location and/or orientation of the chromophore with respect to the gradient give rise to a distribution of fluorescence lifetimes.<sup>67-70</sup> This condition has been reported previously for the NBD chromophore.<sup>71-72</sup> While it may be tempting to ascribe the different lifetime components to specific chemical environments, the dependence of fluorescence lifetime on intramolecular and intermolecular properties is sufficiently complex that it is not possible to make such assignments in the absence of additional information.

Fluorescence anisotropy decay data, in contrast, can be interpreted within the context of well established theoretical models.<sup>37, 73-75</sup> The induced orientational anisotropy decay function,  $R(t)$ , is formulated as the normalized transient difference in emission intensity parallel,  $I_{\parallel}(t)$ , and perpendicular,  $I_{\perp}(t)$ , to the polarization of the incident excitation pulse (Eq. 2.1):

$$R(t) = \frac{I_{\parallel}(t) - I_{\perp}(t)}{I_{\parallel}(t) + 2I_{\perp}(t)} \quad (2.1)$$

This is the functional form of  $R(t)$  that contains chemically relevant information. There are two possible choices for the interpretation of our fluorescence anisotropy data due to the fact that the chromophore is attached to the headgroup of the phospholipid. The

functional form of the anisotropy decay allows us to determine whether this tethered-chromophore behaves as a free rotor or as a hindered rotor.

A free rotor, such as a chromophore in free solution, is characterized by a zero infinite-time anisotropy because the chromophore can assume all orientations with equal probability. The general case for a chromophore tethered to a lipid (as is the case for NBD-PE) is termed a “hindered rotor”, because it is not free to access all possible orientations, resulting in a non-zero infinite-time anisotropy,  $R(\infty)$ .<sup>74-75</sup> The limiting case for a hindered rotor is where the volume accessible to the chromophore is hemispherical, and under this condition it will behave as a free rotor because of the inherent polarization symmetry of the incident electric field. Our experimental data are characterized by a two-component exponential anisotropy decay for each of the three lipid systems used in this study, and for each the infinite-time anisotropy,  $R(\infty)$  is zero to within the experimental uncertainty (Figure 2.3b, Table 2.1). The absence of an infinite-time anisotropy component in the data means that the chromophore is able to reorient within a hemispherical volume and, as such, it can be treated as a free rotor.

We can interpret our anisotropy decay data using a model for molecular reorientation developed by Chuang and Eisenthal.<sup>73</sup> This model was developed for free chromophores with full motional freedom in solution, but the same essential physics underlying the Chuang and Eisenthal model must also apply to the dynamics of a tethered chromophore, especially when the chromophore is free to relax in a hemispherical volume (*i.e.* no confining cone). In this model, the Cartesian axes are assigned so that the  $z$ -axis is perpendicular to the chromophore  $\pi$ -system plane and the exciting and emitting

transition dipole moments are oriented along either the  $x$ -axis (long axis) or  $y$ -axis (short axis) of the chromophore molecular plane.<sup>76</sup> The two limiting cases of this model treat the chromophore as either a Type I or a Type II rotor. The excited and emitting transition dipoles lie coincident with the unique rotational axis for Type I ( $D_x \neq D_y = D_z$ ) and perpendicular to the unique rotational axis for Type II ( $D_x = D_y \neq D_z$ ) rotors. The reorientation decay time constants are related to the Cartesian components of the rotational diffusion constant through the anisotropy decay function,  $R(t)$ , as shown in Eqs. 2.2-2.5:<sup>77</sup>

*Transition dipole oriented along the chromophore long (x) axis*

$$\text{Type I: } r(t) = \left(\frac{4}{10}\right) \exp(-6D_z t) \quad (2.2)$$

$$\text{Type II: } r(t) = \left(\frac{1}{10}\right) \exp(-(2D_x + 4D_z)t) + \left(\frac{3}{10}\right) \exp(-6D_x t) \quad (2.3)$$

*Transition dipole oriented along the chromophore short (y) axis*

$$\text{Type I: } r(t) = \left(\frac{1}{10}\right) \exp(-(2D_z + 4D_x)t) + \left(\frac{3}{10}\right) \exp(-6D_z t) \quad (2.4)$$

$$\text{Type II: } r(t) = \left(\frac{4}{10}\right) \exp(-(2D_z + 4D_x)t) \quad (2.5)$$

In this model, the recovery of a double-exponential decay indicates that the NBD chromophore behaves as either an  $x$ -axis polarized Type II rotor or a  $y$ -axis polarized Type I rotor, according to Eqs. 2.3 and 2.4. Previous studies of the solution phase NBD

chromophore using one and two-photon excitation methods suggest that the  $S_1 \leftarrow S_0$  transition of this chromophore is short-axis polarized, and a two-component anisotropy decay would be consistent with NBD reorienting as a Type I rotor (Eq. 2.4).<sup>57</sup> Based on this assignment, we evaluate the Cartesian components of the rotational diffusion constant for NBD-PE.

The Cartesian components of the diffusion constant (Table 2.2) of tethered NBD in all of the vesicle solutions are similar. These data all indicate that the tethered NBD chromophore is a substantially anisotropic rotor, with an aspect ratio of  $D_x/D_z \sim 8$ . While it may be tempting to consider the subtle differences between the  $D_z$  and  $D_x$  values and the ratio of these constants, the uncertainty in the data is sufficiently large enough that it is not possible to draw any system-dependent conclusions without additional information. Next we will consider the molecular-scale translational diffusion behavior of NBD-PE in our supported lipid bilayer systems.

*Translational Diffusion in Supported Lipid Bilayers:* Rotational diffusion measurements can provide information on the molecular-scale environment of the reorienting chromophore, and the information we obtain for NBD-PE on the molecular length scale suggests that the dynamics of the lipid headgroup are determined to a significant extent by the interactions of the aqueous environment with the lipid bilayer. This finding is consistent with our observation of a two-component fluorescence lifetime, which can be accounted for in the context of the chromophore existing in a dielectric gradient. The molecular-scale information does not provide a complete picture, however,

Table 2.2. Cartesian components of the rotational diffusion constant (MHz) of NBD-PE chromophores in lipid bilayer vesicles.

	$D_x$ (MHz)	$D_z$ (MHz)	$D_x/D_z$
DOPC	$362 \pm 27$	$45 \pm 2$	$7.97 \pm 0.82$
DOPG	$484 \pm 148$	$52 \pm 7$	$9.30 \pm 4.22$
DOPC/DOPG	$303 \pm 131$	$42 \pm 1$	$7.16 \pm 3.18$

of the fluid properties of the lipid bilayers. We also need to consider motion over longer length scales, and we accomplish this task through the use of translational diffusion measurements.

Mobile fractions and translational diffusion coefficients were measured with FRAPP to provide information complementary to our TCSPC fluorescence lifetime and anisotropy decay data. Because vesicles with 98 mol% DOPG did not adsorb to fused silica, FRAPP studies were limited to two systems: 1) 98 mol% DOPC and 2 mol% NBD-PE, and 2) 59 mol% DOPC, 39 mol% DOPG, and 2 mol% NBD-PE. We found that 39 mol% DOPG was the maximum concentration of the anionic lipid that would lead to the establishment of stable fluid solid-supported lipid bilayers. This finding is consistent with previous studies under similar buffer conditions.<sup>46, 78</sup>

For FRAPP experiments, a Ronchi ruling was placed in the rear image plane of the microscope, creating a striped pattern of alternating light and dark fringes on the solid-supported lipid bilayer. Chromophores in illuminated zones are photobleached by exposure to a high intensity laser beam. Unbleached chromophores in the dark zones then diffuse into the photobleached areas, leading to the recovery of a spatially homogeneous fluorescence signal.<sup>79</sup> The time constant and functional form of this recovery are given by,

$$f(t) = f(0) + \frac{m}{2} [1 - f(0)] \left\{ 1 - \left( \frac{8}{\pi^2} \right) \exp\left( -\frac{4\pi^2 Dt}{a^2} \right) + \frac{1}{9} \exp\left( -\frac{36\pi^2 Dt}{a^2} \right) \right\} \quad (2.6)$$

where  $f(t)$  is the post-bleach fluorescence intensity ( $t > 0$ ) normalized with respect to the constant pre-bleach fluorescence intensity ( $t < 0$ ), with  $t = 0$  being the time of the bleach pulse,  $D$  is the average translational diffusion coefficient of the chromophores within the bleached area,  $m$  is the mobile fraction, and  $a$  is the stripe periodicity of the Ronchi ruling in the sample plane.<sup>80</sup> Eq. 2.6 assumes a single diffusing population, corresponding to the chromophores in the solid-supported lipid bilayer for our experiments, and an immobile population of chromophores that reside in intact vesicles attached to the surface.

A typical FRAPP recovery curve for a DOPC/NBD-PE bilayer is shown in Figure 2.4, and calculated translational diffusion coefficients and mobile fractions are given in Table 2.3. The mobile fractions were determined to be statistically the same for both systems using an ANOVA analysis; however, the translational diffusion coefficients were statistically different. For the DOPC bilayer we measured a diffusion coefficient of  $2.91 \pm 0.31 \mu\text{m}^2/\text{s}$ , and for the mixed DOPC/DOPG bilayers we measured  $1.82 \pm 0.41 \mu\text{m}^2/\text{s}$ . It is clear from these data that translational diffusion of NBD-PE is hindered in bilayers containing DOPG. The fact that this difference in translational diffusion times was observed within the experimental uncertainty for the DOPG-containing bilayer, but not in the rotational diffusion measurements suggests that the NBD-PE chromophore does not show a substantial preference for interacting with either DOPC or DOPG lipid headgroups. The intermolecular headgroup-headgroup interactions between lipids seem to mediate the translational motion of the bilayer constituents. This finding is consistent with recent molecular dynamics (MD) simulations involving PC and PG bilayers.<sup>81</sup> The

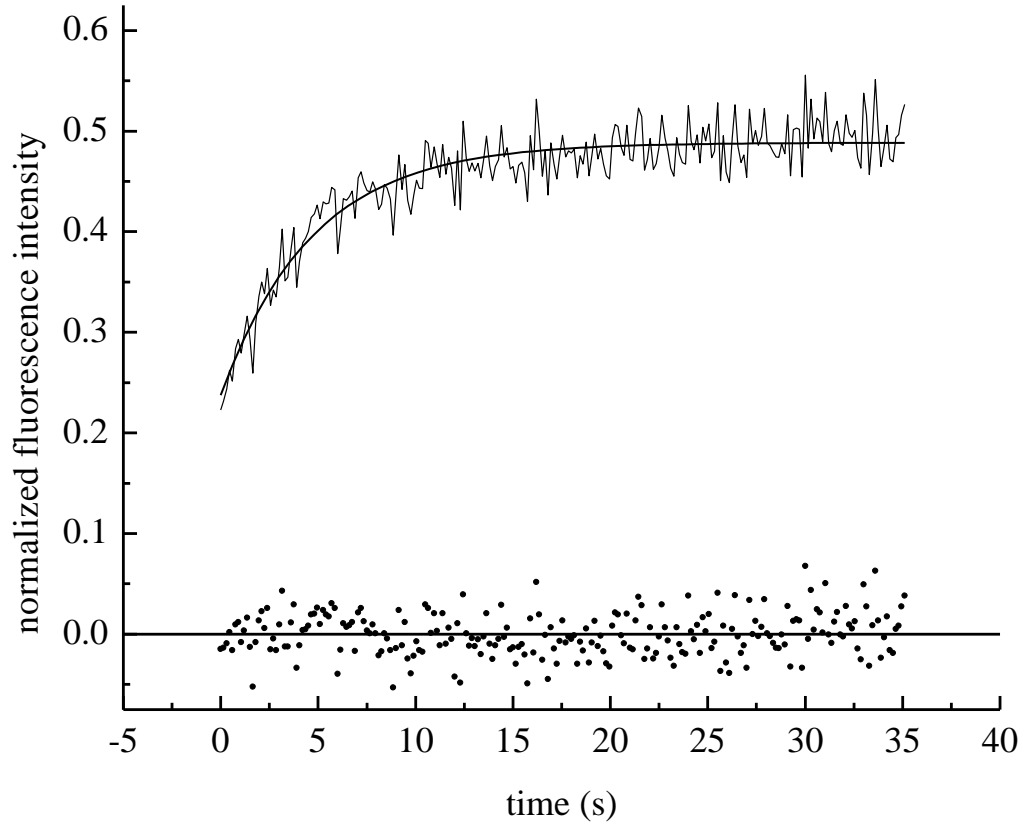


Figure 2.4. A typical FRAPP recovery curve for a DOPC/NBD-PE supported bilayer membrane (above) along with residuals (below). Total photobleaching time was 300 ms.

Table 2.3. Mobilities and diffusion coefficients of NBD-PE in supported lipid bilayers on fused silica. FRAPP data represent average values for three bilayers. At least five different areas were interrogated for each bilayer.

	Mobility (%)	Diffusion Coefficient ( $\mu\text{m}^2/\text{s}$ )
DOPC	$0.79 \pm 0.11$	$2.91 \pm 0.31$
DOPC/DOPG	$0.61 \pm 0.08$	$1.82 \pm 0.24$

strength of the hydrogen bonding interactions ranges from *ca.* 10 to *ca.* 30 kJ/mol.<sup>82</sup> The NBD chromophore contains several hydrogen bonding functionalities so, in principle it can participate in hydrogen bonding interactions. Perhaps of more significance is the fact that the DOPG glycerol headgroup contains two hydroxyl groups that can function as either hydrogen bond donors or acceptors. In contrast, the DOPC headgroup does not contain any hydrogen bonding functionalities and, as such, should not be expected to participate in headgroup-headgroup interactions in a manner analogous to that of DOPG headgroups. MD simulations have reported that pure palmitoyl-oleoyl-phosphatidylglycerol (POPG) bilayers are *ca.* 6 Å thicker than pure palmitoyl-oleoyl-phosphatidylcholine (POPC) bilayers. Therefore, the slower translational diffusion coefficient observed for the DOPG system could also be attributed to its having a thicker bilayer membrane.

We next need to consider how these two bodies of data can be reconciled. The rotational diffusion data indicate that at the molecular level, the rotational motion of chromophores localized in the headgroup region of the bilayer is not mediated significantly by the headgroup structure or organization of the lipids. This situation is explained by the presence of bulk Tris<sup>®</sup> buffer solvent in close contact with the interfacial region of the lipid bilayer structure. The fact that the translational diffusion behavior of these chromophores in the bilayers does depend on lipid headgroup identity arises from the fact that it is the translational motion of entire lipid molecules that is being sensed in the measurement, and translational motion is expected to be significantly dependent on structural heterogeneity present in the bilayer.

In our translational diffusion data there appear to be regions of the supported bilayer structure that are comparatively less mobile than others. The notion of immobile regions is not surprising for the DOPC/DOPG systems in light of the large body of literature which proposes the existence of phase separation in mixed lipid systems. The basis for such phase separation is understood from a thermodynamic point of view for multi-component systems,<sup>83-92</sup> but for single-component systems, it is fair to question the origin of such features. One possibility is that interactions exist between the supported lipid bilayer lower leaflet and the substrate interface, which result in comparatively less mobile regions. Experiments to resolve the physical reason or reasons for these results is a presently under investigation.

## Conclusions

We have investigated the dynamics of a tethered chromophore (NBD-PE) in unilamellar DOPC, DOPG, and mixed DOPC/DOPG vesicles and supported bilayer systems. We used both phosphocholine (PC) and phosphoglycerol (PG) to evaluate the role of headgroup hydrogen bonding interactions in mediating the fluidity of lipid bilayer structures. Within the experimental uncertainty we obtained the same rotational diffusion results for tethered NBD in each system for vesicles of both 100 nm and 2000 nm diameter. Our data also showed that the molecular-scale rotational motion of the NBD chromophore does not depend sensitively on the type of lipid in the bilayer. We also measured the translational diffusion of NBD-PE in planar supported lipid bilayers comprised of pure DOPC and a mixture of DOPC and DOPG. The data indicate a slower rate of translational diffusion in supported lipid bilayers containing DOPG. We believe this is due to hydrogen bonding interactions between the headgroup regions of neighboring lipids, even though the effect on rotational diffusion appears to be much less pronounced.

## CHAPTER 3

### Investigating Membrane Fluidity of Phospholipid Bilayers Using Steady-State Fluorescence Measurements

#### Introduction

Membrane fluidity is an extremely complex and dynamic concept that encompasses a number of molecular motions, including lipid flip-flop, rotational diffusion, and translational diffusion.<sup>23</sup> All lipid motions contribute to membrane fluidity and play an essential role in regulating the life of a cell. Successful membrane protein reconstitution and functionality are largely dependent upon the behavior of lipid bilayers at a molecular level. Therefore, in order to develop a working membrane-based biosensor, the behavior and fluidity of lipids in bilayer vesicle systems needs to be thoroughly understood before proceeding.

Several biological cell processes are mediated by the composition and properties of the cell membrane, some of these include transmembrane protein function, intercellular signaling, and enzyme activity.<sup>42</sup> Biological cell membranes can regulate protein function by manipulating the fluidity of the lipid bilayer to control the diffusive properties of the membrane. Translational diffusion of molecules through the membrane can be mediated in several ways, including altering the phase of the lipids, adding lipids with varied chain lengths or unsaturations, or by introducing an “impurity” to the bilayer. It is possible to vary the phase of the lipid bilayer by altering the system temperature of the lipid environment. All lipids have a characteristic gel-to-fluid phase transition temperature ( $T_m$ ) that is distinguished by an ordered gel phase at temperatures below  $T_m$ ,

and a less ordered fluid phase at temperatures above  $T_m$ . Gel phase lipids have tightly packed acyl chain regions, resulting in limited rotational and translational freedom of the lipids. Fluid phase bilayers have disordered acyl chain regions with increased motional freedom, resulting in more “fluid-like” behavior.

Additionally, the introduction of a bilayer impurity or non-lipid constituent, such as the weak anesthetic ethanol, is thought to disrupt the well ordered structure of the bilayer lipids, which alters the overall fluidity of the membrane. Ethanol is thought to displace water molecules that are associated with the gel phase lipid bilayer interfacial region, destabilizing the interactions between the lipid headgroups, causing the bilayer to dilate. This lipid dilation increases the average surface area of the headgroups, and once a sufficient amount of ethanol is added to the system, it can perturb the bilayer to the extent that it forms an intermediate phase known as the interdigitated phase.<sup>93-95</sup> The interdigitated phase occurs when lipids in opposing leaflets interpenetrate with one another, decreasing the overall bilayer thickness, and eliminating the bilayer midplane. The formation of the interdigitated phase can affect the proper function of integral proteins in biological cells by altering the fluidity of the lipid membrane.<sup>96</sup> Therefore, it is of interest to us to study the effects of ethanol concentration on the fluidity of pure lipid vesicles using a fluorescent molecular probe.

One way of investigating the membrane fluidity or translational mobility of lipids is through the use of a fluorescent molecular probe imbedded in the acyl chain region of the bilayer, which reports on the local environment of the probe. The acyl chain region is the area of the bilayer that undergoes the most dramatic structural reorganization as a

result of the addition of non-lipid constituents and system temperature changes. Therefore, the nonpolar region of the bilayer is of particular interest to us. The local environment of a probe molecule can often directly determine its optical response. Pyrene, a polycyclic aromatic hydrocarbon with a long excited-state lifetime and high quantum yield, has been used extensively to investigate and gauge the local polarity of solvents.<sup>29-33, 97</sup> In lipid mixtures, pyrene intercalates into the nonpolar acyl chain region of the lipid bilayer, providing information on the local polarity of the nonpolar region of lipid vesicles. Pyrene monomer has a characteristic fluorescence spectrum, with five major vibronic bands appearing at 373, 379, 383, 389, and 393 nm (Fig. 3.1).<sup>30, 32</sup> These vibronic bands are assigned values I through V, respectively. The I/III band intensity ratio scales with increasing solvent polarity, and is a result of dipole-induced dipole interactions between the solvent molecules and the vibrational modes of pyrene.<sup>29-33</sup>

Pyrene also possesses the ability to form an excited-state dimer structure known as an excimer. The formation of an excimer,  $(MM)^*$ , occurs when an electronically excited molecule of pyrene ( $M^*$ ) collides and reacts with a ground-state monomer of pyrene ( $M$ ), and the process can be thought of as dynamic fluorescence quenching of the pyrene monomers.<sup>35</sup> The reactions of interest for excimer formation are<sup>35, 97</sup>:





The fluorescence spectrum of pyrene excimer is red-shifted from that of pyrene monomer, and is characterized by the appearance of a broad, featureless emission band at *ca.* 470 nm (Fig. 3.1). The formation of pyrene excimer is concentration-dependent, as an increase in the concentration of pyrene monomer increases the probability of a reaction between an excited-state pyrene molecule and a ground-state pyrene monomer (Fig. 3.2). The ability of pyrene to form excimers when sequestered in the acyl chain region of lipid bilayers also depends on the fluidity of the membrane, or the translational mobility of pyrene molecules through the acyl chain medium. In this way, pyrene fluorescence measurements provide data on the restrictiveness of the local environment of the probe.<sup>26</sup> As more ethanol is added to solutions of pyrene-doped lipid vesicles, the translational mobility of pyrene through the acyl chains becomes less restricted and the propensity of pyrene to form excimers increases. Therefore, by monitoring the fluorescence emission of pyrene excimer in lipid vesicles as a function of ethanol concentration, we are able to gauge the extent to which the incorporation of ethanol mediates the fluid properties of the bilayer structure. We also want to study whether ethanol perturbs the lipid bilayer to the extent that it can induce the formation of the interdigitated phase.

For these experiments we use 100 nm diameter unilamellar vesicles comprised of 1,2-dimyristoyl-*sn*-phosphatidylcholine (14:0 DMPC,  $T_m = 297$  K), and apply steady-state fluorescence techniques to interrogate the properties of pyrene incorporated into

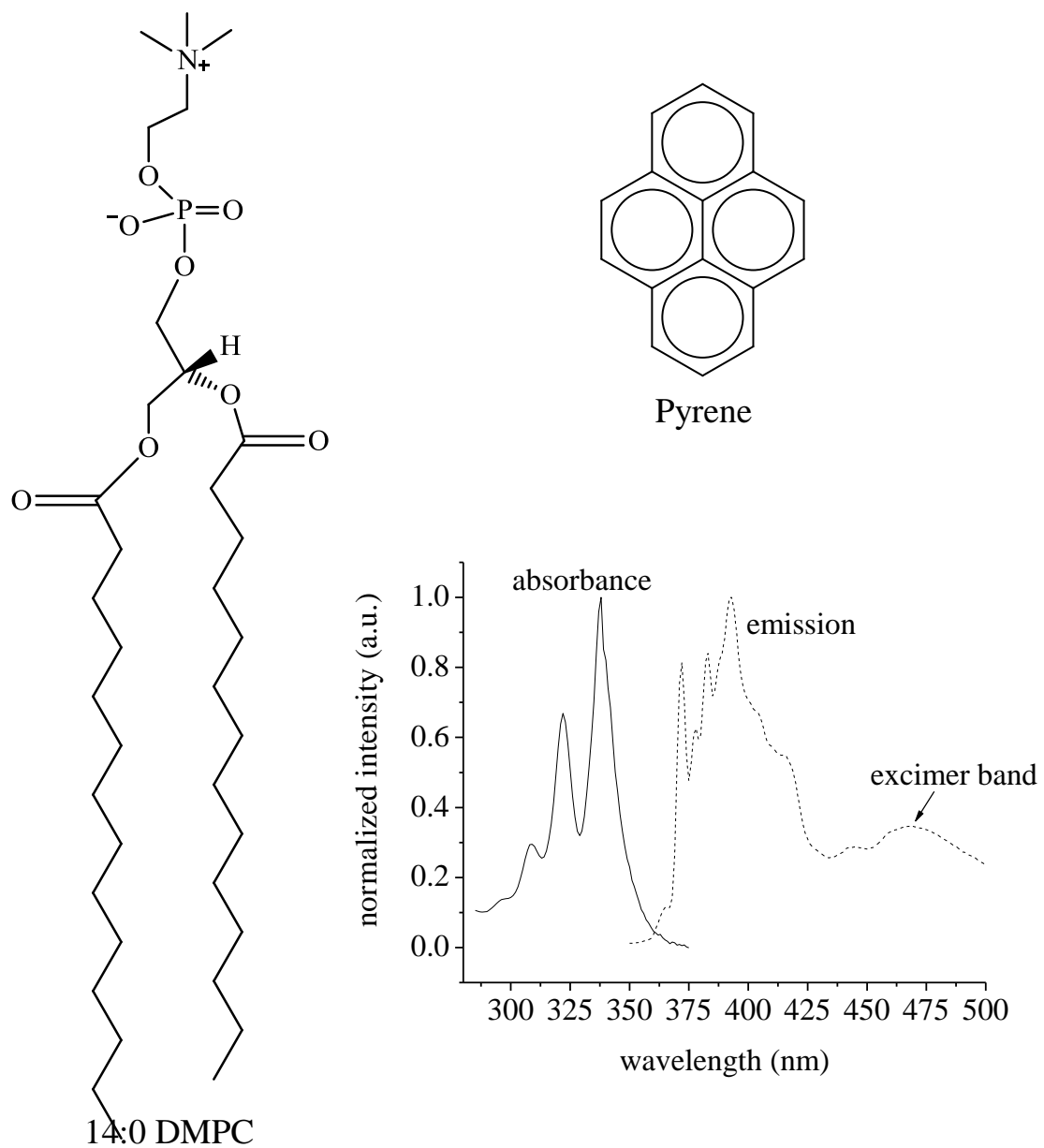


Figure 3.1. Structures of 14:0 DMPC, pyrene, and absorbance and emission spectra of 1e-5 M pyrene in chloroform.

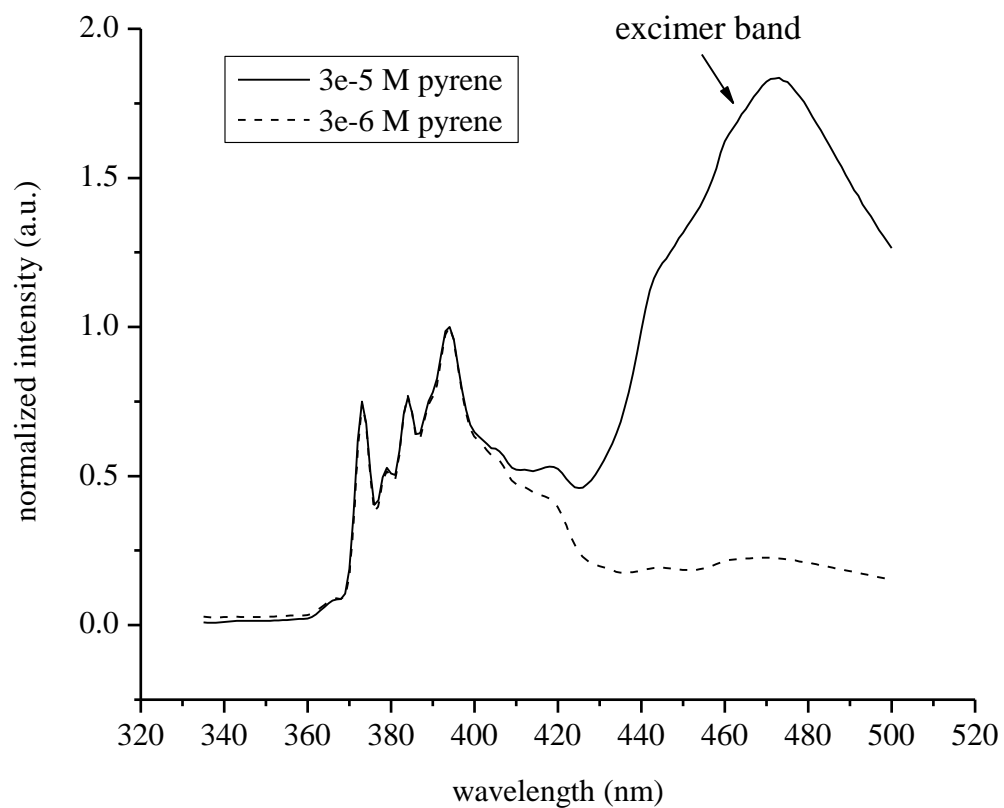


Figure 3.2. Emission spectra of pyrene demonstrating the relationship between concentration and excimer band intensity in 3e-6 M pyrene in DMPC vesicles (dotted line) and 3e-5 M pyrene in DMPC vesicles (solid line).

fluid phase ( $T = 298$  K) vesicle bilayers. Typical biological cell membranes are primarily composed of phospholipids with 16 to 18 carbons per acyl chain, but we use DMPC, which has 14 carbons in each of its aliphatic tails. We chose DMPC because of its characteristic phase transition temperature, which is just below room temperature. This gel-to-fluid phase transition temperature (297 K) allows for easy manipulation of lipid phase at ambient conditions. For steady-state fluorescence experiments we use pyrene because of its aforementioned well-characterized polarity-dependent emission properties and its propensity for excimer formation.<sup>31, 34, 98-102</sup> We found that at ethanol concentrations of *ca.* 0.6 M there appeared to be an increase in the emission intensity of pyrene excimer. This finding indicates that there is an increase in excimer formation at this concentration of ethanol, which could be the result of a fluidizing, or reorganization, of the lipid bilayer acyl chains by the penetration of ethanol molecules into the bilayer of the vesicles.

## Experimental Section

*Vesicle Preparation.* The phospholipid 1,2-dimyristoyl-*sn*-phosphatidylcholine (14:0 DMPC) in chloroform was purchased from Avanti Polar Lipids, Inc. (Alabaster, AL) and used as received. Pyrene (99% optical grade) and perylene (99+ %) were purchased from Sigma-Aldrich (Milwaukee, WI) and used without further purification. For each sample, 10 mg of lipid were mixed with 30.5  $\mu\text{g}$  of chromophore, and the chloroform solvent was evaporated. Tris<sup>®</sup> buffer (Sigma-Aldrich) was then added to each sample to make the lipid concentration 1 mg/mL. Tris<sup>®</sup> buffer (10 mM, pH 8.0) was prepared with purified water from a Milli-Q Plus water purification system (Millipore, Bedford, MA), and was purged with argon prior to use. The lipid and chromophore mixtures were processed five times through a freeze-thaw-vortex cycle to ensure complete mixing of the constituents. Each cycle was comprised of first freezing the solution by immersion in  $\text{N}_2(l)$  (5 min.), then thawing in a 60°C water bath (5 min.), followed by vortexing the mixture (2 min.). After completion of the freeze-thaw-vortex process, sample solutions were extruded eleven times through a polycarbonate membrane (Whatman, Piscataway, NJ) with a nominal pore diameter of 100 nm using a mini-extruder apparatus (Avanti Polar Lipids, Inc.).<sup>25, 103</sup> Once the vesicle solutions were extruded, controlled amounts of 95% ethanol (Sigma-Aldrich) were added to the bulk mixtures, and the samples were allowed to equilibrate under ambient conditions prior to fluorescence acquisition. A time study (results not shown) showed that the amount of lipid-ethanol equilibration time needed to achieve reproducible fluorescence results was *ca.* 24 hours.

*Steady-State Fluorescence Measurements.* Steady-state emission spectra were acquired for three trials each of the DMPC/pyrene vesicles with ethanol held at a constant temperature of 298 K. Samples were excited at 339 nm, and emission was collected from 350-500 nm using a Spex Fluorolog 3 emission spectrometer with 2 nm resolution for both excitation and emission monochromators. The sample temperature was regulated to  $\pm 0.1^\circ\text{C}$  with a water-circulating bath (Neslab EX-100DD) connected to a temperature-controlled glass cell jacket which held the sample cuvette. All samples were allowed to thermally equilibrate for 10 min. prior to data acquisition.

## Results and Discussion

The goal of the work we report here is to gauge the effects of ethanol concentration on the molecular-scale dynamics and fluidity of unilamellar lipid vesicles. We have used pyrene imbedded in the acyl chain region of the vesicles for our steady-state emission measurements because of the probe's sensitivity to polarity and its propensity to form excimers. Pyrene excimer formation depends on the chromophore's ability to diffuse through the acyl chain environment. So, in other words, the more fluid the local environment of pyrene, the higher the concentration and the more intense the fluorescence emission band for pyrene excimer. These data provide insight into the interdigitation process and suggest that interdigitation proceeds heterogeneously across the bilayer surface, rather than in a coordinated manner.

Pyrene is well established as a polarity-sensitive fluorescent probe in lipid membranes,<sup>34, 98, 104</sup> and because of its nonpolar nature, it partitions selectively into the aliphatic region of lipid bilayers. The emission spectrum of pyrene consists of five vibronic bands,<sup>30</sup> and the ratio of the I/III emission band intensities has been correlated with the polarity of the chromophore immediate environment.<sup>31</sup> This somewhat unusual spectral property is a consequence of the electronic structure of pyrene and is a consequence of the differences in the nature of vibronic coupling for the I and III transitions.<sup>31</sup> A I/III band intensity ratio  $> 1$  is characteristic of pyrene being sequestered in a polar environment, while a ratio  $< 1$  is indicative of the chromophore being in a nonpolar environment. The I/III pyrene emission band ratio (*Py* scale) remained constant for all of our steady-state measurements with a value of 0.96, a value that suggests that

the chromophore remains in the nonpolar bilayer acyl chain region under all conditions examined here. We note that the *Py* band ratio has a reported value of 1.18 for pyrene in ethanol, 1.87 in water and 0.60 for hexadecane. The value we obtain is consonant with solvents of polarity similar to *p*-xylene and *iso*-propyl ether.<sup>105</sup>

Pyrene also has the ability to form excited-state dimers or excimers, which are products from the reaction of electronically excited pyrene molecules with ground-state pyrene molecules. The characteristic signature of pyrene excimer formation is the appearance of a broad structureless emission feature centered near 470 nm. Excimer formation is limited by both concentration and translational diffusion through the surrounding medium. The probability of excimer formation scales with the fluidity of the bilayer structure, and we can use this spectroscopic feature as a gauge of local fluidity in our work.

We are interested in understanding changes in the molecular-scale organization of lipid bilayers as a function of ethanol concentration, and whether the subsequent perturbation to the interfacial region of the bilayer can trigger the formation of the interdigitated phase. It has been proposed before that lipid bilayer interdigitation results in a subsequent decrease in membrane fluidity.<sup>106-107</sup> The rationale for this assertion is that the presence of ethanol, which has been known to initiate lipid interdigitation, gives rise to an increase in the average spacing between lipid headgroups.<sup>108</sup> Losses in lipid-lipid headgroup interactions are compensated by interdigitation, which increases inter-leaflet acyl chain interactions. While this condition could lead to a less fluid membrane, the interchain spacing in the interdigitated bilayer must remain substantially the same as

that of the non-interdigitated bilayer because of the intermolecular forces acting between the acyl chains.<sup>96, 109</sup> Our steady-state fluorescence measurements can help to resolve this issue.

Steady-state fluorescence emission data were acquired for pyrene incorporated into 100 nm diameter DMPC vesicles as a function of solution ethanol concentration (Fig. 3.3). There is an overall trend of increasing excimer band intensity with increasing ethanol concentration, with a noticeable excimer intensity enhancement near 0.6 M ethanol. We view the data presented in Figure 3.3 as showing an essentially continuous change in the amount of excimer formed with increasing ethanol concentration, with an anomalous increase near 0.6 M ethanol. We understand the continuous trend in the context of increasing pyrene excimer content of the bilayer structure as the solution-phase ethanol concentration increases. While there are no data we are aware of that relate ethanol concentration to changes in lipid bilayer acyl chain viscosity, the dilation of the acyl chains by ethanol could lead to increased translational mobility of constituents within the bilayer. The anomalous increase in excimer formation in the region of 0.6 M ethanol has been seen for other bilayer systems, albeit at different ethanol concentrations. We believe that this anomalous feature represents the heterogeneous onset of interdigitation, a phenomenon which should depend on the structural identity of the lipid. If the solubility of pyrene is different in the interdigitated bilayer regions than in the non-interdigitated regions, then the formation of interdigitated areas would give rise to an increase in pyrene concentration in the region of preferential solubility. Once the bilayer structure became more structurally homogeneous, this concentration modulation effect would no longer be operative, and the ethanol concentration-dependence would return

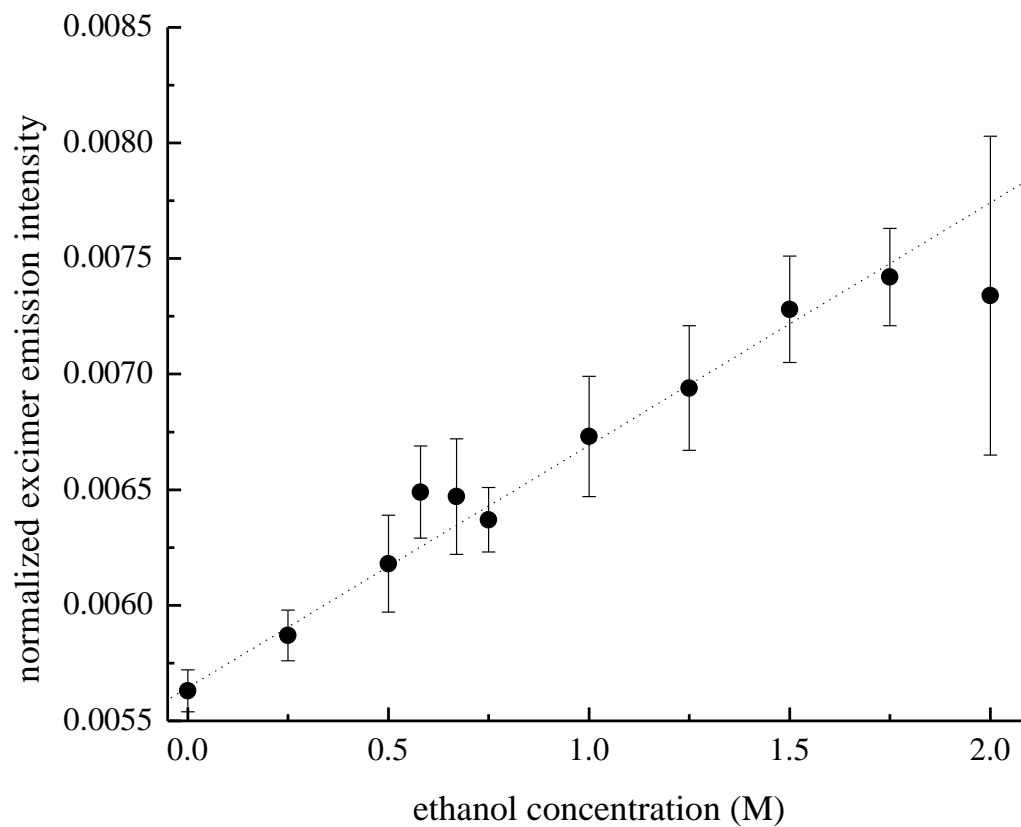


Figure 3.3. Pyrene excimer band intensity for the chromophore incorporated into 100 nm diameter DMPC vesicles, as a function of ethanol concentration. Error bars are  $\pm 1\sigma$  for three individual determinations at each ethanol concentration. The dashed line is a linear regression fit to the data.

to what is expected for a homogeneous bilayer-ethanol system.

A previous ethanol-induced interdigitation study conducted by LÖbbecke *et al.* found that for carboxyfluorescein-imbedded 1,2-dipalmitoyl-*sn*-glycero-3-phosphocholine (DPPC) bilayers, interdigitated domains began to form at ethanol concentrations of *ca.* 0.45 M, while full interdigitation was not observed until 1.0 M.<sup>110</sup> DPPC has 16 carbons in each of its aliphatic tails and DMPC has only 14 carbons, so qualitatively similar behavior is expected. Because the strength of van der Waals interactions is expected to scale with acyl chain length, a higher ethanol concentration for DPPC interdigitation may be expected. However, there are two factors that argue for the fact that our DMPC data exhibit signs of interdigitation occurring at lower ethanol concentrations than is seen for DPPC. If we consider the driving force for formation of the interdigitated bilayers to be the attractive interactions between acyl chains of opposing lipid molecules, and that all other interactions are independent of acyl chain length, then it is reasonable to expect longer lipids to undergo interdigitation at lower concentrations of ethanol.<sup>96</sup> Also contributing to the slight difference between our findings and those of LÖbbecke *et al.* is the fact that the use of a carboxyfluorescein dye could be more disruptive to bilayer structure than the pyrene chromophore we use.<sup>110</sup> Their finding that interdigitation was not complete until a concentration of 1.0 M ethanol was added to the system is based on calorimetric data and a correlated change in the ethanol concentration dependence of the carboxyfluorescein emission intensity. The pyrene emission data we report here, while loosely related to the emission processes

Löbbecke *et al.* reported, sense different phenomena and it is therefore not surprising that these data do not provide exact correspondence.

We have also examined the average size of the vesicles as a function of solution ethanol concentration using dynamic light scattering measurements. Our interest in measuring the average size of the vesicles lies in the fact that the process of interdigitation is likely to alter vesicle diameter due to the interweaving of the lipid acyl chains, and a consequent decrease in bilayer thickness. We assert that the intermolecular spacing of phospholipids is dominated by the van der Waals interactions between acyl chains. If this spacing is to remain the same in both non-interdigitated and interdigitated bilayers, the size of the vesicle must change upon interdigitation. We observe a discontinuous change in vesicle size in the region of 0.6 M ethanol, consistent with interdigitation (Fig. 3.4). We note that this anomalous behavior is consonant with that observed for the steady-state fluorescence emission of pyrene excimer as a function of the ethanol. There is an apparent increase in vesicle diameter with increasing alcohol concentration up to *ca.* 1.0 M ethanol. We ascribe this trend to the disruption of lipid headgroup-headgroup interactions by ethanol molecules (*vide infra*), which cause the bilayer to dilate. The anomalous increase in diameter near 0.6 M likely signals the onset of a structural phase transition, possibly to the interdigitated phase.

We note that there is significant uncertainty in some of the data, especially for the higher ethanol concentrations (Fig. 3.4). We understand this uncertainty in the context of there being an intrinsic vesicle size distribution, and that the functional form of this distribution may change with increasing ethanol concentration due to vesicle-vesicle or other unaccounted-for processes. For ethanol concentrations exceeding 1.0 M, we

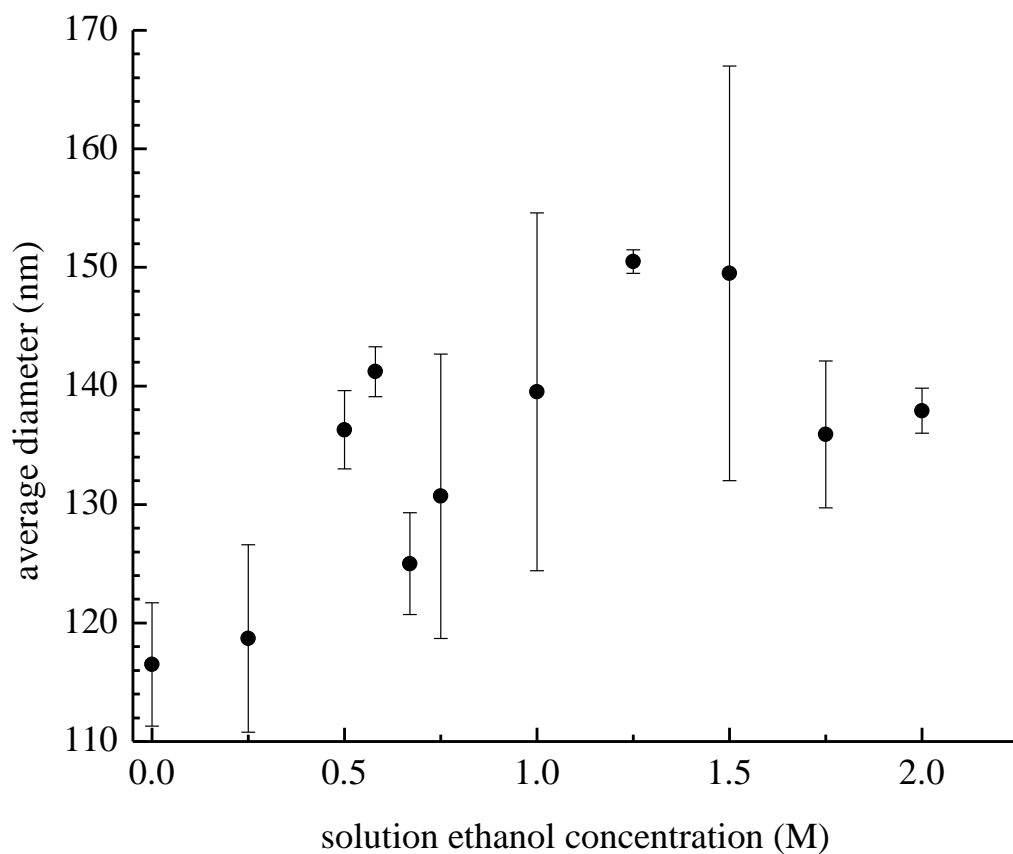


Figure 3.4. Dynamic light scattering data on vesicle size as a function of solution ethanol concentration. Uncertainties reported are  $\pm 1\sigma$  for at least three determinations.

observe a plateau effect in vesicle diameter, and this may be due to the saturation of interactions between ethanol molecules and the vesicles. Clearly, more detailed measurements of the vesicle size distribution will be required to resolve this issue, but the central point of the data we present here is that there appears to be a predictable correlation between the average diameter of the vesicles and the solution ethanol concentration. It is important for us to note that although we were not able to sense any resolvable change in the local environment of the chromophore upon the addition of ethanol, we believe our vesicle systems are experiencing a structural phase transition in the vicinity of 0.6 M ethanol.

Over the last two decades a variety of scientific techniques have been used to study the ethanol-induced interdigitation of lipid bilayers, all of which have demonstrated that ethanol does in fact promote lipid interdigitation.<sup>100, 110-117</sup> The one point, however, that appears to be lipid-dependent is the ethanol concentration at which interdigitation is first observed. Our steady-state spectroscopic (Fig. 3.3) and DLS (Fig. 3.4) results point to ethanol-induced lipid interdigitation in DMPC vesicles doped with pyrene at *ca.* 0.6 M. However, our steady-state results alone do not clarify whether interdigitation first begins in isolated regions of the bilayer, followed by a more homogeneous interdigitated structure as ethanol concentration increases.

## Conclusions

The effects of ethanol on both membrane fluidity and lipid structure have been examined. We have used steady-state fluorescence measurements of pyrene excimer formation to monitor changes in the translational mobility of pyrene sequestered within the acyl chain region of lipid vesicles. We observed a linear trend of increasing excimer formation as the bulk ethanol concentration was increased, with the exception of an anomalous increase near 0.6 M solution ethanol concentration, which we believe to be the point at which interdigitation begins to occur in DMPC vesicles. Dynamic light scattering data also point to a structural anomaly in the average diameter of DMPC vesicles in the region of 0.6 M ethanol, indicating that we are sensing a structural phase transition which is a necessary consequence of the interdigitation process. We assert that van der Waals interactions mediate bilayer structure, suggesting that inter-acyl chain spacing should be the same for both interdigitated and non-interdigitated systems. In order to better gauge the structure and molecular motion of lipids in the presence of ethanol, we will next need to perform time-resolved fluorescence measurements to study the dynamic behavior of both gel phase and fluid phase DMPC bilayers. These experiments are discussed in Chapter 4.

## CHAPTER 4

### Interrogating the Effects of Ethanol on the Organization of Lipid Vesicles Using Time-Resolved Fluorescence Measurements

#### Introduction

Mammalian cell membranes are highly complex biological structures that function as regulators of cell life, allowing specific chemical species to pass into and out of the cell. Plasma membranes are heterogeneous structures composed primarily of glycerophospholipids, sphingolipids, cholesterol, and proteins arranged in a bilayer structure.<sup>118-120</sup> Even in compositionally simple systems, phospholipids self-assemble in aqueous environments to form nominally spherical bilayer liposomes, a structure which serves to minimize interactions between hydrophobic acyl chains and the aqueous solvent. In such structures the hydrophobic acyl chain regions of lipids comprise the interior of a double-leaflet arrangement, while the polar headgroups act to shield the acyl chains from the aqueous environment and, as such, are located at the surfaces of the bilayer in direct contact with the solution in which they are suspended. In this structural format the acyl chain terminal methyl groups of the opposing lipid monolayers are oriented facing one another. This lipid packing arrangement is the most energetically favorable, where the number of *gauche* rotamers in the acyl chain region is minimized, and van der Waals interactions between chains are optimized. The process of optimizing van der Waals interactions represents a balance between attractive acyl chain interactions and the thermal energy present in the system. Lipid bilayer assemblies are known to undergo phase transitions from ordered to disordered acyl chains, with the transition

temperature depending on the length of the acyl chain and the presence of any unsaturations.

A variety of cellular processes are mediated by both lipid bilayer composition and dynamic properties of cell membranes, including intercellular and intracellular signaling, protein and enzyme activity, and cellular response to environmental stresses.<sup>42</sup> One way in which cells can regulate these functions is by controlling or manipulating the physical properties of the membrane, such as membrane fluidity, which is mediated by viscous drag effects between the membrane constituents.<sup>23</sup> Such interactions, along with membrane composition and structural heterogeneity, determine the motional freedom of these constituents in the membrane.<sup>121</sup> Membrane fluidity as it relates to the motional freedom of lipids refers to translational diffusion, rotational diffusion, and lipid translocation.<sup>23, 121</sup> One way of experimentally altering the membrane fluidity of a bilayer is by changing the temperature of the local environment of the membrane. Phospholipid vesicles exhibit a characteristic phase transition at  $T_m$ , where the dynamic properties of lipids are altered due to changes in the organization of the lipid acyl chains. At temperatures below  $T_m$ , lipids exist in the gel phase, characterized by highly ordered acyl chain packing, where the acyl chains are tilted slightly away from the bilayer normal.<sup>122</sup> The close-packed arrangement of lipids in the gel phase results from van der Waals interactions in the hydrophobic acyl chain region of the membrane. Inter-acyl chain van der Waals interactions limit lipid rotational and translational freedom. At temperatures above  $T_m$ , lipid bilayers exist in a disordered fluid phase, characterized by

an increase in the number of *trans-gauche* conformers and, as a result, an increase in the average interfacial area subtended by the lipid headgroups.<sup>24</sup> Lipids in the fluid phase experience greater translational and rotational freedom than lipids in the gel phase, resulting in increased overall membrane fluidity. The fluid phase has been shown experimentally to support a number of protein functions.<sup>123-124</sup>

The gel-to-fluid phase transition described above is dominated by acyl chain interactions, with the lipid headgroups playing a secondary role. Membrane fluidity and organization can also be controlled by the introduction of short-chain alcohols to the interfacial region of the bilayer. Alcohols such as ethanol are amphipathic and can displace some of the water molecules associated with the gel phase lipid bilayer interfacial region, penetrating to some extent into the nonpolar region of the bilayer.<sup>96</sup>

The displacement of water molecules in the vicinity of the lipid headgroups weakens the interactions between the headgroups, allowing the bilayer structure to dilate, thus increasing the average surface area per headgroup. The addition of a sufficient amount of alcohol can perturb the bilayer interfacial region to the extent that a phase transition to an interdigitated structure occurs.<sup>93-95, 125</sup> Ethanol has been used widely to induce the

formation of the interdigitated phase, with much of the early work being done by Rowe *et al.*<sup>114, 126-127</sup> and Simon *et al.*<sup>109, 128</sup> The interdigitated phase occurs when the acyl chains of lipids from one leaflet interpenetrate with the chains from the opposing leaflet, eliminating the bilayer mid-plane, and leading to a consequent decrease in bilayer thickness. The decrease in bilayer thickness can have a dramatic effect on the function of proteins imbedded within biological cell membranes as well.<sup>96</sup> This explanation does

not resolve whether the interdigitation process is spatially homogeneous or heterogeneous, or whether there are any molecular-scale changes in the acyl chain region as a consequence of interdigitation. It is the purpose of this work to address the issue of ethanol concentration-dependent changes in the molecular-scale organization of these bilayers.

Several analytical techniques have been used in the past to elucidate the packing arrangement and properties of phospholipids in interdigitated bilayer arrangements, including differential scanning calorimetry,<sup>129-130</sup> fluorescence,<sup>111, 131-132</sup> NMR,<sup>133-134</sup> and X-ray diffraction.<sup>110, 113</sup> A significant limitation of conventional diffraction techniques for interrogating the structure and organization of unilamellar vesicles is their relatively low sensitivity, and calorimetric data provide limited molecular-scale insight. Fluorescence and NMR methods provide the requisite molecular-scale information and fluorescence is easily capable of detecting low chromophore concentrations. For time-resolved fluorescence measurements, a chromophore can be selected to interrogate a specific region of the bilayer (*i.e.* the nonpolar acyl chain region or the polar headgroup region). We are interested in interrogating the interior acyl chain region of phospholipid vesicles because this region undergoes substantial structural and dynamic changes as a result of temperature- or alcohol-induced phase transitions.

In this work we use 100 nm diameter unilamellar vesicles comprised of 1,2-dimyristoyl-*sn*-phosphatidylcholine (14:0 DMPC,  $T_m = 297$  K),<sup>135</sup> and time-resolved fluorescence techniques to interrogate the properties of a chromophore incorporated into the vesicle bilayer. We measured the anisotropy decay dynamics of the fluorescent probe

perylene in vesicle-containing solutions at 289 K (gel phase DMPC) and 303 K (fluid phase DMPC) with controlled amounts of ethanol to gauge the extent to which the lipid phase and ethanol concentration mediate the properties of the bilayer structure, as sensed by perylene rotational motion. We have used perylene for time-resolved fluorescence measurements because of its well characterized anisotropy decay dynamics<sup>136-138</sup> and because its fluorescence lifetime and anisotropy decay time constants are similar, allowing for efficient collection of the requisite data. We measured the reorientation dynamics of perylene using time-correlated single photon counting (TCSPC), and found that this chromophore appears to be sensitive to the ethanol-induced phase transition from the gel phase to the interdigitated phase in DMPC at 289 K. We also observed a similar, more pronounced change in the reorientation behavior of perylene as a function of ethanol concentration at 303 K, a temperature at which DMPC is in the fluid phase. The interactions between lipid bilayers and ethanol produce measurable changes in lipid bilayer organization in both the gel and fluid phases.

## Experimental Section

*Vesicle Preparation.* The phospholipid 1,2-dimyristoyl-*sn*-phosphatidylcholine (14:0 DMPC) in chloroform was purchased from Avanti Polar Lipids, Inc. (Alabaster, AL) and used as received. Perylene (99+ %) was purchased from Sigma-Aldrich (Milwaukee, WI) and used without further purification. For each sample, 10 mg of lipid was mixed with 30.5  $\mu$ g of chromophore, and the chloroform solvent was evaporated. Tris<sup>®</sup> buffer (Sigma-Aldrich) was then added to each sample to make the lipid concentration 1 mg/mL. Tris<sup>®</sup> buffer (10 mM, pH 8.0) was prepared with purified water from a Milli-Q Plus water purification system (Millipore, Bedford, MA), and was purged with Ar prior to use. The lipid and chromophore mixtures were processed five times through a freeze-thaw-vortex cycle to ensure complete mixing of the constituents. Each cycle was comprised of first freezing the solution by immersion in N<sub>2</sub>(l) (5 min.), then thawing in a 60°C water bath (5 min.), followed by vortexing the mixture (2 min.). After completion of the freeze-thaw-vortex process, sample solutions were extruded eleven times through a polycarbonate membrane (Whatman) with a nominal pore diameter of 100 nm using a mini-extruder apparatus (Avanti Polar Lipids, Inc.).<sup>25, 103</sup> Once the vesicle solutions were extruded, controlled amounts of 95% ethanol (Sigma-Aldrich) were added to the bulk mixtures, and the samples were allowed to equilibrate under ambient conditions prior to fluorescence acquisition. A time study (results not shown) indicated that the amount of lipid-ethanol equilibration time needed to achieve reproducible fluorescence results was *ca.* 24 hours.

*Time-Resolved Fluorescence Measurements.* All fluorescence lifetime and anisotropy decay data were acquired using a time-correlated single photon counting (TCPSC) instrument. The light source is a CW passively mode-locked, diode-pumped Nd:YVO<sub>4</sub> laser (Spectra Physics Vanguard) that produces 2.5 W average power at 355 nm and 2.5 W of average power at 532 nm at 80 MHz repetition rate, with 13 ps pulses at both wavelengths. The output of the Nd:YVO<sub>4</sub> laser pumps a cavity-dumped dye laser (Coherent 702-2), which operates in the range of 430 nm to 850 nm, producing 5 ps pulses. The repetition rate of the dye laser is adjustable between 80 MHz and 80 kHz by means of the cavity dumping electronics (Gooch & Housego). The dye laser was operated with Stilbene 420 dye (Exciton) to produce the excitation wavelength of *ca.* 430 nm. The fundamental excitation pulse from the dye laser is divided, with one portion of the pulse directed to a reference photodiode (Becker & Hickl PHD-400-N), and the other portion directed to the sample. Emission is collected using a 40x reflecting microscope objective. The collected emission is separated into polarization components parallel ( $0^{\circ}$ ) and perpendicular ( $90^{\circ}$ ) to the vertically polarized excitation pulse using a polarizing cube beam splitter. The parallel and perpendicular polarized signal components are detected simultaneously using microchannel plate photomultiplier tubes (MCP-PMT, Hamamatsu R3809U-50), each equipped with a subtractive double monochromator (Spectral Products CM-112) for wavelength selection. The detection electronics (Becker & Hickl SPC-132) resolve the parallel and perpendicular transients separately, yielding *ca.* 30 ps response functions for each detection channel. The detection electronics include a time-to-amplitude converter (TAC) and a constant fraction discriminator (CFD) that temporally resolves the fluorescence signal for each polarization component. Data

are collected using multichannel analyzers (MCAs), which are integral components of the SPC-132 electronics. Data acquisition, detector bias, and collection wavelength are all controlled using an in-house written LabVIEW<sup>®</sup> (National Instruments) program on a PC. The sample temperature was regulated to  $\pm 0.1^{\circ}\text{C}$  with a water-circulating bath (Neslab RTE-110) connected to a temperature-controlled brass cell jacket which held the sample cuvette. All samples were allowed to thermally equilibrate for 10 minutes prior to data acquisition.

## Results and Discussion

The goal of the work we report here is to gain a better understanding of the effects of ethanol concentration and system temperature on the fluidity and molecular-scale organization of the lipid acyl chain region of 100 nm diameter DMPC vesicles. As noted above, we have used perylene for time-resolved measurements because its anisotropy decay dynamics are well understood and are sensitive to changes in its local environment. Perylene (Fig. 4.1) partitions into the hydrophobic region of DMPC vesicles. The reorientation dynamics of perylene thus provide information useful for understanding the behavior of the bilayer acyl chain region as it experiences structural changes associated with temperature and exposure to solution phase ethanol. The results of our time-resolved fluorescence measurements show that the organization of DMPC in both the gel and fluid phases is influenced by the presence of ethanol.

When incorporating a chromophore into the lipid bilayer structure, there is always a chance that the fluorescent probe can perturb the bilayer to the extent that it could alter the phase transitions sensed by the probe. Previous work has shown, however, that perylene does not change the observed gel-to-fluid phase transition temperature (297 K)<sup>135</sup> measurably in DMPC bilayers.<sup>25</sup> We have used an even smaller probe-to-lipid ratio in this work than we have in the past, and for this reason we do not expect to perturb the gel-to-fluid phase transition temperature from its reported value.<sup>135</sup> Another important characteristic of perylene to be considered is where, within the bilayer, the chromophore localizes. Perylene is thought to locate amongst the acyl chains of the

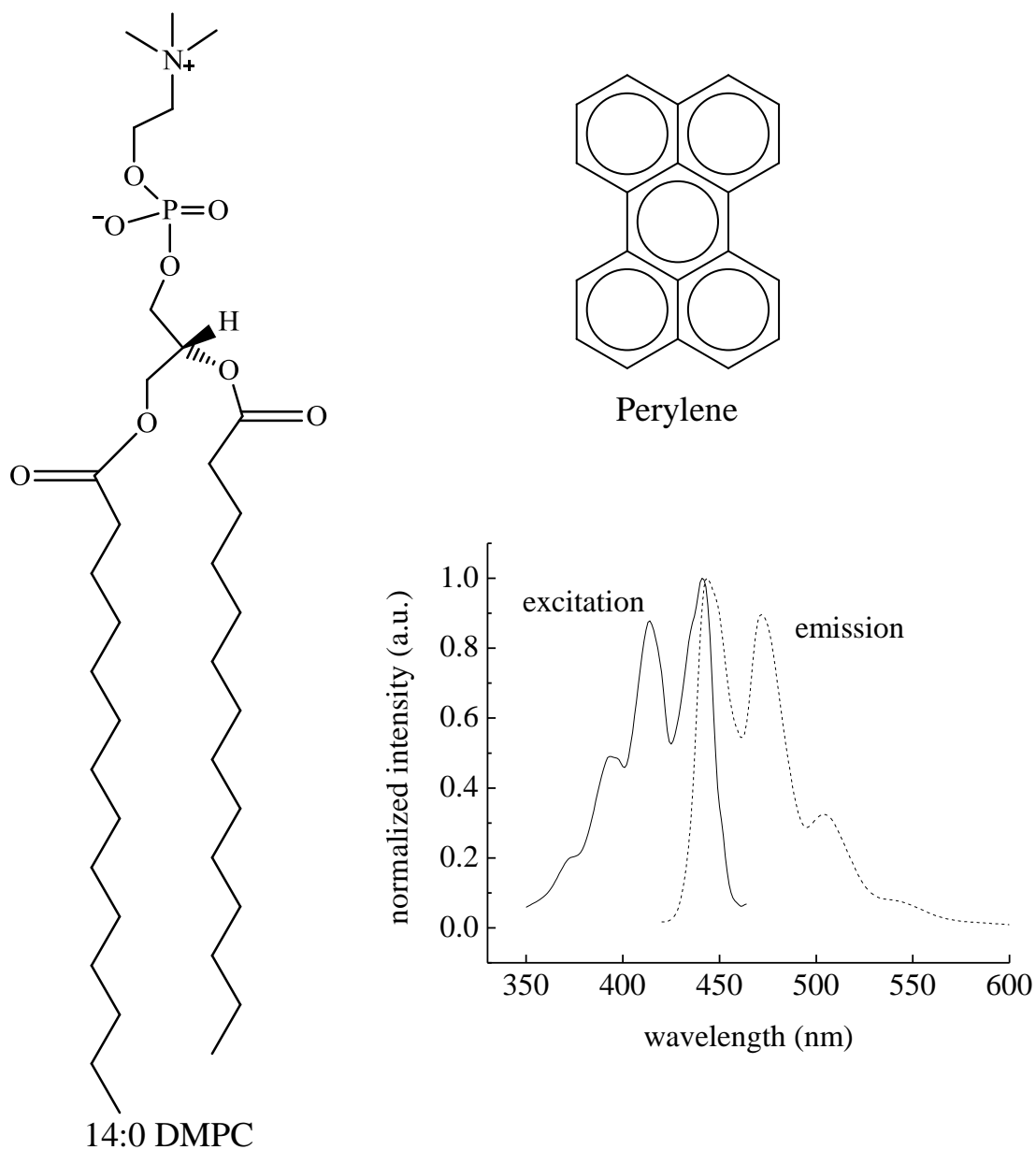


Figure 4.1. Structures of 14:0 DMPC and perylene, and normalized absorption and emission spectra of perylene in DMPC vesicles.

bilayer leaflets. Some recent work has indicated that perylene moves within the bilayer to be in closest proximity to the acyl chain terminal methyl groups for vesicles of *ca.* 1  $\mu\text{m}$  diameter and larger.<sup>76</sup> Those changes in perylene local environment were sensed by anisotropy decay measurements. We consider next the time-resolved emission behavior of perylene in both the gel and fluid phases of 100 nm diameter lipid vesicles as a function of solution phase ethanol concentration to gain insight into the alcohol-mediated changes in the organization of DMPC bilayer structures.

It is useful to consider at this point the nature of the interactions between the lipid bilayers and the solution phase ethanol. Because the lipid bilayers are present in the form of unilamellar vesicles, and ethanol is introduced to the vesicle-containing solutions, at least the initial interactions between the vesicles and ethanol must of necessity be at the outer vesicle leaflet. The asymmetric perturbation to the structure of the outer leaflet must therefore be the first step in the ethanol-induced changes we observe. If the chromophore is sequestered within the acyl chain region in a location that is asymmetric with respect to the inter-leaflet gallery, as our previous data on small vesicles suggest,<sup>25,</sup><sup>76</sup> then we would expect more pronounced dynamical effects for the chromophore residing in the outer leaflet than in the inner leaflet.

For fluorescence anisotropy decay measurements, polarized fluorescence transients are collected for polarizations parallel and perpendicular to the vertically polarized excitation pulse. These quantities,  $I_{\parallel}(t)$  and  $I_{\perp}(t)$ , respectively, are combined to produce the induced orientational anisotropy function,  $R(t)$ , (Eq. 4.1),

$$R(t) = \frac{I_{\parallel}(t) - I_{\perp}(t)}{I_{\parallel}(t) + 2I_{\perp}(t)} \quad (4.1)$$

The chemical information available from these measurements is contained in the functional form of the  $R(t)$  decay. There are several theoretical treatments that relate the anisotropy decay to the Cartesian components of the rotational diffusion constant and the transition dipole moment orientation(s) of the reorienting chromophore.<sup>139-141</sup> We treat the reorientation dynamics of perylene in DMPC bilayers in the context of a free rotor rather than a hindered rotor<sup>74-75</sup> because perylene is not tethered to the lipid acyl chains, and the planar shape and aspect ratio of perylene is such that when incorporated into the bilayer structure of DMPC, there is no intrinsic limit on the rotational motion the chromophore can execute. We note that the nonpolar chromophore 1,6-diphenyl-1,3,5-hexatriene (DPH) has been used previously in the examination of lipid bilayer structures, and in that work it was treated as a hindered rotor.<sup>142</sup> We assert that perylene rotational motion cannot be treated in the same context as that of DPH in lipid bilayers because of the substantially different structures and aspect ratios of these two molecules.

For the majority of anisotropy decay data, a single exponential decay is observed, and the chemical information contained in such data is limited. Perylene is well suited as a probe of local organization because it can exhibit either a one- or two-component anisotropy decay, depending on its immediate environment. We observe a two-component anisotropy decay in this work, a condition which yields information on each of the Cartesian components of the chromophore rotational diffusion constant,  $D$ . It is

the relative values of  $D_x$ ,  $D_y$ , and  $D_z$  that are useful in probing the ethanol- and temperature-induced lipid bilayer organizational changes of interest.

Relating the functional form of the anisotropy decay to the components of the rotational diffusion constant requires the assignment of axes and the assumption of a rotor shape, *i.e.* the volume swept out by the reorienting molecule. The excited and emitting transition dipole moments of perylene accessed in our experiments ( $S_1 \leftrightarrow S_0$ ) lie along the chromophore long in-plane axis, which we designate as the  $x$ -axis. The short in-plane axis is the  $y$ -axis, and the  $z$ -axis is perpendicular to the chromophore  $\pi$ -system plane. Given these assignments, a single-exponential anisotropy decay indicates the probe reorients as a prolate rotor ( $D_x > D_y = D_z$ ),<sup>139</sup>

$$R(t) = 0.4 \exp(-6D_z t) \quad (4.2)$$

and a two-component exponential decay indicates the probe reorients as an oblate rotor ( $D_z > D_x = D_y$ ), and is described by,<sup>139</sup>

$$R(t) = 0.1 \exp(-(2D_x + 4D_z)t) + 0.3 \exp(-6D_x t) \quad (4.3)$$

For the data we report here, the decay of  $R(t)$  was fit best by a two-component exponential decay (Fig. 4.2), consistent with Eq. 4.3. We have reported previously on the reorientation dynamics of perylene in DMPC vesicles.<sup>25, 76</sup> For vesicles ranging in size from 100 nm to 5  $\mu$ m in diameter, a two-component exponential decay was found. The data we report here, both above and below the known  $T_m$  of DMPC, show perylene to

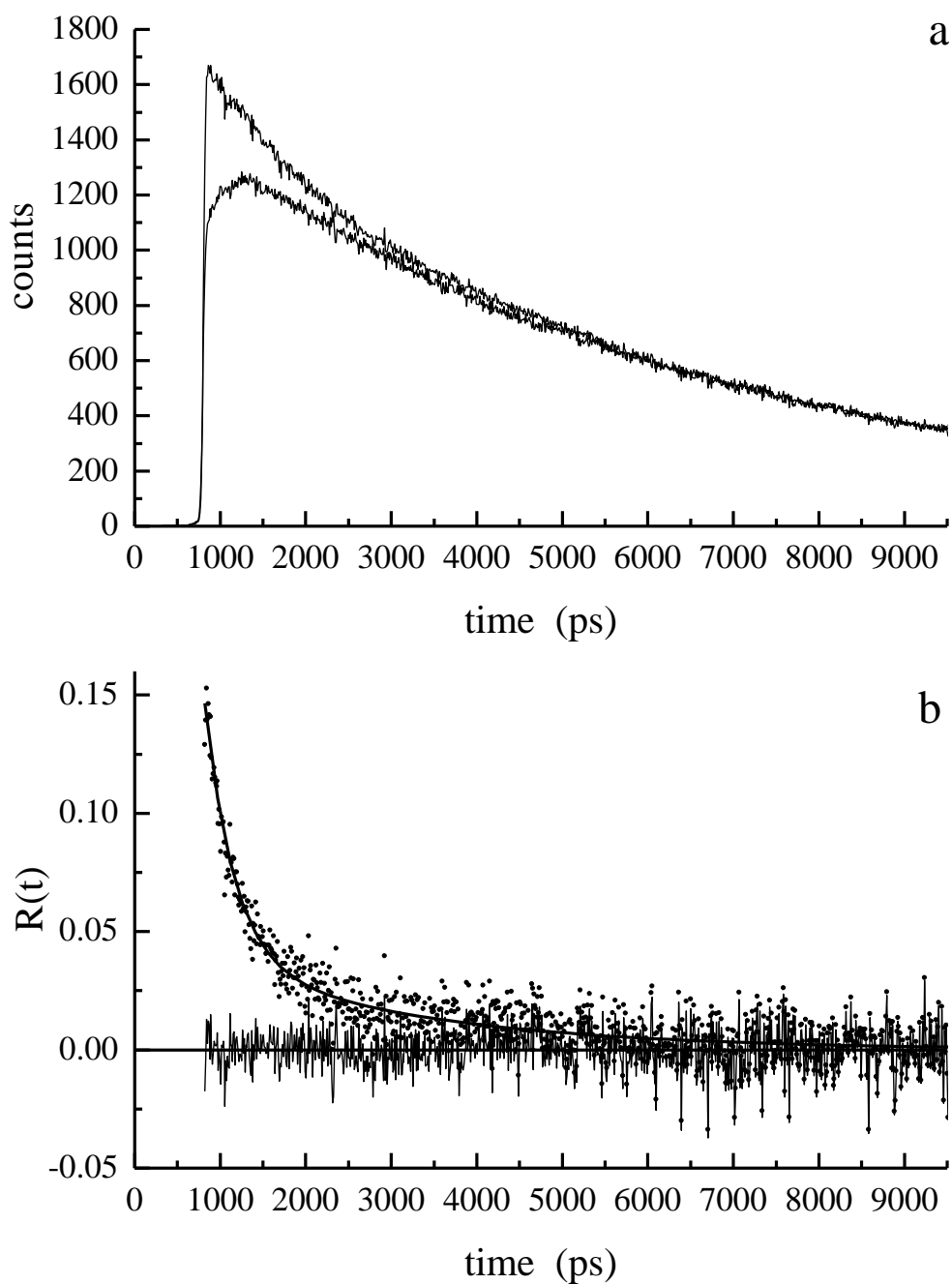


Figure 4.2. (a) Experimental data for perylene reorientation in a 100 nm diameter DMPC vesicle, with 0.25 M ethanol concentration at 289 K. (b) Induced orientational anisotropy decay function for the data shown in panel (a), along with the best-fit function to the data. For this fit the function is:  
 $f(t) = (0.11 \pm 0.004)\exp(-t/(339 \pm 24 \text{ ps})) + (0.04 \pm 0.003)\exp(-t/(2483 \pm 185 \text{ ps}))$ .

reorient as an oblate rotor. From the experimental anisotropy decay data we extract the Cartesian components of the rotational diffusion constant,  $D$ . As noted above, Eq. 4.3 assumes  $D_z > D_x = D_y$ . We present in Table 4.1 the experimental values of  $D_z$ ,  $D_x (=D_y)$  and the ratio  $D_z/D_x$ , as a function of system temperature and solution phase ethanol concentration. These data contain several interesting features.

At the outset of this discussion it is important to consider the extent to which subtle trends in reorientation data can be relied upon. The rotational diffusion constants we report here are the average and standard deviation ( $1\sigma$ ) for at least four individual determinations. We understand that the data we report reveal subtle ethanol concentration dependencies, a fact that results from the nature of the physico-chemical phenomena we are examining.

In previous work, the ratio of  $D_z/D_x$  was shown to be a useful gauge of changes in the immediate environment of the chromophore,<sup>136</sup> but such a permutation of our data provides limited insight into the systems we report on here. Of more immediate benefit, however, is a direct examination of the ethanol concentration-dependence of the  $D_z$  and  $D_x$  values at both 289 K and 303 K. We present these data in Fig. 4.3, revealing measurable differences in the effect of solution phase ethanol on the local environment of perylene for the two temperatures. We ascribe the differences in the ethanol concentration dependencies of  $D_z$  and  $D_x$  at the two different temperatures to be the result of the lipid bilayer existing in the gel phase at 289 K and the fluid phase at 303 K, at least for modest ethanol concentrations.<sup>25</sup> The  $D_z$  values reported at 289 K over all

Table 4.1. Cartesian components of the rotational diffusion constant and aspect ratio  $D_z/D_x$  as a function of solution phase ethanol concentration at 289 K and 303 K. Errors are  $\pm 1\sigma$  for at least four individual determinations at each ethanol concentration.

	T = 289 K, Gel Phase			T = 303 K, Fluid Phase		
[Ethanol], M	$D_z$ (MHz)	$D_x$ (MHz)	$D_z/D_x$	$D_z$ (MHz)	$D_x$ (MHz)	$D_z/D_x$
0	$600 \pm 50$	$55 \pm 2$	$10.9 \pm 1.2$	$888 \pm 80$	$70 \pm 5$	$12.7 \pm 1.1$
0.25	$703 \pm 117$	$59 \pm 3$	$11.8 \pm 1.9$	$851 \pm 65$	$65 \pm 5$	$13.1 \pm 1.7$
0.50	$689 \pm 51$	$54 \pm 3$	$12.8 \pm 1.0$	$879 \pm 92$	$73 \pm 4$	$12.1 \pm 1.5$
0.58	$665 \pm 35$	$49 \pm 2$	$13.6 \pm 0.8$	$923 \pm 73$	$58 \pm 5$	$16.0 \pm 1.8$
0.67	$737 \pm 89$	$61 \pm 7$	$12.1 \pm 2.0$	$762 \pm 50$	$52 \pm 3$	$14.8 \pm 0.5$
0.75	$651 \pm 72$	$56 \pm 3$	$11.5 \pm 1.0$	$816 \pm 89$	$57 \pm 3$	$14.3 \pm 1.8$
1.00	$676 \pm 36$	$52 \pm 2$	$12.9 \pm 0.4$	$882 \pm 76$	$68 \pm 8$	$13.0 \pm 1.2$

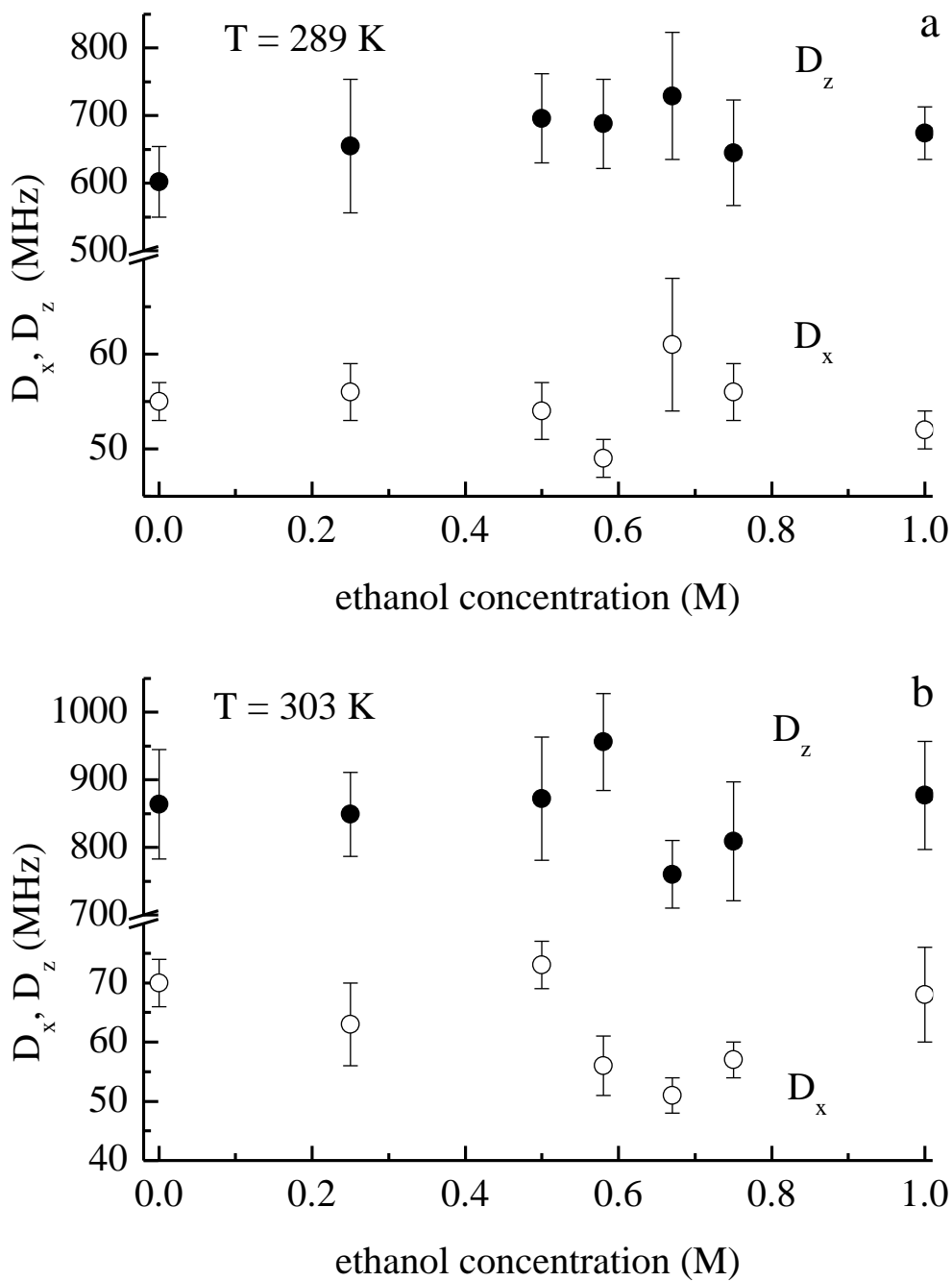


Figure 4.3. (a) Dependence of perylene  $D_x$  and  $D_z$  on ethanol concentration for 100 nm diameter DMPC vesicles at 289 K. (b) Dependence of perylene  $D_x$  and  $D_z$  on ethanol concentration for 100 nm diameter DMPC vesicles at 303 K. Errors are  $\pm 1\sigma$  for at least four individual determinations at each ethanol concentration.

ethanol concentrations (Fig. 4.3a) were found to be statistically the same using an ANOVA analysis at the 99% ( $\alpha = 0.01$ ) confidence level, while the  $D_x$  values were found to be statistically different for ethanol concentrations in the proximity of 0.6 M. It should be noted that all ANOVA analyses were tested at both a 95% ( $\alpha = 0.05$ ) and 99% ( $\alpha = 0.01$ ) confidence level. In all cases the same conclusion was reached in both instances. The value of  $D_x$  at 0.58 M is anomalously low and the value at 0.67 M appears to be slightly high relative to the corresponding values at other ethanol concentrations, albeit within the uncertainty of the  $D_x$  values at 0.50 and 0.75 M. These results suggest that near 0.6 M ethanol, there is some perturbation to the lipid bilayer structure that makes rotation of perylene about its  $x$ -axis somewhat more restricted than for other ethanol concentrations, and that for 0.67 M ethanol, the value of  $D_x$  has at least recovered, if not increased slightly. It is thought that for small diameter vesicles, perylene resides in the bilayer between acyl chains, and if this is the case, the chromophore may be sensing the onset of an interdigitation process. Such a process would be most pronounced in the region between leaflets, and perylene is likely in close proximity to this portion of the bilayer. The fact that there is no observable change in  $D_z$  over this ethanol concentration range suggests that the confining, quasi-lamellar structure created within the bilayer acyl chain region is not disrupted significantly by the structural events responsible for the changes in  $D_x$ .

The  $D_x$  ( $=D_y$ ) and  $D_z$  data for perylene in DMPC vesicles at 303 K provide a qualitatively different picture of ethanol-dependent changes in bilayer organization (Fig.

4.3b). For these data we also find, through the use of an ANOVA analysis, that values of  $D_x$  in the vicinity of 0.6 M ethanol are statistically different, while the values of  $D_z$  are statistically not distinguishable. Interestingly, as ethanol concentration increases at 303 K, the value of  $D_x$  decreases. If the ethanol-dependent change in behavior we observe is associated with an interdigitation process, it appears that the onset of interdigitation causes the acyl chain region of the bilayer to become more restrictive to perylene out-of-plane rotation. The same general trend is seen for  $D_z$ , despite the fact that ANOVA analysis shows that  $D_z$  is statistically independent of ethanol concentration. However, the ethanol concentration at which the apparently anomalous behavior in  $D_z$  occurs is not commensurate with that observed for  $D_x$  (Fig. 4.3b). This finding may be related to modulation of the acyl chain density by the interdigitation process. The ethanol-dependent reorientation dynamics of perylene at 289 K and 303 K are measurably different from one another, and we correlate this difference with DMPC being in the gel phase at 289 K and the fluid phase at 303 K, at least for modest ethanol concentrations.<sup>25</sup>

In comparing the data taken at 289 K to those taken at 303 K, we note that the rotational diffusion constants at 303 K are uniformly faster than those at 289 K. This is not surprising, for two reasons. The first is that the local frictional (viscous) interactions experienced by perylene are expected on theoretical grounds to be temperature dependent,<sup>39, 143-144</sup> and the second is that, for pure DMPC, there is a phase transition between the two temperatures at which we recorded data. The difference in phases is seen in the different  $D_z/D_x$  ratios for perylene at the two temperatures. ANOVA analysis

showed that the value of  $D_z/D_x$  for perylene at 289 K is independent of ethanol concentration to within the experimental uncertainty, at a value of  $12.2 \pm 0.5$ . The same analysis applied to the  $D_z/D_x$  ratio for perylene at 303 K is ethanol-dependent. The acyl chain environment for perylene is slightly more anisotropic at 303 K (Table 4.1) than it is at 289 K. Such behavior may reflect either a difference in the relative location of the chromophore in the acyl chain region at the two temperatures, or a change in the environment at a specific location within the bilayer acyl chain region. Regardless, the local environment sensed by perylene appears to be different at the two temperatures.

It is possible to gauge the frictional intermolecular interactions experienced by perylene in the bilayer structures. We can calculate the rotational diffusion constant,  $D$ , using the Cartesian components  $D_x (=D_y)$  and  $D_z$  given in Table 4.1.

$$D = \frac{D_x + D_y + D_z}{3} \quad (4.4)$$

The rotational diffusion constant is related to the viscosity of the local environment sensed by the probe according to the modified Debye-Stokes-Einstein equation,<sup>39, 143-</sup>

144

$$\frac{1}{6D} = \frac{\eta Vf}{k_B T S} \quad (4.5)$$

where  $\eta$  is the viscosity of the surrounding medium of the reorienting chromophore,  $V$  is the hydrodynamic volume of the chromophore,  $f$  is a frictional term to compensate for solvent-solute interactions,  $k_B$  is the Boltzmann constant,  $T$  is the temperature, and  $S$  is a shape factor determined from Perrin's equations to account for the nonspherical shape of

the chromophore.<sup>39</sup> We used the rotational diffusion constants calculated from Eq. 4.4, the shape factor,  $S = 0.70$ ,<sup>145</sup> and the hydrodynamic volume of perylene,  $V = 225 \text{ \AA}^3$ ,<sup>146</sup> to determine the viscosity,  $\eta$ , of the perylene local environment as a function of ethanol concentration. We find that there is no resolvable ethanol concentration dependence of the acyl chain micro-viscosity sensed by perylene using ANOVA analysis, indicating that the ethanol is not penetrating fully into the acyl chain region, but is instead acting primarily on the lipid headgroup region. For data taken at 289 K, we calculate  $\eta = 7.9 \pm 0.3 \text{ cP}$  and at 303 K,  $\eta = 6.6 \pm 0.2 \text{ cP}$ . These values are consistent with those we have measured previously, indicative of an acyl chain region that does not contain constituents other than phospholipids.<sup>25</sup> We attribute the difference in calculated viscosity to the temperature difference between the two measurements and the fact that DMPC is initially in the gel phase at 289 K and the more disordered fluid phase at 303 K. It is significant that these values are consistent with those reported for DMPC without the addition of ethanol,<sup>25</sup> suggesting that ethanol penetration of the DMPC bilayer does not proceed to the extent of perturbing the acyl chain region of the structure, at least prior to the point of causing interdigitation.

It is known that the ethanol-induced interdigitated phase results when amphipathic molecules disrupt the lipid headgroup interactions to the extent that the bilayers dilate and eventually interpenetrate.<sup>94</sup> When lipid interdigitation takes place, it is characterized by a closely-packed gel phase structure, and a consequent decrease in membrane fluidity.<sup>107</sup> At a concentration of *ca.* 0.6 M ethanol in our systems, perylene experiences

a decrease in its motional freedom for  $D_x$  at 289 K and 303 K. These data are consistent with the DMPC lipid bilayers becoming interdigitated at *ca.* 0.6 M ethanol. One might expect there to be a requisite increase in  $D_x$  and/or  $D_z$  with the onset of lipid headgroup dilation preceding interdigitation, but this is not seen. We believe that this is due to the fact that perylene resides in the lipid acyl chain region, relatively well isolated from the phospholipid headgroups, and that up to the point of interdigitation the van der Waals interactions between acyl chains dominate the local environment experienced by perylene. For ethanol concentrations above 0.6 M, it is likely that the lipid headgroup interactions become further disrupted, eventually giving rise to the loss of bilayer integrity. Up to the point of bilayer destruction, however, it is likely that the perturbation to the headgroup organization is resisted by the van der Waals attractive interactions between lipid acyl chains. For ethanol concentrations of *ca.* 1 M, we observe dynamics that differ little from those measured for aqueous vesicle solutions, underscoring the importance of dispersion forces in mediating lipid local organization.

Our data on 100 nm diameter DMPC lipid vesicles at 303 K, a temperature above the known gel-to-fluid phase transition temperature (Fig. 4.3b), show an ethanol concentration-dependence that is qualitatively similar, albeit different in detail, from that seen for the 289 K data (Fig. 4.3a). Much work has been conducted in the last two decades on ethanol-induced interdigitation of gel phase lipid bilayers, all of which have demonstrated through a variety of techniques that ethanol does promote lipid interdigitation.<sup>95, 110-114</sup> While there are no data we are aware of that have reported on the existence of an ethanol-induced interdigitation in fluid phase lipid bilayers, our data

reveal fluid phase behavior that is commensurate with gel phase behavior. Our data reveal ethanol concentration-dependent changes in  $D_x$  in the vicinity of 0.6 M ethanol. While the details of changes in  $D_x$  at 303 K differ from those seen at 289 K, they do show a change in lipid acyl chain environment, consistent with an interdigitation phase transition seen for gel phase DMPC. Further experiments will be required to resolve the details of this anomalous organizational change in fluid phase DMPC, and those experiments are underway in our laboratory.

## Conclusions

We have found that the presence of solution phase ethanol has an effect on the organization of DMPC lipid bilayer structures, both below and above the gel-to-fluid phase transition temperature. At 289 K, we observe that the rotational diffusion dynamics of perylene incorporated in the bilayer acyl chain region experience a perturbation about their long in-plane rotational axis for ethanol concentrations in the vicinity of 0.6 M. Interestingly, there is no measurable effect on the rotation of perylene about the axis normal to its molecular plane. For the same measurements performed at 303 K, we similarly observe a perturbation to out-of-plane ( $D_x$ ,  $D_y$ ) perylene rotational motion when the solution phase ethanol concentration is in the vicinity of 0.6 M, although the onset of the perturbation occurs at slightly different ethanol concentrations, which is likely the result of the extent of structural perturbation experienced by the lipid acyl chain region. Again, there is no measurable perturbation to the in-plane ( $D_z$ ) rotational motion of perylene. Our findings are consistent with the known phases of the lipid vesicles. Phospholipids are known to undergo interdigitation phase transitions in their gel phases at ethanol concentrations in the vicinity of 0.6 M.<sup>110</sup> Our findings point to the influence of ethanol in mediating a structural perturbation for DMPC in the fluid phase as well, although the structural details of this perturbation remain to be resolved fully. Further work is underway to understand this effect more thoroughly.

## CHAPTER 5

### Effects of Localized Energy Dissipation on the Motional Dynamics of Unilamellar Vesicles

#### Introduction

There has been a great deal of research interest in the organization and dynamics of lipid bilayer structures because of their intrinsic importance to life processes<sup>42</sup> and their complexity. Mammalian plasma membranes contain between 100 and 500 different chemical constituents, with the identity and amount of these constituents depending on the type of cell. This structural complexity appears to be a central factor in mediating the organization and function of transmembrane proteins, and it is the broad issue of how lipid bilayer constituents interact with transmembrane proteins and other bilayer constituents that remains to be understood in detail. Specific areas of importance relating to the organization of lipid bilayer structures are the relationship between bilayer composition and fluidity, and the nature of the coupling between the bilayer structures and transmembrane proteins.<sup>23</sup> There are a variety of ways to address issues of intermolecular organization, and one of them is to evaluate the efficiency of energy transfer between constituents.

Lipid bilayers are known to behave as fluids, and this factor allows for the facile incorporation of transmembrane proteins. The viscosity of a bilayer membrane has been the subject of some debate since the early 1970s.<sup>147-150</sup> Initial estimates of the average

bilayer viscosity predicted a value of 100 cP.<sup>150</sup> Subsequent estimates, however, have likened the bilayer lipid viscosity to that of olive oil or “crocodile fat on a warm summer’s day”.<sup>150</sup> The fluidity of lipid bilayer structures has been examined somewhat more quantitatively by a number of groups, and perhaps one of the most direct means of evaluating this property is through orientational relaxation measurements of selected species incorporated in the bilayer structure. This type of measurement, which is sensitive to molecular rotational motion, has been used to improve our understanding of lipid bilayer fluidity. It has been found from this work that the addition of selected bilayer constituents can mediate the microscopic viscosity of the acyl chain environment and lower the temperature at which phase transitions occur in the bilayers. Multicomponent systems can exhibit viscosities on the order of several cP, consistent with high mobility of bilayer constituents within the membrane, but the details of this fluidity depend sensitively on the composition of the bilayer. The term “fluidity” encompasses a number of physical and chemical properties within the bilayer. These include microscopic viscosity, translational diffusion of the bilayer constituents, and inter-leaflet translocation of lipids. Addressing the full complexity of the fluid properties of lipid bilayers ultimately requires the examination of these structures from a number of perspectives.

In simple bilayer systems, composed of a single phospholipid species, membrane viscosity can be altered by changing the system temperature. Such lipid bilayers are characterized by a phase transition temperature ( $T_m$ ), where the extent of order within the acyl chain region of the bilayer goes from an ordered (gel) phase to a less ordered (fluid)

phase. The transition temperature  $T_m$  depends sensitively on the functionality of the headgroup, the presence of any acyl chain unsaturations, and the length of the acyl chains.<sup>24</sup> The phase of the lipid bilayer can affect the activity of transmembrane proteins contained within the bilayer structure.<sup>123, 151</sup>

The gel-to-fluid phase transition within the bilayer can be sensed on the molecular level by measuring the orientational relaxation time,  $\tau_{OR}$ , of a fluorescent probe molecule imbedded in the nonpolar acyl chain region of the bilayer.<sup>25</sup> The acyl chain interior is the region of the bilayer most affected structurally and dynamically by phase changes, and as such is the moiety of interest. Several studies have employed molecular reorientation measurements to study the dynamic behavior of lipid vesicles as a function of temperature,<sup>10</sup> vesicle diameter,<sup>76</sup> headgroup functionality,<sup>152-154</sup> and the presence of impurities.<sup>1, 25</sup> These reports demonstrate collectively that the use of molecular reorientation measurements is well suited to the interrogation of molecular scale properties within lipid bilayer structures.

We are concerned in this work with the issue of local, rather than systemic, temperature change within lipid bilayer structures. Specifically, we are interested in understanding how the localized deposition of thermal energy into a bilayer structure perturbs the system, and to gauge the physical extent of this perturbation on a timescale relevant to molecular motion. In order to address these issues, we have used the chromophore perylene as a local “radiator”, and compare its molecular reorientation

dynamics when little if any excess thermal energy is deposited into the chromophore immediate environment versus when *ca.* 2 eV of thermal energy are dissipated nonradiatively. We use the phospholipid 1,2-dimyristoyl-*sn*-phosphatidylcholine (14:0 DMPC,  $T_m = 297$  K)<sup>135</sup> to create unilamellar vesicles of *ca.* 100 nm diameter and compare the rotational diffusion behavior of perylene<sup>1, 25</sup> when excited to two different electronic states. We find that there is indeed an excitation state-dependence to the reorientation dynamics of perylene and we relate our findings to the dissipation of excess excitation energy.

We excite the  $S_1 \leftarrow S_0$  and the  $S_2 \leftarrow S_0$  transitions of perylene and monitor emission from the  $S_0 \leftarrow S_1$  transition. Because of the small Stokes shift exhibited by perylene and its high fluorescence quantum yield, there is little if any local heating that results from excitation of the  $S_1 \leftarrow S_0$  transition. The perylene  $S_2 \leftarrow S_0$  transition is 1.92 eV higher in energy than the  $S_1 \leftarrow S_0$  transition, and subsequent to  $S_2 \leftarrow S_0$  excitation, rapid nonradiative relaxation to the  $S_1$  state occurs. The dissipation of 1.92 eV of excess excitation energy into the surrounding lipid acyl chain bath will result in local heating. By monitoring the state-dependent change in reorientation dynamics of the chromophore and through the application of a simple model, we can estimate the temperature change experienced by the chromophore local environment.<sup>155</sup> The transient temperature change of the lipid bilayer is on the order of 4 K, with a possible dependence on the phase of the lipids surrounding the chromophore. Our data also suggest that the spatial

extent of the local heating phenomenon depends sensitively on the extent of organization of the lipid acyl chains.

## Experimental Section

*Vesicle Preparation.* The phospholipid 1,2-dimyristoyl-*sn*-phosphatidylcholine (14:0 DMPC) in chloroform was purchased from Avanti Polar Lipids, Inc. (Alabaster, AL) and used as received. Perylene (99+ %) was purchased from Sigma-Aldrich (Milwaukee, WI) and used without further purification. For each sample, 10 mg of lipid was mixed with 30.5  $\mu\text{g}$  of chromophore, and the chloroform solvent was evaporated. Tris<sup>®</sup> buffer (Sigma-Aldrich) was then added to each sample to make the lipid concentration 1 mg/mL. Tris<sup>®</sup> buffer (10 mM, pH 8.0) was prepared with purified water from a Milli-Q Plus water purification system (Millipore, Bedford, MA), and was purged with Ar prior to use. The lipid and chromophore mixtures were processed through five freeze-thaw-vortex cycles to ensure complete mixing of the constituents. Each cycle consisted of freezing the solution by immersion in  $\text{N}_2(l)$  (5 min.), followed by thawing in a 60°C water bath (5 min.), then vortexing the mixture (2 min.). After completion of the freeze-thaw-vortex process, sample solutions were extruded eleven times through a polycarbonate membrane (Whatman) with a nominal pore diameter of 100 nm using a mini-extruder apparatus (Avanti Polar Lipids, Inc.) to produce unilamellar vesicles.<sup>25, 103</sup>

*Time-Resolved Fluorescence Measurements.* All fluorescence lifetime and anisotropy decay data were acquired using a time-correlated single photon counting (TCSPC) instrument. The light source is a CW passively mode-locked, diode-pumped Nd:YVO<sub>4</sub> laser (Spectra Physics Vanguard) that produces 2.5 W average power at 355 nm and 2.5 W of average power at 532 nm at 80 MHz repetition rate, with nominally the

same 13 ps pulses at both wavelengths. The output of the Nd:YVO<sub>4</sub> laser pumps a cavity-dumped dye laser (Coherent 702-2), which operates in the range of 430 nm to 850 nm, producing 5 ps pulses. The repetition rate of the dye laser is adjustable between 80 MHz and 80 kHz by means of the cavity dumping electronics (Gooch & Housego). For excitation of the S<sub>1</sub> ← S<sub>0</sub> transition, the dye laser was operated with Stilbene 420 dye (Exciton) to produce the excitation wavelength of *ca.* 435 nm. For the S<sub>2</sub> ← S<sub>0</sub> transition, Coumarin 500 dye (Exciton) was used to produce an excitation pulse of 520 nm. For both excitation wavelengths, the laser output is linearly polarized with a polarization extinction ratio of *ca.* 100. The 520 nm excitation pulses were frequency doubled using a Type I BBO crystal to produce a pulse of *ca.* 260 nm. The 260 nm pulse polarization was rotated to vertical using a UV-grade quartz polarization rotating Fresnel rhomb pair (CVI). The fundamental excitation pulse from the dye laser is divided, with one portion of the pulse directed to a reference photodiode (Becker & Hickl PHD-400-N), and the other portion directed to the sample. Emission is collected using a 40x reflecting microscope objective (Ealing). The collected emission is separated into polarization components parallel (0°) and perpendicular (90°) to the vertically polarized excitation pulse using a polarizing cube beam splitter (Newport, extinction ratio ≥ 500:1). The parallel and perpendicular polarized signal components are detected simultaneously using microchannel plate photomultiplier tubes (MCP-PMT, Hamamatsu R3809U-50), each equipped with a subtractive double monochromator (Spectral Products CM-112) for wavelength selection. The detection electronics (Becker & Hickl SPC-132) resolve the parallel and perpendicular transients separately, yielding *ca.* 30 ps response functions for

each detection channel. The detection electronics include a time-to-amplitude converter (TAC) and a constant fraction discriminator (CFD) that temporally resolves the fluorescence signal for each polarization component. Data are collected using multichannel analyzers (MCAs), which are integral components of the SPC-132 electronics. Data acquisition, detector bias, and collection wavelength are all controlled using an in-house written LabVIEW<sup>®</sup> (National Instruments) program on a PC. The sample temperature was regulated to  $\pm 0.1^\circ\text{C}$  with a water-circulating bath (Neslab RTE-110) connected to a temperature-controlled brass cell jacket which held the sample cuvette. All samples were allowed to equilibrate thermally for 10 minutes prior to data acquisition.

*Steady-State Fluorescence Measurements.* Excitation and emission spectra were acquired for our vesicle samples in order to determine the perylene band positions. We used a Hitachi F-4500 fluorescence spectrophotometer for excitation measurements, and a Spex Fluorolog 3 emission spectrometer for emission measurements. Both instruments were set to a spectral band pass of 1 nm for both excitation and emission monochromators.

## Results and Discussion

Although it is clear that there are thermally driven phase transitions within lipid bilayer structures, it is not clear whether or not such transitions can proceed in isolation or in areas of molecular-dimension for a bilayer exposed to a point source thermal transient. This issue may appear to be relatively esoteric, but it is of central importance to the study of bilayers. Many spectroscopic and electrochemical studies of bilayer structure, organization and dynamics are performed using probe molecules to report on their local environment. The results of such studies make the underlying assumption that the presence of the probe and any excess energy that it may dissipate do not alter the properties of the lipid bilayer. We assert that this is, at least in certain cases, a poor assumption, and seek to explore the consequences of a spectroscopic probe being present in a bilayer system. It is clear that probe molecules are not the only non-lipid constituents in plasma membrane structures, and the data we present here bear, in principle, on the influence of any bilayer non-lipid constituent.

We use perylene as a probe of local organization in lipid bilayers. We use this chromophore in low concentrations to minimize large scale disruption of bilayer organization. Previous work using higher perylene concentrations showed that the presence of the chromophore did not lower the gel-to-fluid phase transition temperature.<sup>25</sup> The work we report here, where two different perylene transitions are accessed, makes use of nonradiative energy transfer from the chromophore to the lipid bath modes to infer information on local organization within the lipid bilayer. The spectroscopic properties of perylene are well understood and characterized, and the

measurement we use, fluorescence anisotropy decay, can provide information on the short range dissipation of energy that is not readily obtainable by other means.

The goal of the work presented here is to gain insight into the effects of transient local heating in simple lipid vesicle systems, and to gauge the spatial extent of the thermal perturbation to the bilayer structure on the timescale of molecular motion. Understanding the extent to which an energetic perturbation within a lipid bilayer can influence its fluidity is important because of the dependence of cellular regulation processes on plasma membrane properties.<sup>49, 156-157</sup> The chromophore we have chosen for this work partitions selectively into the nonpolar acyl chain region of the bilayer, and it is thought that this region undergoes the most marked organizational changes during a phase transition. Previous studies have shown that the location of perylene within the DMPC acyl chain region depends on the diameter of the extruded vesicle.<sup>76</sup> For relatively small vesicles (*i.e.* 100 - 800 nm diameter), the phase transition of DMPC ( $T_m = 297$  K) influences the motional freedom of the chromophore, while in larger diameter vesicles (*i.e.*  $\geq 1$   $\mu\text{m}$ ) chromophore motion is not sensitive to the phase transition. This vesicle size-dependent change in the sensitivity of the chromophore to the phase transition is associated with a discontinuous change in its reorientation dynamics, indicating that the location of perylene within the bilayer acyl chain region changes according to vesicle size and curvature. One explanation consistent with these findings is that perylene is located interstitially, between acyl chains, in small DMPC vesicles, and that as the diameter of the vesicle increases, minimizing any structural or organizational difference between inner and outer leaflets, the chromophore relocates into the bilayer

mid-plane region. It is important to consider the location of perylene in the lipid bilayer as we interpret the results of our fluorescence anisotropy decay measurements for perylene in unilamellar vesicles as a function of system temperature. Because of the diameter of the vesicles we use here, we assert that perylene is located within the acyl chains and not in the inter-layer gallery.

We measured the fluorescence anisotropy decay of perylene (Fig. 5.1) in DMPC unilamellar vesicles at temperatures above and below  $T_m$  for this phospholipid. For such measurements, polarized fluorescence transients are acquired for polarizations parallel,  $I_{\parallel}(t)$ , and perpendicular,  $I_{\perp}(t)$ , to the vertically-polarized excitation pulse. These two quantities are combined to produce the induced orientational anisotropy function,  $R(t)$ , (Eq. 5.1).

$$R(t) = \frac{I_{\parallel}(t) - I_{\perp}(t)}{I_{\parallel}(t) + 2I_{\perp}(t)} \quad (5.1)$$

The functional form of the  $R(t)$  decay contains the chemical information of interest. Chromophores can produce anisotropy decays with as many as five exponential components, but in most cases only a one- or two-component anisotropy decay is observed experimentally. Perylene can exhibit a one- or two-component decay, depending upon the nature of its local environment. For our experiments, we observe a two-component anisotropy decay for excitation of the  $S_1 \leftarrow S_0$  transition ( $\lambda_{S_1} = 435$  nm) and a one-component decay for excitation of the  $S_2 \leftarrow S_0$  transition ( $\lambda_{S_2} = 260$  nm).

For both excitation conditions, we monitor emission from the  $S_0 \leftarrow S_1$  transition. The excitation and emission spectra of perylene are shown in Figure 5.1. To understand the information content of these data, we first consider their treatment in the context of ellipsoids of rotation.

There have been several theoretical treatments relating time-domain fluorescence anisotropy decay to the Cartesian components ( $D_x$ ,  $D_y$ , and  $D_z$ ) of the rotational diffusion constant,  $D$ , and the orientation of the emitting transition dipole moment of the chromophore.<sup>38, 139-140</sup> The rotational diffusion constant is defined as:

$$D = \frac{D_x + D_y + D_z}{3} \quad (5.2)$$

Chuang and Eisenthal derived a series of expressions for the functional form of  $R(t)$  based on the assignment of Cartesian axes and the assumption of a rotor shape.<sup>139</sup> The rotor shapes are described as being either oblate or prolate ellipsoids, and they represent the volume swept out by the reorienting chromophore. For perylene, both the excited and emitting transition dipole moments for the  $S_1 \leftrightarrow S_0$  transition lie along the long in-plane axis, designated as the  $x$ -axis. The  $y$ -axis is defined as the short in-plane axis and the  $z$ -axis is perpendicular to the chromophore  $\pi$ -system plane. For excitation of the perylene  $S_1 \leftarrow S_0$  transition, reorientation as a prolate rotor ( $D_x > D_y = D_z$ )<sup>139</sup> gives rise to a single-component exponential anisotropy decay,

$$R(t) = 0.4 \exp(-6D_z t) \quad (5.3)$$

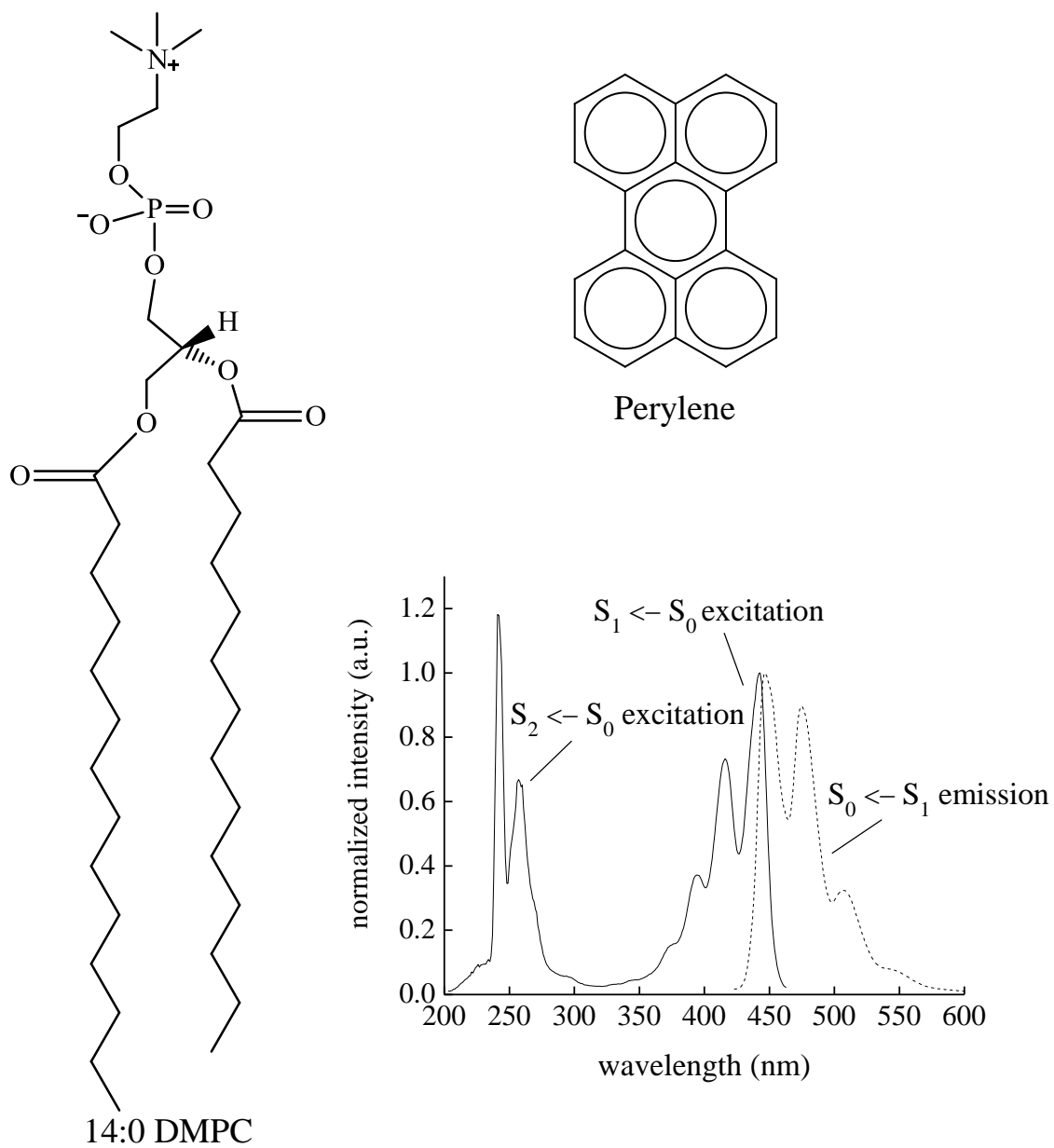


Figure 5.1. Structures of 14:0 DMPC and perylene, and normalized excitation and emission spectra of perylene in DMPC vesicles.

and reorientation as an oblate rotor ( $D_z > D_x = D_y$ ) produces an anisotropy decay with two exponential decay components,

$$R(t) = 0.1\exp(-2D_x + 4D_z)t + 0.3\exp(-6D_x t) \quad (5.4)$$

Our data for excitation of the  $S_1 \leftarrow S_0$  transition were fit best by a double-exponential decay (Fig. 5.2b), indicating that perylene behaves as an oblate rotor (Eq. 5.4) in DMPC, above and below  $T_m$ . These findings are fully consistent with previous reports.<sup>1, 25, 76</sup> Because perylene reorients as an oblate rotor, we are able to extract the values of the Cartesian components of the diffusion constant. These values, along with the ratio  $D_z/D_x$ , are presented as a function of system temperature in Table 5.1. We will consider their significance in the context of our data for excitation of the  $S_2 \leftarrow S_0$  transition (*vide infra*).

The  $S_2 \leftarrow S_0$  transition of perylene is polarized nominally perpendicular to the  $S_1 \leftarrow S_0$  transition and for excitation of  $S_2 \leftarrow S_0$  and monitoring  $S_0 \leftarrow S_1$ ,  $R(t)$  for an oblate rotor is given by

$$R(t) = 0.1\exp(-6D_x t) - 0.3\exp(-(2D_x + 4D_z)t) \quad (5.5)$$

Based on the results for excitation of the  $S_1 \leftarrow S_0$  transition, indicating that perylene reorients as an oblate rotor, we assume that the rotor shape and aspect ratio ( $D_z/D_x$ ) of perylene are independent of the state to which the molecule is excited. Eq. 5.5 predicts

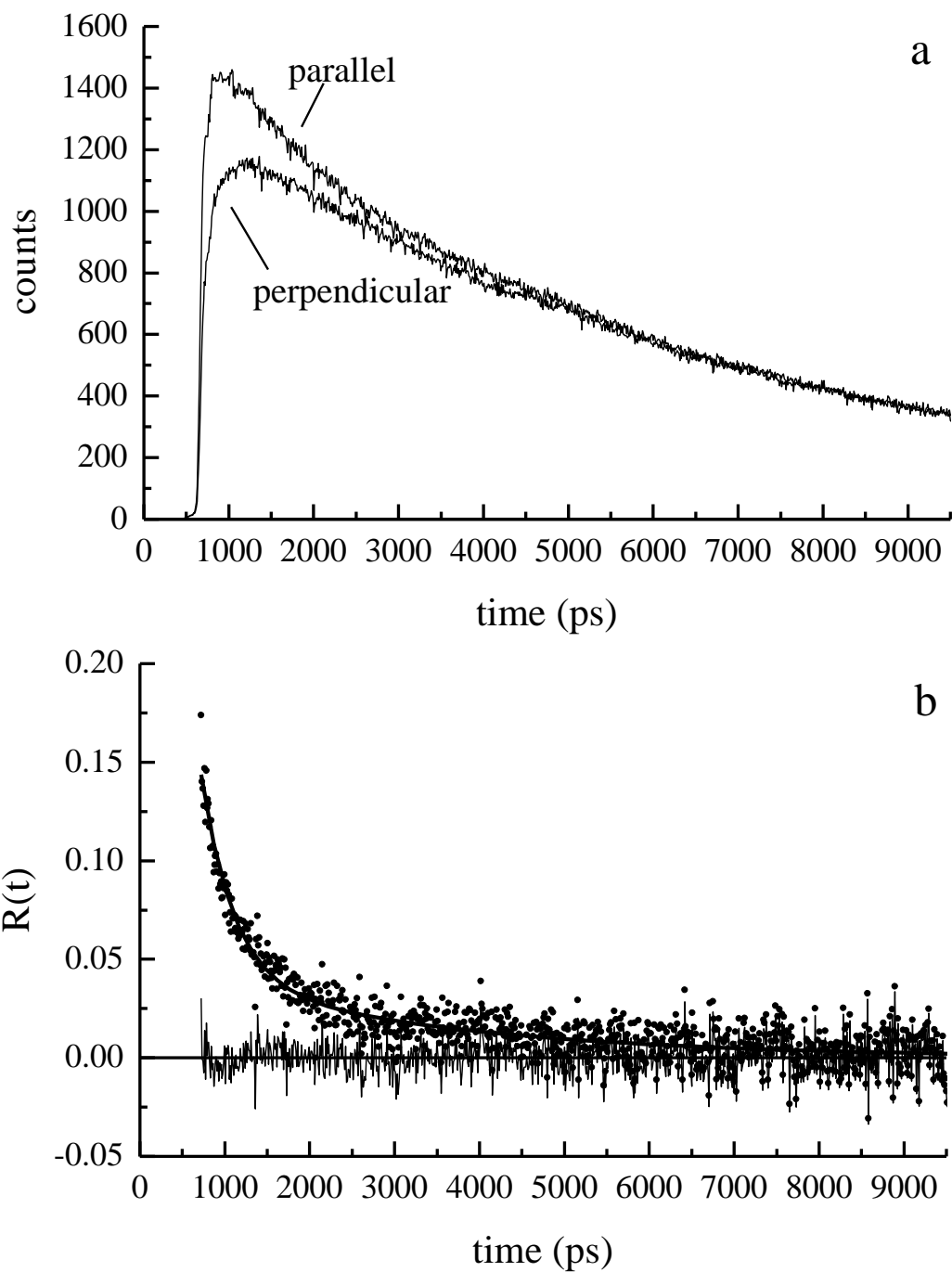


Figure 5.2. (a) Experimental data for perylene reorientation in 100 nm diameter DMPC vesicles at 292 K, excited at 435 nm ( $S_1 \leftarrow S_0$ ). (b) Induced orientational anisotropy decay function for the data shown in panel (a), along with the best-fit function to the data.

Table 5.1. The rotational diffusion constant, aspect ratio  $D_z/D_x$ , and calculated local viscosity as a function of temperature.

	$\lambda_{S_1} = 435 \text{ nm}, S_1 \leftarrow S_0$			$\lambda_{S_2} = 260 \text{ nm}, S_2 \leftarrow S_0$		
Temp. (K)	$D_z/D_x$	D (MHz)	$\eta$ (cP)	$D_z/D_x$	D (MHz)	$\eta$ (cP)
292	$11.8 \pm 0.8$	$254 \pm 13$	$8.3 \pm 0.4$	$11.8^a$	$311 \pm 5$	$6.7 \pm 0.1$
294	$11.8 \pm 0.1$	$269 \pm 1$	$7.8 \pm 0.1$	$11.8^a$	$346 \pm 6$	$6.1 \pm 0.1$
296	$11.9 \pm 0.4$	$294 \pm 7$	$7.2 \pm 0.2$	$11.9^a$	$406 \pm 2$	$5.2 \pm 0.1$
296.5	$12.6 \pm 0.7$	$322 \pm 14$	$6.6 \pm 0.3$	$12.6^a$	$438 \pm 2$	$4.8 \pm 0.1$
298	$12.5 \pm 0.4$	$386 \pm 10$	$5.5 \pm 0.1$	$12.5^a$	$527 \pm 8$	$4.1 \pm 0.1$
300	$12.5 \pm 0.3$	$396 \pm 8$	$5.4 \pm 0.1$	$12.5^a$	$530 \pm 16$	$4.1 \pm 0.1$
302	$13.2 \pm 0.4$	$427 \pm 10$	$5.1 \pm 0.1$	$13.2^a$	$561 \pm 22$	$3.9 \pm 0.1$

<sup>a</sup> The values of the aspect ratio ( $D_z/D_x$ ) for the  $S_2 \leftarrow S_0$  transition were assumed to remain unchanged from those determined experimentally for the  $S_1 \leftarrow S_0$  transition. Errors are  $\pm 1\sigma$  for at least four individual determinations at each temperature.

that the recovered anisotropy decay function will be characterized by a negative zero-time anisotropy because of the perpendicular polarizations of the excited and emitting transitions. Despite the prediction of a two-component anisotropy decay, we resolve only one of the decay components (Fig. 5.3). We understand the reason for this finding in the context of more than one fluorophore being present in the solution. An examination of the steady-state and time-resolved anisotropy measurements of solutions containing only 10 mM Tris<sup>®</sup> buffer solution reveals the presence of a weak emission component (data not shown). Exciting the Tris<sup>®</sup> buffer solution at 260 nm produces emission in the range of 375 nm to 475 nm, with the excitation and emission transition moments for the contaminant polarized parallel to one another. In solutions containing TRIS<sup>®</sup>-buffered DMPC but no perylene, we recover an anisotropy decay for the contaminant that is given by

$$R(t) = 0.06 \exp\left(\frac{-t}{3000 \pm 225 \text{ ps}}\right) \quad (5.6)$$

This emissive species, when present in solutions containing small amounts of perylene, interferes with the slow ( $\tau_{OR} \sim 2800$  ps) (negative) anisotropy decay of the chromophore and as a result we can only resolve the fast component of the perylene anisotropy decay. With the assumption that the rotor shape and aspect ratio are the same for the two excitation conditions, we can recover  $D_z$  and  $D_x$  using Eq. 5.7.

$$\tau_{OR1} = \frac{1}{2D_x + 4D_z} \quad (5.7)$$

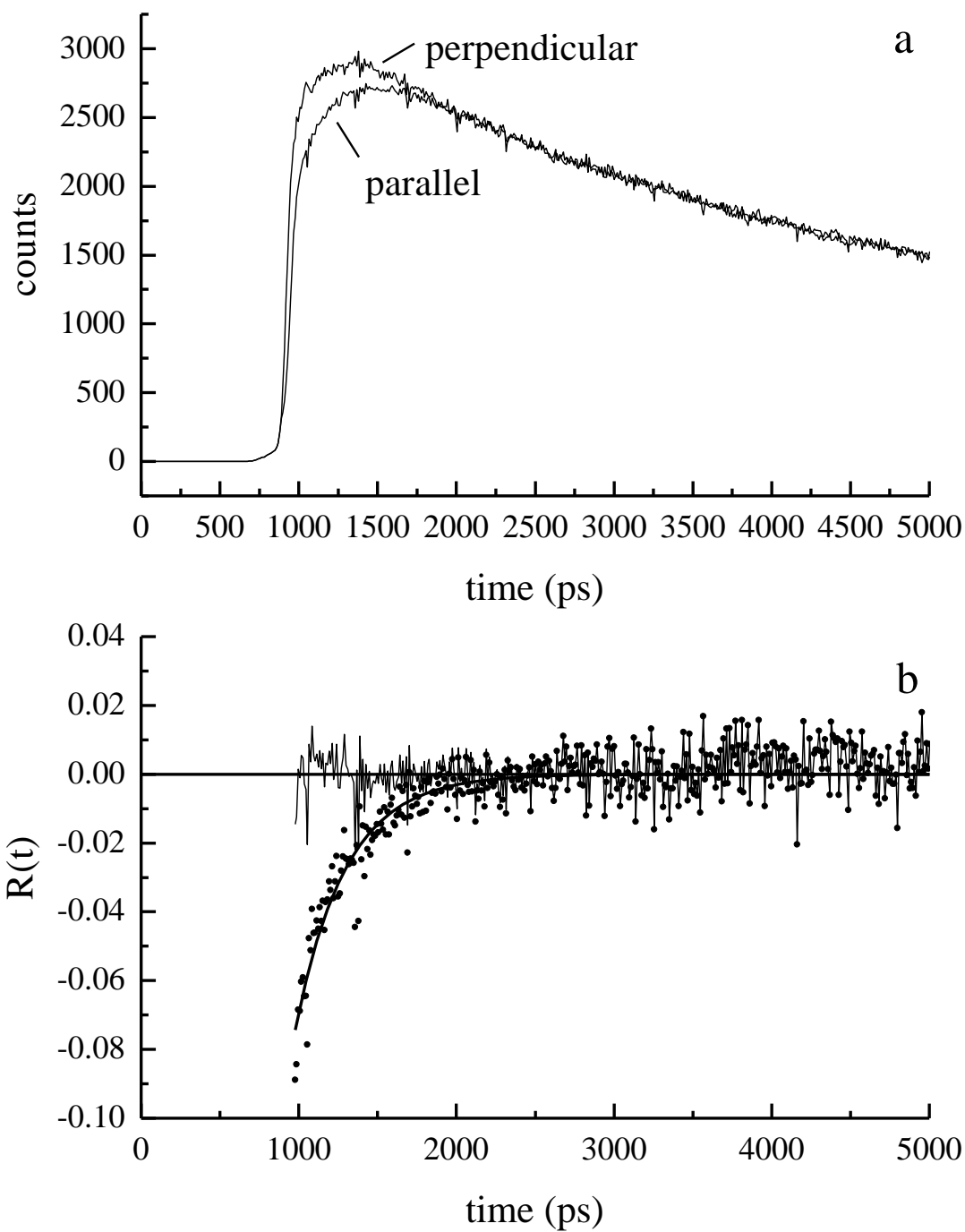


Figure 5.3. (a) Experimental data for perylene reorientation in 100 nm diameter DMPC vesicles at 292 K, and excited at 260 nm ( $S_2 \leftarrow S_0$ ). (b) Induced orientational anisotropy decay function for the data shown in panel (a), along with the best-fit function to the data.

We present these results in Table 5.1. The data show that excitation of the  $S_2 \leftarrow S_0$  transition gives rise to faster rotational diffusion constants than excitation of the chromophore  $S_1 \leftarrow S_0$  transition. We have observed this phenomenon before for a rhodamine chromophore<sup>155</sup> and understand this behavior in the context of local heating due to the dissipation of excess excitation energy by nonradiative transfer to the bath.

Based on the data presented in Table 5.1, it is clear that  $D$  for excitation of the  $S_2 \leftarrow S_0$  transition of perylene is larger than  $D$  for excitation of the  $S_1 \leftarrow S_0$  transition. We can relate the rotational diffusion constant,  $D$ , to the viscosity of the medium in which the chromophore resides through the modified Debye-Stokes-Einstein (DSE) equation. This equation is intended to describe the rotational motion of an ellipsoidal rotor in a continuum solvent, a situation that does not describe the environment formed within a lipid bilayer accurately. Despite this issue, we apply the DSE model to the same chromophore under conditions of excitation at two different wavelengths. Thus any issues relating to the application of this model to our data are consistent throughout. The modified Debye-Stokes-Einstein equation is given by<sup>39, 143</sup>

$$\frac{1}{6D} = \frac{\eta Vf}{k_B T S} \quad (5.8)$$

In this equation  $\eta$  is the solvent bulk viscosity,  $V$  is the hydrodynamic volume of the reorienting chromophore,  $f$  is a frictional term used to compensate for interactions between the solute and the solvent,  $k_B$  is the Boltzmann constant,  $T$  is the temperature of

the system, and  $S$  is a shape factor that is calculated using Perrin's equations to account for the non-spherical shape of the chromophore.<sup>39</sup> We take  $V = 225 \text{ \AA}^3$  for the hydrodynamic volume of perylene,<sup>158</sup>  $S = 0.70$  for the shape factor,<sup>145</sup> and  $f = 1$  for the frictional coefficient. In this equation the only temperature-dependent terms are the solvent bulk viscosity and the temperature of the system. The essential issues to understanding these data are knowledge of the amount of excess excitation energy deposited in the system and an understanding of the temperature dependence of the viscosity of the lipid bilayer medium. The amount of excess energy deposited into the system can be calculated in a straightforward manner. This energy is the difference in energy between the  $S_2 \leftarrow S_0$  transition ( $\lambda_{\text{ex}} = 260 \text{ nm}$ ,  $E_{\text{ex}} = 4.77 \text{ eV}$ ) and the  $S_1 \leftarrow S_0$  transition ( $\lambda_{0-0} = 435 \text{ nm}$ ,  $E_{0-0} = 2.85 \text{ eV}$ ), which is  $1.92 \text{ eV}$ . This  $1.92 \text{ eV}$  of energy is dissipated nonradiatively into the bath modes of the surrounding lipid acyl chains. Figure 5.4 shows that the dissipated energy from the excitation of the  $S_2 \leftarrow S_0$  transition results in faster reorientation times for this transition, as opposed to the  $S_1 \leftarrow S_0$  transition, because the excess excitation energy is presumably disordering the local environment of the chromophore, and decreasing the local viscosity.

We relate the state-dependent rotational diffusion behavior to a change in both the viscosity of the medium and the temperature of the system using the modified DSE equation.

$$\Delta\tau_{OR} = \Delta\left(\frac{\eta}{T}\right)\left(\frac{Vf}{k_B S}\right) \approx \frac{\Delta\eta Vf}{k_B T S} \quad (5.9)$$

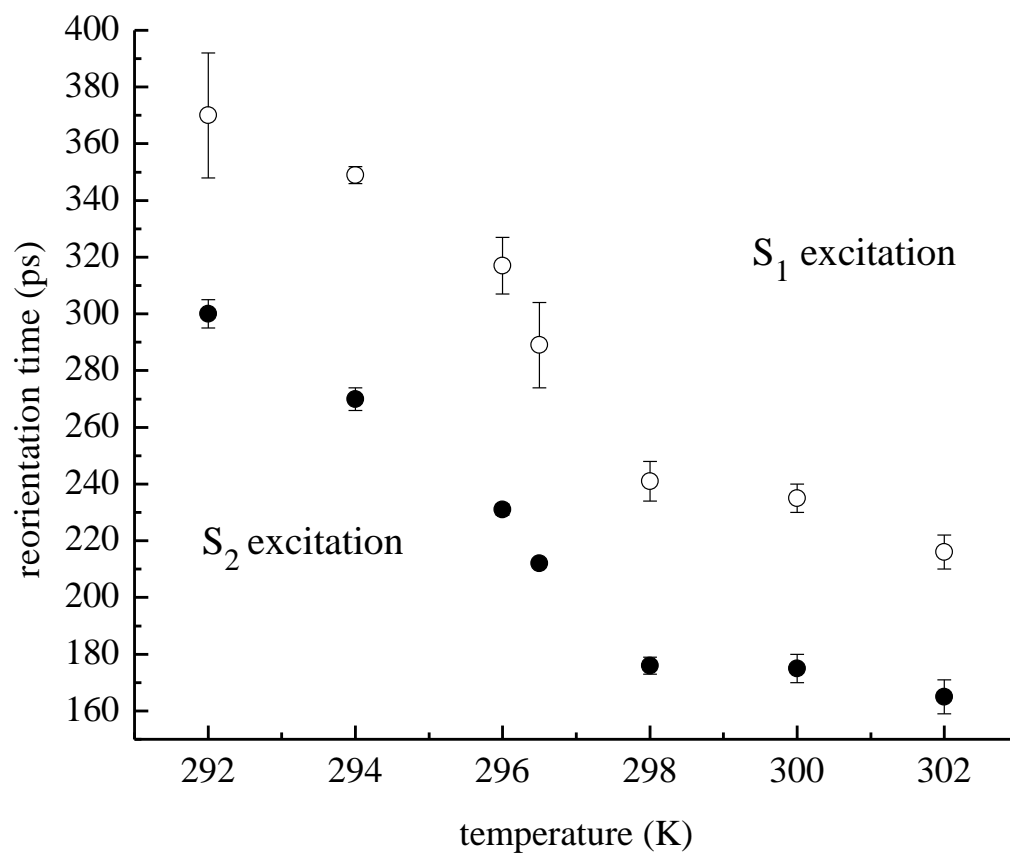


Figure 5.4. Dependence of reorientation time on temperature for 100 nm diameter DMPC vesicles, for excitation of the  $S_1 \leftarrow S_0$  transition ( $\circ$ ) and the  $S_2 \leftarrow S_0$  transition ( $\bullet$ ). Errors are  $\pm 1\sigma$  for at least four individual determinations at each temperature.

Using Eq. 8 we can calculate the value of  $\Delta\eta$  at each temperature for which fluorescence anisotropy data were recorded, and we show these results in Table 5.2. In order to determine the change in local temperature ( $\Delta T$ ) that gives rise to the state-dependent reorientation times, we must have a model for the temperature dependence of the lipid acyl chain viscosity.

The temperature dependence of viscosity depends on the physical properties of the medium, and has been determined experimentally for a variety of liquids.<sup>159</sup> The same is not true for lipids, however, and we know of no reliable evaluation of the temperature-dependent viscosity characteristics of DMPC.<sup>150</sup> Previous rotational diffusion studies of perylene in DMPC have shown that the viscosities of the lipid acyl chain region, at temperatures in the vicinity of the lipid  $T_m$ , are similar to those of normal alcohols.<sup>25</sup>

Based on the data we report here, we estimate the viscosity of the DMPC acyl chain region to be similar to that of *n*-octanol ( $\eta = 7.4$  cP)<sup>159</sup> for temperatures below  $T_m$ , and similar to the viscosity of *n*-heptanol ( $\eta = 5.8$  cP) for temperatures above  $T_m$  (Table 5.1). If we use the model of *n*-alcohols for the lipid acyl chains, and assume that their local viscosity obeys the same temperature dependence (on length scales short enough that we do not have to consider a mesoscopic phase transition), we can use Eq. 5.10 to estimate the temperature change associated with the experimentally observed  $\Delta\tau_{OR}$ . A parameterized fit can be used to relate  $\eta$  to  $T$ <sup>159</sup>

Table 5.2. Experimental reorientation times and calculated changes in local viscosity and temperature associated with internal conversion of perylene.

Temp. (K)	$\tau_{\text{OR1}} (S_1)$ (ps)	$\tau_{\text{OR1}} (S_2)$ (ps)	$\Delta\tau_{\text{OR1}} (S_2 - S_1)$ (ps)	$\Delta\eta$ (cP)	$\Delta T$ (K)
292	$370 \pm 22$	$300 \pm 5$	$-70 \pm 23$	$-0.88 \pm 0.28$	$3.6 \pm 1.2$
294	$349 \pm 3$	$270 \pm 4$	$-79 \pm 5$	$-1.00 \pm 0.06$	$4.1 \pm 0.3$
296	$317 \pm 10$	$231 \pm 2$	$-86 \pm 10$	$-1.09 \pm 0.13$	$4.5 \pm 0.5$
296.5	$289 \pm 15$	$212 \pm 1$	$-77 \pm 15$	$-0.98 \pm 0.19$	$4.1 \pm 0.8$
298	$241 \pm 7$	$176 \pm 3$	$-65 \pm 8$	$-0.83 \pm 0.10$	$4.0 \pm 0.5$
300	$235 \pm 5$	$175 \pm 5$	$-60 \pm 7$	$-0.77 \pm 0.09$	$3.7 \pm 0.4$
302	$216 \pm 6$	$165 \pm 6$	$-51 \pm 8$	$-0.66 \pm 0.11$	$3.2 \pm 0.5$

Errors are  $\pm 1\sigma$  for at least four individual determinations at each temperature.

$$T = \frac{A}{\eta} - \eta B + C \quad (5.10)$$

$A$ ,  $B$ , and  $C$  in this expression are empirical constants. The temperature dependence of the viscosity is given by Eq. 5.11.<sup>155</sup>

$$\left. \frac{d\eta}{dT} \right|_{T_0} = \frac{-\eta^2}{A + \eta^2 B} \quad (5.11)$$

where  $T_0$  is the ambient temperature of the vesicle-containing solution. Literature values for  $A$  and  $B$  were used along with the viscosities for  $n$ -octanol and  $n$ -heptanol, and the experimentally derived values of  $\Delta\eta \sim d\eta$  (Eq. 5.9) in order to calculate  $dT \sim \Delta T$  (Table 5.2). The calculated value of  $\Delta T$  is an estimate of the amount of transient heating that occurs to the lipid acyl chains, which in turn gives rise to the observed  $\Delta\tau_{\text{OR}}$ .<sup>155</sup> We calculate an average value of  $\Delta T$  of 4 K, but for temperatures below the DMPC phase transition ( $< 297$  K) the average value of  $\Delta T$  is slightly higher (*i.e.* 4.1 K) than it is for system temperatures above the  $T_m$  of DMPC (*i.e.* 3.7 K), although this apparent difference lies within the uncertainty of the measurements.

We note in passing that it is possible, in principle, to treat the transient temperature change associated with point source heating with the well-known time-dependent partial differential heat equation.<sup>160</sup> We have chosen not to present an analysis of our data in the context of the heat equation because the results calculated in this manner are highly dependent on assumed input parameters, and the qualitative result is always that the heat deposited into the system dissipates very rapidly. There is little or

no insight to be gained into the intermolecular processes responsible for the effects we observe using this model.

We have discussed our data in the context of a transient change in the temperature of the chromophore immediate environment. Because of the time scales involved in both the energy dissipation process and in our measurement of the associated system changes, we sense an average temperature change rather than an instantaneous change. The time scale of energy dissipation in this system is determined by the time required to transfer energy from the chromophore to the vibrational modes of the surrounding lipid acyl chains. The nonradiative relaxation from the perylene  $S_2$  state to the  $S_1$  state will proceed within a picosecond.<sup>161</sup> The heating process for the sample as a whole will occur over the duration of the excitation pulse, but for any given chromophore, the relaxation process will be on the order of a ps or less. This conservative estimate of the relaxation time includes IVR (intramolecular vibrational relaxation) within the  $S_2$  manifold and  $S_2 \rightarrow S_1$  relaxation. Once the excitation energy has been deposited into the lipid bath modes, the rate at which intermolecular vibrational energy transfer proceeds is determined by the nature of the energy transfer process and the efficiency of intramolecular vibrational relaxation within the lipid acyl chains. The former process, assuming resonant energy transfer dominates, will proceed on the *ca.* 10 ps time scale,<sup>136-137, 162-165</sup> and the latter process, which depends on the density of vibrational states within the acyl chains, may take a similar period of time, at most. Thus it is fair to estimate that the energy dissipation into the bath is complete within less than 20 ps, and

quite possibly much less than 20 ps. This time scale is fast relative to the time scale associated with perylene reorientation. Our experimental data show that the reorientation time of perylene varies between 165 ps and 370 ps, depending on the state excited and the temperature of the system (Table 5.2). If we average the transient temperature change over several hundred ps, it is clear that the instantaneous temperature change associated with excitation is much higher than the  $\Delta T$  values we report. While it is tempting to calculate the transient temperature change based on the time scales involved, doing so is not straightforward because of changes in the order of the lipid acyl chains. Specifically, the transient temperature change can drive phase transition(s) in the lipid acyl chain region, leading to a more disordered system. The persistence time for the thermally induced disorder may be significantly longer than the actual thermal transient used to create the disorder and, as a consequence, the chromophore is sensing a disordered environment that does not re-organize fully on the time scale of the measured reorientation. Thus, owing to the time scales and intrinsic molecular-scale complexity of the systems we have examined, it is not possible to quantitate either the maximum  $\Delta T$  achieved or the duration of the thermal transient associated with the  $S_2 \rightarrow S_1$  relaxation of perylene.

## Conclusions

We have examined the time-resolved fluorescence anisotropy decay behavior of perylene in DMPC vesicles as a function of system temperature, lipid phase and the state to which perylene is excited. The excitation state-dependent reorientation dynamics of perylene reveal the effect of the deposition of excess excitation energy on the lipid bilayer acyl chain environment in closest proximity to the chromophore. Our findings are consistent with a transient temperature change of *ca.* 4 K for excitation of perylene to its  $S_2$  state, with there being a subtle difference in the temperature change for the lipid gel and fluid phases, albeit not outside of the experimental uncertainty. It appears that thermal energy may be transferred to lipid (bath) molecules somewhat more efficiently when the bath is relatively well organized, and that for phases of comparatively low order, such as the lipid fluid phase, the absence of organization can potentially limit the efficiency of vibrational intermolecular energy transfer on the timescale of the reorientation experiment. Our data provide insight into the effect of transient heating in lipid bilayer systems and suggest that the least perturbative way to perform spectroscopic experiments in any medium is to excite the chromophore to the same excited state from which the experimental signal is derived.

## CHAPTER 6

### Consequences of Transient Heating on the Motional Dynamics of Cholesterol-Containing Phospholipid Vesicles

#### Introduction

Biological plasma membranes are dynamic fluid structures that are composed of an assortment of chemical constituents, which work together to promote the regulation and function of the cell.<sup>42</sup> The interactions of these chemical constituents, which include phospholipids, glycerophospholipids, sphingolipids, sterols, and proteins, are crucial to the organization of the membrane and the proper function of integral proteins. Among the primary constituents in plasma membranes are phospholipids and cholesterol. It is well-established that the amount of cholesterol present in the membrane supports cell structure, dynamics, and function.<sup>166-168</sup> It is for this reason that a number of studies on synthetic bilayer structures have focused on comparatively simple systems that contain phospholipid, sphingomyelin, and cholesterol.<sup>153, 169-171</sup> Cholesterol is an amphipathic molecule (Fig. 6.1), and the  $\beta$ -hydroxyl group on its A ring produces an orientational preference in bilayer structures, with the fused-ring system aligning parallel to the lipid acyl chains and the  $\beta$ -hydroxyl group directed toward the bilayer headgroup region.<sup>166</sup> The incorporation of cholesterol into phospholipid bilayers is believed to disrupt the interactions between neighboring lipids, which leads to the creation of an intermediate

“liquid-ordered” phase and consequently alters the lipid’s main phase transition temperature ( $T_m$ ).<sup>172</sup>

Bilayers that contain cholesterol exhibit regions of phase separation,<sup>173</sup> and are known to exist in a liquid-ordered phase at low temperatures and a liquid-disordered phase at higher temperatures.<sup>174</sup> The temperature at which this phase transition occurs depends sensitively on the functionality of the lipids comprising the bilayer and the amount of cholesterol present. This phase transition is analogous to the “melting” gel-to-fluid phase transition seen in bilayers comprised solely of phospholipid. The addition of cholesterol to a phospholipid bilayer typically leads to a decrease in the observed phase transition temperature, consistent with the introduction of a loss of molecular-scale organization within the system.

Phase separation in model lipid bilayer systems has been associated with the notion of “lipid rafts”, the existence of which in plasma membranes remains a subject of debate.<sup>175-179</sup> It is clear that in model systems the presence of cholesterol in phospholipid bilayers mediates lateral organization and local motional freedom of individual phospholipids within the membrane. In most bilayer systems cholesterol is believed to act in concert with other constituents. Cholesterol and sphingomyelin, in particular, are thought to play a cooperative role in mediating bilayer organization, as well as protein function in plasma membranes.<sup>179</sup>

We are interested in learning about the consequences of local temperature change within bilayer structures containing cholesterol. We have recently investigated the structural effects of local temperature change in bilayers comprised entirely of a

phospholipid, DMPC.<sup>180</sup> In the work we present here, we examine the effects of transient heating on vesicles comprised of phospholipid and cholesterol. We measure the rotational diffusion dynamics of perylene imbedded in the non-polar region of the vesicles, as a function of electronic excitation energy. Perylene functions as a local “radiator” of thermal energy in these systems. For  $S_1 \leftarrow S_0$  excitation, little excess energy is released nonradiatively, owing to the high fluorescence quantum yield and small Stokes shift of this chromophore. For  $S_2 \leftarrow S_0$  excitation, rapid nonradiative relaxation (*ca.* 1 ps)<sup>28</sup> from the  $S_2$  manifold to the  $S_1$  manifold deposits *ca.* 1.92 eV of thermal energy into the immediate environment of the chromophore, resulting in a transient change in local temperature and, possibly, organization within the bilayer. Consistent with our earlier work,<sup>180</sup> the reorientation dynamics of perylene in DMPC/cholesterol vesicles are excitation state-dependent, and from this state dependence we are able to estimate the transient temperature change in the chromophore local environment, averaged over its reorientation time. The average temperature change we observe is on the order of *ca.* 7 K below what we believe to be the liquid-ordered to liquid-disordered phase transition, and *ca.* 13 K above this phase transition. The reorientation data suggest a significant change in the chromophore local environment at the onset of a phase transition, with a lower degree of organization and, consequently, molecular order above the phase transition.

## Experimental Section

*Vesicle Preparation.* The phospholipid 1,2-dimyristoyl-*sn*-phosphatidylcholine (14:0 DMPC) dissolved in chloroform was purchased from Avanti Polar Lipids, Inc. (Alabaster, AL) and was used without further purification. Cholesterol powder (ovine wool, > 98 %) was also purchased from Avanti Polar Lipids, Inc. and used as received. Perylene (99+ %) was purchased from Sigma-Aldrich (Milwaukee, WI) and used without further purification. For each sample, DMPC and cholesterol were first mixed in a 2:1 ratio of 66.7 mol % and 33.2 mol %, respectively, with 0.1 mol % perylene added and the chloroform solvent was evaporated under vacuum. 10 mM Tris<sup>®</sup> buffer (Fluka) was then added to each sample, making the final sample concentration 1 mg/mL. Tris<sup>®</sup> buffer was prepared with water from a Milli-Q Plus water purification system (Millipore, Bedford, MA), buffered to pH 8, and purged with Ar (*g*) prior to use. Lipid/cholesterol/chromophore mixtures were mixed with five freeze-thaw-vortex cycles. Each cycle consisted of freezing the solution by immersion in N<sub>2</sub> (*l*) for 5 min., followed by thawing of the sample in a 60°C water bath for 5 min., then vortexing the mixture for 2 min. The resulting solutions were extruded eleven times through a polycarbonate membrane (Whatman) with a nominal pore diameter of 100 nm using a mini-extruder apparatus (Avanti Polar Lipids, Inc.) to produce unilamellar vesicles.<sup>103</sup>

*Time-Resolved Fluorescence Measurements.* Fluorescence lifetime and anisotropy decay data were acquired using a time-correlated single photon counting (TCSPC) instrument. This system has been described in detail elsewhere,<sup>1</sup> and we briefly summarize the pertinent features below. The light source is a CW passively

mode-locked, diode-pumped Nd:YVO<sub>4</sub> laser (Spectra Physics Vanguard) that produces 13 ps pulses at 1064 nm at a repetition rate of 80 MHz. The output is frequency doubled and tripled, providing 2.5 W average power with the same pulse characteristics at 355 nm and 532 nm. The second and third harmonic outputs of the Nd:YVO<sub>4</sub> laser excite cavity-dumped dye lasers (Coherent 702-2), which can operate in the range of 430 nm to 850 nm, producing 5 ps pulses with a repetition rate of 4 MHz. For excitation of the S<sub>1</sub> ← S<sub>0</sub> transition at 430 nm, the dye laser was operated with Stilbene 420 dye (Exciton) to produce the excitation wavelength. For the S<sub>2</sub> ← S<sub>0</sub> transition at 260 nm, Coumarin 500 dye (Exciton) was used to produce 520 nm pulses that were frequency doubled using a Type I BBO crystal to produce 260 nm pulses. For both excitation wavelengths, the laser output is linearly polarized with a polarization extinction ratio of *ca.* 100:1. The polarization of the 260 nm pulse was rotated to vertical using a UV-grade quartz polarization rotating Fresnel rhomb pair (CVI), which ensured an extinction ratio > 500:1. The fundamental excitation pulse from the dye laser is divided, with one portion of the pulse directed into a reference photodiode (Becker & Hickl PHD-400-N), and the other portion directed into the sample. Emission is collected at right angles to the excitation axis and directed to the detectors using a 40x reflecting microscope objective (Ealing). The collected emission is separated into polarization components parallel (0°) and perpendicular (90°) to the vertically polarized excitation pulse using a polarizing cube beam splitter. The polarized signal components are simultaneously detected with microchannel plate photomultiplier tubes (MCP-PMT, Hamamatsu R3809U-50), each equipped with a subtractive double monochromator (Spectral Products CM-112). The

detection electronics (Becker & Hickl SPC-132) record the parallel and perpendicular transients separately, yielding *ca.* 30 ps response functions for each detection channel. The instrument is controlled using an in-house written LabVIEW<sup>®</sup> (National Instruments) program on a PC. The sample temperature was regulated to  $\pm 0.1^\circ \text{C}$  with a water-circulating bath (Neslab RTE-110) connected to a temperature-controlled brass cell jacket which held the sample cuvette. All samples were allowed to equilibrate thermally for 10 minutes prior to data acquisition.

*Steady-State Fluorescence Measurements.* Excitation and emission spectra were acquired for our vesicle samples to determine the perylene band positions. We used a Hitachi F-4500 fluorescence spectrophotometer to collect both the excitation and emission spectra of perylene in our samples. The instrument was set to a spectral band pass of 1 nm for both excitation and emission monochromators.

## Results and Discussion

The purpose of this work is to study the effects of thermal energy dissipation in lipid bilayer structures. Cholesterol in the membrane is critical to the regulation of cellular processes.<sup>49, 167, 181-183</sup> Also important to the understanding of cellular function and overall bilayer behavior is the mechanism by which thermal energy is dissipated within the lipid matrix. We do know that thermal energy influences the organization of the bilayer constituents,<sup>25, 76, 184</sup> but it remains unclear whether the presence of a point source of thermal energy is capable of creating a local or longer range change in that organization. In order to study this phenomenon in greater detail, we use a fluorescent probe molecule to obtain information about its local environment. In this case, the local environment of interest is the acyl chain region of a lipid bilayer, as changes in this region can help to elucidate the structure, packing, and overall dynamics of the bilayer. This is the area of the bilayer most greatly affected by the addition of “impurities”, such as ethanol<sup>1</sup> or cholesterol, and by changes in the thermal energy of the system.<sup>180</sup>

The use of any molecule as a “probe” can, in principle, lead to the acquisition of information that is not necessarily reflective of the system of interest. This is because the probe molecule is itself a perturbation to the system. In an attempt to minimize the consequences of this limitation, relatively low concentrations of chromophore are typically used. The concentration of perylene we use is sufficiently low that, for DMPC vesicles less than 800 nm in diameter, we observe the same phase transition temperature ( $T_m = 297$  K) that has been measured using variable temperature NMR spectroscopy.<sup>180</sup>

For this reason, we assert that the phenomena we report here are reflective of the chromophore local environment formed by the lipids and cholesterol, and that the chromophore functions as a largely non-disruptive probe.

As noted above, we have reported previously on the dissipation of thermal energy in pure phospholipid bilayers using the same spectroscopic technique. In that work, we observed a *ca.* 4 K change in local temperature associated with the nonradiative relaxation of perylene from the  $S_2$  to  $S_1$  manifold. We calculated the average temperature change of the chromophore immediate environment using a model that relates the excitation state-dependent change in the anisotropy decay time constant to a change in local viscosity, and then related the change in viscosity to a change in temperature.<sup>180</sup> The data we report here indicate that the addition of cholesterol to this bilayer system reduces the efficiency of intermolecular vibrational energy transfer, thus keeping the thermal energy in close spatial proximity to the probe and giving rise to a larger measured temperature increase.

Perylene was chosen for these experiments because of our past experience with this probe,<sup>1, 25</sup> and because it is a nonpolar polycyclic aromatic hydrocarbon (Fig. 6.1) that partitions selectively into the hydrophobic region of the lipid bilayer. The actual location of the chromophore within the acyl chain region of the bilayer has been shown to depend sensitively on the diameter of the extruded vesicles.<sup>76</sup> As the diameter of the vesicle exceeds *ca.* 800 nm, perylene becomes insensitive to the gel-to-fluid phase transition in DMPC unilamellar vesicles, suggesting its relocation to the bilayer midplane.<sup>76</sup> In small vesicles (< 800 nm diameter), the gel-to-fluid phase transition is

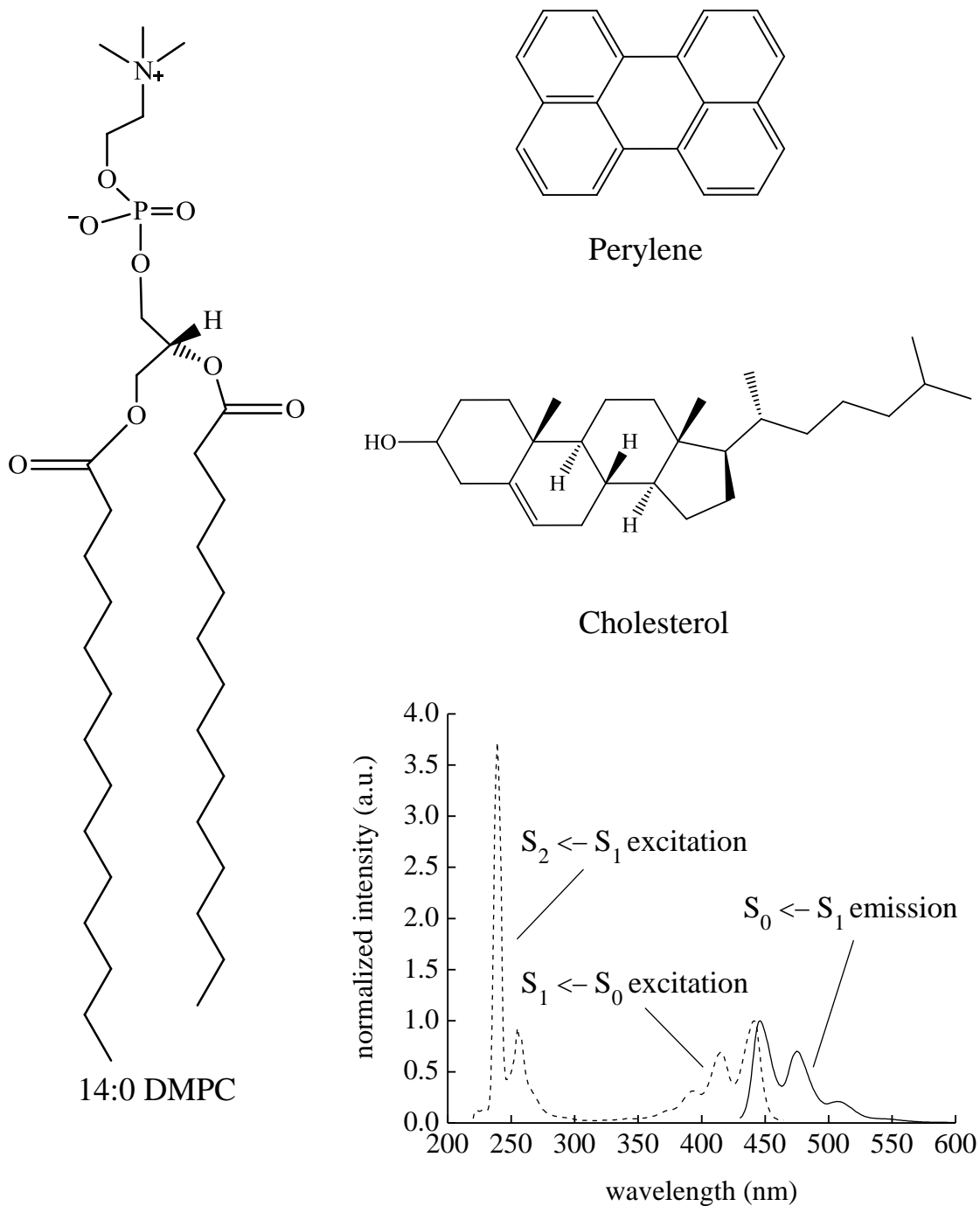


Figure 6.1. Structures of 14:0 DMPC, perylene, cholesterol, and normalized excitation and emission spectra of perylene in DMPC vesicles.

sensed, suggesting that perylene is most likely situated between the lipid acyl chain moieties.<sup>76, 180</sup> Understanding the approximate location of the probe within the bilayer acyl chains allows for a more meaningful interpretation of the fluorescence dynamics measurements.

Two sets of experiments were performed to study the consequences of transient heating in DMPC/cholesterol vesicles. The first was to measure the rotational diffusion dynamics of perylene excited to its  $S_1$  state ( $\lambda_{S1} = 430$  nm) at a series of system temperatures, and the second was to perform the same measurements, except exciting the chromophore to the  $S_2$  state ( $\lambda_{S2} = 260$  nm). For all measurements, emission from the  $S_1$  state is monitored, and excitation state-dependent differences in the chromophore reorientation dynamics are related to transient heating in the bilayer.

For fluorescence anisotropy measurements, the polarized fluorescence transients are combined to produce the induced orientational anisotropy function,  $R(t)$ ,

$$R(t) = \frac{I_{\parallel}(t) - I_{\perp}(t)}{I_{\parallel}(t) + 2I_{\perp}(t)} \quad (6.1)$$

where  $I_{\parallel}(t)$  is the emission transient polarized parallel to the vertically polarized excitation pulse and  $I_{\perp}(t)$  is the emission transient polarized perpendicular to the excitation pulse. For these experiments, the pertinent chemical information is contained in the number of exponential decays exhibited in  $R(t)$  and the time constant of each decay. There are several theoretical treatments that relate the decay functionality of  $R(t)$  to the Cartesian components of the chromophore rotational diffusion constant,  $D$ .<sup>38, 139-</sup>

140 Perylene is known to produce either a one- or two-exponential component fluorescence anisotropy decay, depending on its local environment. In this work, we have observed a two-component anisotropy decay for excitation of the  $S_1 \leftarrow S_0$  ( $\lambda_{S1} = 430$  nm) transition at all temperatures studied (Fig. 6.2b). Excitation of the  $S_2 \leftarrow S_0$  transition ( $\lambda_{S2} = 260$  nm) produces a two-component decay for temperatures of 278 K and below (Fig. 6.3b), and a one-component decay for temperatures above 278 K (Fig. 6.4b). We consider the implications of these findings and the chemical information content of these data next.

Chuang and Eisenthal developed theoretical expressions relating fluorescence anisotropy decay functionality to the Cartesian components of the diffusion constant,  $D$ ,<sup>139</sup>

$$D = \frac{D_x + D_y + D_z}{3} \quad (6.2)$$

It is the magnitude of  $D$  and relative values of  $D_x$ ,  $D_y$ , and  $D_z$  that reflect the interactions with and constraints imposed upon the chromophore by its local environment. Because of the number of independent variables in the model and the number of experimental observables, it is necessary to assume that molecules reorient according to the general condition  $D_i \neq D_j = D_k$ . It is not possible to unambiguously resolve three Cartesian components of  $D$ . It is most common to interpret reorientation data in the context of the chromophore reorienting as either a prolate or oblate rotor,<sup>139</sup> but these representations can lead to ambiguity in the interpretation of anisotropy decay data under certain

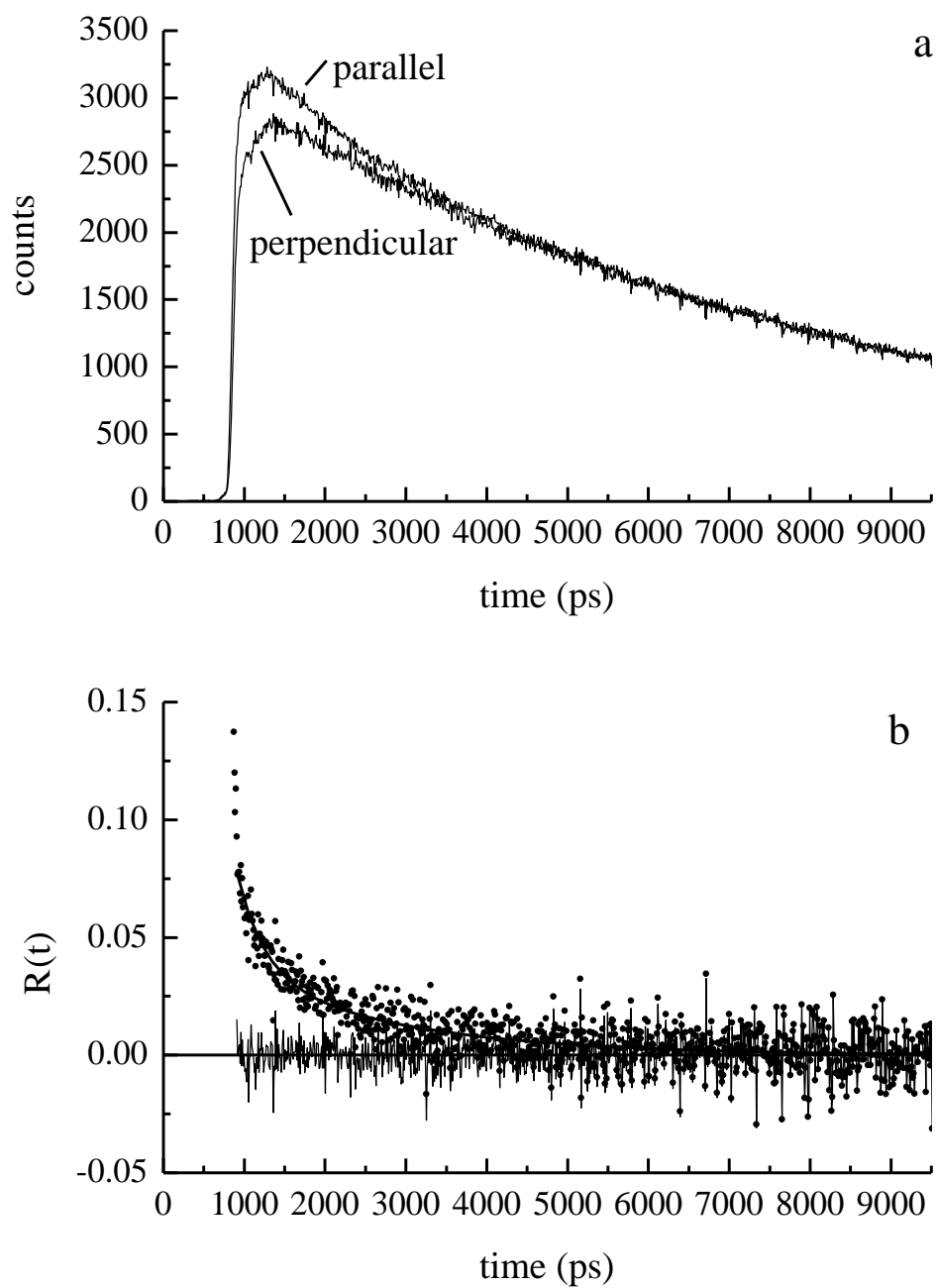


Figure 6.2. (a) Experimental data for perylene reorientation in 100 nm diameter DMPC vesicles at 270.5 K, excited at 430 nm ( $S_1 \leftarrow S_0$ ). (b) Induced orientational anisotropy decay function for the data shown in panel (a), along with the best-fit function to the data.

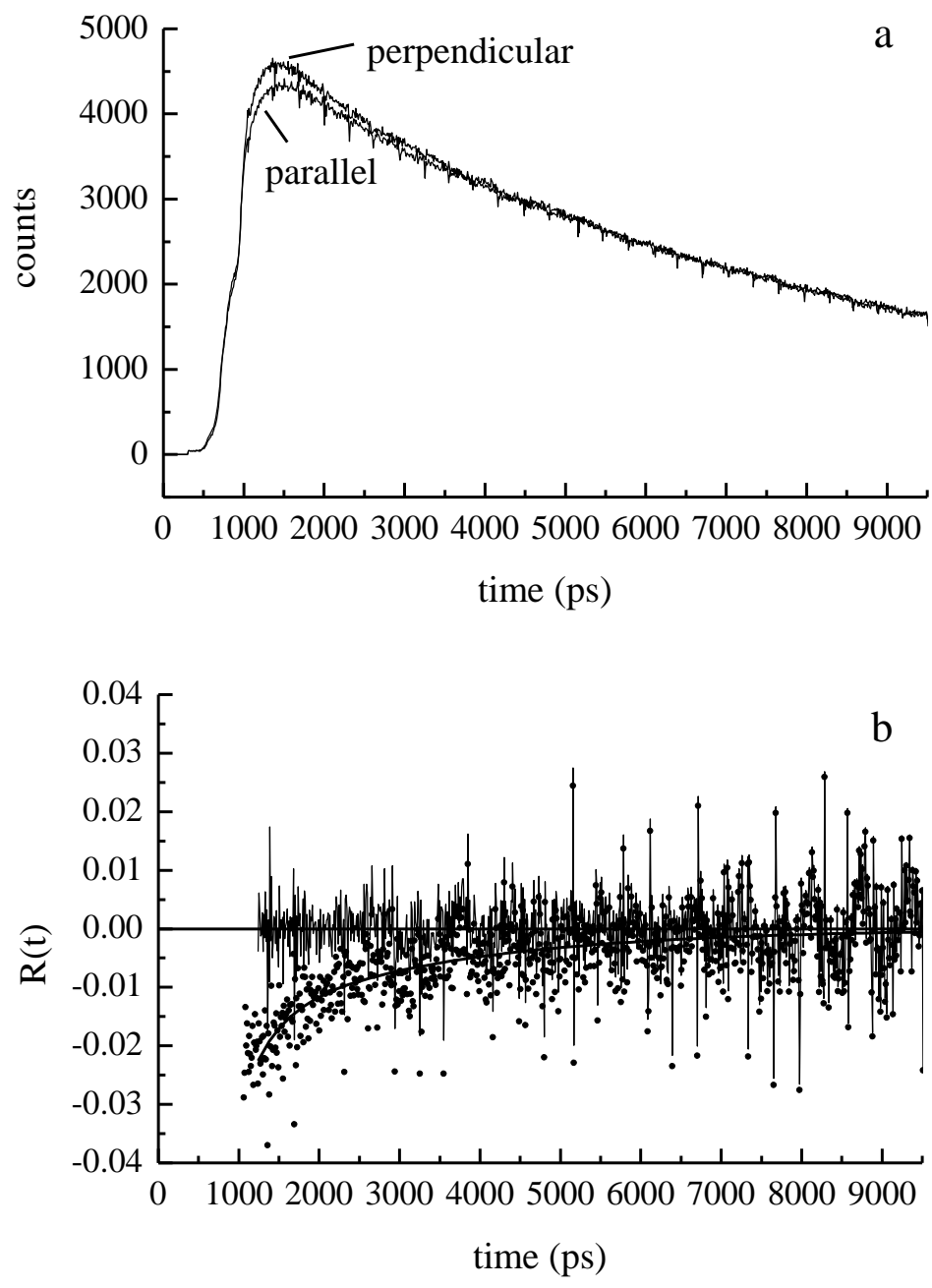


Figure 6.3. (a) Experimental data for perylene reorientation in 100 nm diameter DMPC vesicles at 273 K, excited at 260 nm ( $S_2 \leftarrow S_0$ ). (b) Induced orientational anisotropy decay function for the data shown in panel (a), along with the best-fit function to the data.

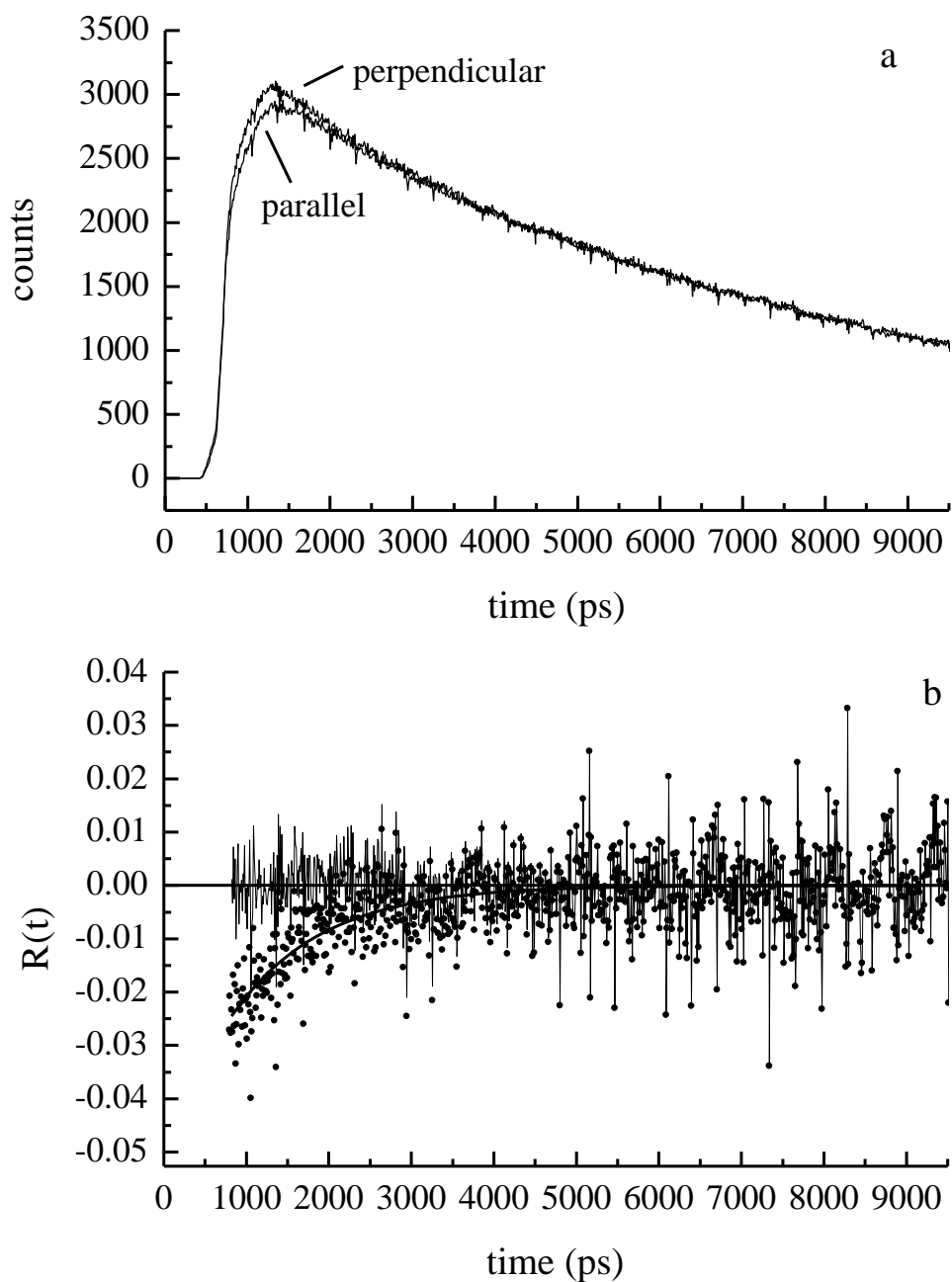


Figure 6.4. (a) Experimental data for perylene reorientation in 100 nm diameter DMPC vesicles at 283 K, excited at 260 nm ( $S_2 \leftarrow S_0$ ). (b) Induced orientational anisotropy decay function for the data shown in panel (a), along with the best-fit function to the data.

circumstances, such as those we encounter here. It is the relative orientations of the absorbing and emitting transition dipole moments with respect to the major axis of rotation that defines the types of possible rotors. We designate these rotors as Type I, Type II, and Type III,<sup>76</sup> and define them below.

In addition to the perylene  $S_2 \leftarrow S_0$  transition being 1.92 eV higher in energy than the  $S_1 \leftarrow S_0$  transition, these transitions are polarized perpendicular to one another. Thus, using Chuang and Eisenthal's treatment of  $R(t)$ , there will be different anisotropy decay equations to describe each excitation condition. For perylene, we define the long in-plane axis as the  $x$ -axis, the short in-plane axis as the  $y$ -axis, and the out-of-plane axis perpendicular to the  $\pi$ -system plane as the  $z$ -axis. A Type I rotor has a unique axis of rotation coincident with the chromophore emission transition moment (the axis of observation). For perylene, both the absorption and emission transition dipole moments for the  $S_1 \leftrightarrow S_0$  transition lie along the  $x$ -axis. Using Chuang and Eisenthal's nomenclature for a Type I rotor,<sup>139</sup> where  $q$  is the unit vector describing the orientation of the absorbing transition dipole moment and  $\gamma$  is the unit vector describing the emitting transition dipole moment,  $q_x^2 = 1$ ,  $\gamma_x^2 = 1$  and  $D_x \neq D_y = D_z$ . The anisotropy decay function is:

$$R(t) = 0.4 \exp(-6D_z t) \quad (6.3)$$

For the perylene  $S_2 \leftarrow S_0$  transition, which is  $y$ -axis polarized ( $q_y^2 = 1$ ,  $\gamma_x^2 = 1$ ), the functional form of the anisotropy decay is:

$$R(t) = -0.2 \exp(-6D_z t) \quad (6.4)$$

Note that Eq. 6.4 predicts a negative zero-time anisotropy because the absorption transition is polarized perpendicular to the emission transition.

A Type II rotor is defined as having its unique axis of rotation oriented perpendicular to its transition dipole moment(s). For perylene this corresponds to  $D_z \neq D_x = D_y$ . For excitation of the  $S_1 \leftarrow S_0$  transition,

$$R(t) = 0.1 \exp(-2D_x + 4D_z)t + 0.3 \exp(-6D_x t) \quad (6.5)$$

And for excitation of the  $S_2 \leftarrow S_0$  transition,

$$R(t) = 0.1 \exp(-6D_x t) - 0.3 \exp(-2D_x + 4D_z)t \quad (6.6)$$

A Type III rotor is defined as having its unique axis of rotation perpendicular to the emission transition dipole moment, but not necessarily perpendicular to the absorbing transition dipole moment. For perylene, this condition corresponds to  $D_y \neq D_x = D_z$ . For excitation of the  $S_1 \leftarrow S_0$  transition, where the absorbing and emitting transition moments are oriented perpendicular to the unique rotational axis,

$$R(t) = 0.3 \exp(-4D_y + 2D_z)t + 0.1 \exp(-6D_z t) \quad (6.7)$$

And for the  $S_2 \leftarrow S_0$  transition, where the absorption transition moment is parallel to the unique rotational axis,

$$R(t) = -0.2 \exp(-6D_z t) \quad (6.8)$$

For perylene, a Type I rotor is characterized by a single exponential anisotropy decay for both excitations, a Type II rotor is characterized by a two-component exponential anisotropy decay for both excitations, and a Type III rotor is characterized by a two-

component anisotropy decay for  $S_1 \leftarrow S_0$  excitation and a one component anisotropy decay for  $S_2 \leftarrow S_0$  excitation.

In a previous report, we recovered two-component exponential anisotropy decays when exciting the perylene  $S_1 \leftarrow S_0$  transition in DMPC vesicles at a series of temperatures.<sup>1, 180</sup> We also have recovered two-component anisotropy decays for perylene in DMPC/cholesterol vesicles ( $S_1 \leftarrow S_0$  excitation) (Fig. 6.2b). In our earlier report, we predicted that  $S_2 \leftarrow S_0$  excitation of perylene would give rise to a two-component exponential decay, consistent with this chromophore behaving as a Type II rotor in DMPC vesicles, both above and below the gel-to-fluid phase transition. However, due to the presence of a fluorophore contaminant in our samples, we were only able to resolve one exponential decay component. It is also important to note that the functionality of  $R(t)$  did not change with respect to temperature for these experiments. This contamination issue has since been resolved, and we expect perylene to behave as a Type II rotor upon  $S_2 \leftarrow S_0$  excitation. In the work we report here, we observe a temperature-dependent anisotropy decay for  $S_2 \leftarrow S_0$  excitation. Specifically, for temperatures of 278 K and lower, we observe a two-component anisotropy decay, consistent with a Type II rotor. For temperatures above 278 K, however, we observe a one component anisotropy decay for  $S_2 \leftarrow S_0$  excitation. This change is indicative of a transition from a Type II rotor to a Type III rotor.

Because of the change in rotor shape observed for  $S_2 \leftarrow S_0$  excitation at temperatures above 278 K, and the transient heating effect associated with this excitation (*vide infra*), it is not possible to discern unambiguously whether  $S_1 \leftarrow S_0$  excitation data manifest the analogous change of rotor shape at the same system temperature. Eqs. 6.5 and 6.7 are similar to one another, with the only difference being the exponential prefactors, indicating a transposition of the unique axis of rotation from the  $z$ - to the  $y$ -axis. The quantitation of anisotropy prefactors is not as reliable as the measurement of the decay time constants, rendering the resolution of the change of rotor type somewhat less apparent for  $S_1 \leftarrow S_0$  excitation. Regardless of this uncertainty, it is clear that perylene in our bilayers undergoes a change from a Type II to a Type III rotor in the vicinity of 278 K.

For temperatures below 278 K, the Type II rotor behavior we observe is consistent with other reports of perylene reorientation in lipid bilayers.<sup>1, 76, 185</sup> Above 278 K we recover anisotropy decay functionalities that are different for the two excitations, consistent with perylene reorienting as a Type III rotor. The change of unique rotational axis from  $D_z$  to  $D_y$  reflects a substantial alteration in the environment of the reorienting chromophore.

Assuming that at temperatures below 278 K perylene behaves as a Type II rotor, all the components of the diffusion constant can be extracted from the measured reorientation times (Table 6.1) using Eqs. 6.9 and 6.10, and the model condition that  $D_z \neq D_x = D_y$ .

Table 6.1. Measured reorientation times as a function of system temperature.

	$\lambda_{S_1} = 430 \text{ nm}, S_1 \leftarrow S_0$		$\lambda_{S_2} = 260 \text{ nm}, S_2 \leftarrow S_0$	
Temp. (K)	$\tau_{OR1}$ (ps)	$\tau_{OR2}$ (ps)	$\tau_{OR1}$ (ps)	$\tau_{OR2}$ (ps)
268	$543 \pm 27$	$2550 \pm 14$	$405 \pm 18$	$3102 \pm 56$
270.5	$548 \pm 16$	$2401 \pm 66$	$445 \pm 24$	$2756 \pm 78$
273	$546 \pm 12$	$2255 \pm 40$	$435 \pm 27$	$2531 \pm 80$
278	$489 \pm 11$	$2099 \pm 35$	$353 \pm 21$	$2224 \pm 64$
280.5	$387 \pm 56$	$2063 \pm 83$	$1277 \pm 57$	-
283	$405 \pm 8$	$2014 \pm 42$	$1167 \pm 78$	-
288	$340 \pm 17$	$1871 \pm 51$	$1036 \pm 51$	-

Errors are  $\pm 1\sigma$  for at least four individual determinations at each temperature.

$$\tau_{OR1} = \frac{1}{2D_x + 4D_z} \quad (6.9)$$

$$\tau_{OR2} = \frac{1}{6D_x} \quad (6.10)$$

The aspect ratio,  $D_{major}/D_{minor}$ , ( $D_z/D_x$  for a Type II rotor) can be calculated for each temperature (Table 6.2). The aspect ratio is related to the nature of the surrounding chromophore environment (*i.e.* the acyl chains). For example, a chromophore in an unhindered environment, such as a continuum solvent, would exhibit reorientation about the  $x$ -,  $y$ -, and  $z$ -axes, with the relationship between  $D_x$ ,  $D_y$ , and  $D_z$  being determined by the structure of the chromophore. For a spherical rotor,  $D_{major}/D_{minor} \approx 1$ . The larger the aspect ratio, the more influence is being exerted on the chromophore by its local environment. Our experimental data for temperatures below 278 K indicate  $D_z/D_x \sim 6$  for  $S_1$  excitation and  $\sim 9$  for  $S_2$  excitation. This change in aspect ratio for the two excitation conditions indicates that the chromophore is becoming more anisotropic as a result of the transient heating effect and the subsequent change in local temperature. We believe that at system temperatures in the vicinity of 278 K, our system is nearing a phase transition, and that the excess excitation energy dissipated by perylene is sufficient enough to initiate a phase transition in these systems. This phase transition, and its consequent structural reorganization, could then trigger a change in the location of the chromophore within the bilayer, presumably from between the acyl chains to the bilayer midplane. A past study demonstrated that it is possible for perylene to relocate from the acyl chains to the midplane.<sup>76</sup> Perylene molecules located in this region of the bilayer

would sense a local environment that is structurally much different than one located between acyl chain moieties, which could explain why the aspect ratios for the chromophore after  $S_2$  excitation are more anisotropic than those for  $S_1$  excitation. The role of cholesterol in mediating the dynamics of these systems is yet to be determined.

For temperatures above 278 K, perylene reorients as a Type III rotor (Eqs. 6.7 and 6.8), and we can use Eqs. 6.11 and 6.12, with the measured reorientation time constants for  $S_1$  excitation (Table 6.1) to solve for the Cartesian components of  $D$ .

$$\tau_{OR1} = \frac{1}{4D_y + 2D_z} \quad (6.11)$$

$$\tau_{OR1} = \frac{1}{6D_z} \quad (6.12)$$

Again, the aspect ratio,  $D_{major}/D_{minor}$ , ( $D_y/D_z$  for a Type III rotor) can be calculated using this set of equations (Table 6.2).

Table 6.2. The rotational diffusion constant, aspect ratio  $D_{\text{major}}/D_{\text{minor}}$ , and calculated local viscosity as a function of temperature.

	$\lambda_{S_1} = 430 \text{ nm}, S_1 \leftarrow S_0$			$\lambda_{S_2} = 260 \text{ nm}, S_2 \leftarrow S_0$		
Temp. (K)	$D_{\text{maj.}}/D_{\text{min.}}$	D (MHz)	$\eta$ (cP)	$D_{\text{maj.}}/D_{\text{min.}}$	D (MHz)	$\eta$ (cP)
268	$6.6 \pm 0.4$	$186 \pm 8$	$10.3 \pm 0.4$	$11.0 \pm 0.6$	$233 \pm 9$	$8.2 \pm 0.3$
270.5	$6.1 \pm 0.3$	$187 \pm 4$	$10.4 \pm 0.2$	$8.8 \pm 0.6$	$218 \pm 10$	$8.9 \pm 0.4$
273	$5.7 \pm 0.1$	$190 \pm 4$	$10.3 \pm 0.2$	$8.1 \pm 0.6$	$226 \pm 14$	$8.7 \pm 0.5$
278	$5.9 \pm 0.1$	$210 \pm 4$	$9.5 \pm 0.2$	$9.0 \pm 0.5$	$274 \pm 15$	$7.3 \pm 0.4$
280.5	$7.7 \pm 1.4$	$259 \pm 31$	$7.8 \pm 0.9$	$7.7^a$	$421 \pm 19$	$4.8 \pm 0.2$
283	$7.0 \pm 0.2$	$247 \pm 4$	$8.2 \pm 0.1$	$7.0^a$	$439 \pm 34$	$4.7 \pm 0.4$
288	$7.8 \pm 0.6$	$290 \pm 12$	$7.1 \pm 0.3$	$7.8^a$	$525 \pm 27$	$3.9 \pm 0.2$

<sup>a</sup> The values of the aspect ratio ( $D_{\text{major}}/D_{\text{minor}}$ ) for the  $S_2 \leftarrow S_0$  transition were assumed to remain constant from those at the corresponding temperatures determined for the  $S_1 \leftarrow S_0$  transition. Errors are  $\pm 1\sigma$  for at least four individual determinations at each temperature.

For excitation of the  $S_2 \leftarrow S_0$  transition at temperatures  $> 278$  K, perylene behaves as a Type III rotor (Eq. 6.8), allowing the recovery of one component of the diffusion constant ( $D_z$ ) according to Eq. 6.13.

$$\tau_{OR} = \frac{1}{6D_z} \quad (6.13)$$

To calculate  $D$  (Eq. 6.2) from our  $S_2$  excitation data above 278 K, we assume that  $D_{major}/D_{minor}$  is the same as for  $S_1$  excitation (Table 6.2). While it may be tempting to use the same change in  $D_{major}/D_{minor}$  as for the Type II rotor (temperatures  $\leq 278$  K), we believe this assumption would not be justified based on the bilayer phase transition and, more importantly, the change in rotor type. These data indicate that excitation of the  $S_2 \leftarrow S_0$  transition results in larger rotational diffusion constants than  $S_1$  excitation for perylene. We understand this phenomenon in terms of nonradiative energy transfer between perylene and its immediate environment.<sup>155, 180</sup> The change in the rotor shape from a Type II to a Type III rotor at  $\sim 278$  K is likely the result of a change in the chromophore local environment. As perylene relaxes nonradiatively from the  $S_2$  state to the  $S_1$  state, excess excitation energy released into the surroundings can alter the organization and viscosity of the lipid medium. We consider next the extraction of approximate average transient temperature changes that result.

The rotational diffusion constant,  $D$ , is related to the viscosity of the local environment of the chromophore through the modified Debye-Stokes-Einstein (DSE) equation.<sup>39, 143</sup> This model describes the rotational motion of a chromophore in a

continuum solvent, which is not the case for perylene imbedded in lipid bilayers. Despite this limitation, we apply the DSE model to our data. Any errors that arise from the application of the model to our data will apply to all of the data uniformly, so that excitation-dependent changes in  $D$  will accurately reflect changes in  $\eta$ . The modified Debye-Stokes-Einstein equation is<sup>39, 143</sup>

$$\frac{1}{6D} = \frac{\eta Vf}{k_B T S} \quad (6.14)$$

In this equation  $\eta$  is the viscosity of the bath (cP),  $V$  is the hydrodynamic volume of the chromophore ( $\text{\AA}^3$ ),  $f$  is a frictional term used to account for interactions between the solvent and solute molecules,  $k_B$  is the Boltzmann constant,  $T$  is the system temperature, and  $S$  is a solute shape factor calculated using Perrin's equations<sup>39</sup> to account for the non-spherical (ellipsoidal) shape of the reorienting chromophore.  $V = 225 \text{ \AA}^3$  for perylene,<sup>158</sup>  $S = 0.70$  for perylene,<sup>145</sup> and  $f$  is taken to be 1 for the frictional coefficient. The DSE equation contains only two terms that depend on temperature: solvent bulk viscosity ( $\eta$ ) and system temperature ( $T$ ). Knowing the temperature dependence of the viscosity of the lipid bilayer and the amount of excess excitation energy that is dissipated by the chromophore is vital for accurate interpretation of our data.

The first step in the determination of the temperature dependence of the lipid bilayer viscosity is to use the DSE equation (Eq. 6.14) to calculate the bulk viscosity of the DMPC/cholesterol lipid bilayers at each experimental system temperature and each excitation ( $S_1$  and  $S_2$ ). We can then determine the change in bulk viscosity ( $\Delta\eta$ ) by

difference (Table 6.2). To determine the amount of excitation energy released into the surrounding bath, we simply calculate the difference in energy between the two excitation transitions according to

$$E = \frac{hc}{\lambda} \quad (6.15)$$

So, for the  $S_2 \leftarrow S_0$  transition,  $\lambda_{ex} = 260$  nm and  $E_{ex} = 4.77$  eV, and for the  $S_1 \leftarrow S_0$  transition,  $\lambda_{0-0} = 435$  nm and  $E_{0-0} = 2.85$  eV. Therefore, 1.92 eV of energy is nonradiatively dissipated into the surrounding bath of lipid acyl chains. To calculate the change in local temperature ( $\Delta T$ ) that results from the nonradiative dissipation of *ca.* 1.92 eV of energy into the lipid environment surrounding the chromophore, we will use a model for the temperature dependence of the lipid acyl chain viscosity.

The chemical identity of the medium plays a central role in the temperature dependence of the viscosity, and this relationship has been determined experimentally for a variety of liquids.<sup>159</sup> The temperature dependence of DMPC/cholesterol lipid bilayer viscosity is, however, not known.<sup>150</sup> It was found previously that the lipid acyl chain environment sensed by perylene in DMPC vesicles had a viscosity similar to those of normal alcohols at temperatures near  $T_m$ .<sup>25</sup> Although we measure dynamics at temperatures lower than the expected  $T_m$  of DMPC, the viscosity data reported in Table 6.2 show what appear to be three distinct viscosity ranges for both excitations, which we refer to as “phases”. The first phase is observed from 268 – 273 K, a second one at 278 K, and a third from 280.5 – 288 K. It is important to note that the viscosity values calculated for the  $S_1 \leftarrow S_0$  transition are significantly larger than those determined for the

$S_2 \leftarrow S_0$  transition at all measured temperatures. These data are consistent with a phase transition in our bilayer at *ca.* 278 K, which is sensed by the rotational diffusion dynamics of perylene.

To estimate the overall temperature change ( $\Delta T$ ) that corresponds to the measured change in local viscosity ( $\Delta\eta$ ), we use Eq. 6.16, a parameterized fit relating  $\eta$  to  $T$ .<sup>159</sup>

$$T = \frac{A}{\eta} - \eta B + C \quad (6.16)$$

$A$ ,  $B$ , and  $C$  are empirical constants. We do not have an independent measure of the viscosity of DMPC acyl chains at ambient temperature. We estimate the behavior of the lipid acyl chains to be similar to that of normal alcohols. Using the viscosities determined for the first excited state transition ( $S_1 \leftarrow S_0$ ) as our reference, we estimate the viscosity of the DMPC acyl chain region to be similar to that of *n*-decanol ( $\eta = 10.9$  cP) over the range of 268 – 273 K, *n*-nonanol ( $\eta = 9.1$  cP) at 278 K, and *n*-octanol ( $\eta = 7.3$  cP) above 278 K.<sup>159</sup> By substituting the viscosity of the *n*-alcohol (at 298 K) for the lipid acyl chain region viscosity, and assuming that the local viscosity of the acyl chains has a similar temperature dependence to that of the alcohols, we can use the expression below to calculate  $\Delta T$ ,

$$\left. \frac{d\eta}{dT} \right|_{T_0} = \frac{-\eta^2}{A + \eta^2 B} \quad (6.17)$$

where  $T_0$  is the ambient temperature of the DMPC/cholesterol vesicle solution. In Eq. 6.17,  $A$  and  $B$  are literature values used along with the viscosities of the normal alcohols (*n*-decanol, *n*-nonanol, and *n*-octanol) and the experimentally determined values of  $\Delta\eta \sim d\eta$  to solve for  $dT \sim \Delta T$  (Table 6.3).  $\Delta T$  is the estimated average amount of transient

Table 6.3. Experimental reorientation times and calculated changes in local viscosity and temperature associated with internal conversion of perylene.

Temp. (K)	$\eta (S_1)$ (cP)	$\eta (S_2)$ (cP)	$\Delta\eta (S_2 - S_1)$ (cP)	$\Delta T$ (K)
268.0	$10.3 \pm 0.4$	$8.2 \pm 0.3$	$-2.1 \pm 0.5$	$7 \pm 2$
270.5	$10.4 \pm 0.2$	$8.9 \pm 0.4$	$-1.5 \pm 0.5$	$5 \pm 2$
273.0	$10.3 \pm 0.2$	$8.7 \pm 0.5$	$-1.6 \pm 0.5$	$6 \pm 2$
278.0	$9.5 \pm 0.2$	$7.3 \pm 0.4$	$-2.2 \pm 0.5$	$8 \pm 2$
280.5	$7.8 \pm 0.9$	$4.8 \pm 0.2$	$-3.0 \pm 0.9$	$12 \pm 4$
283.0	$8.2 \pm 0.1$	$4.7 \pm 0.4$	$-3.5 \pm 0.4$	$14 \pm 2$
288.0	$7.1 \pm 0.3$	$3.9 \pm 0.2$	$-3.2 \pm 0.4$	$13 \pm 2$

Errors are  $\pm 1\sigma$  for at least four individual determinations at each temperature.

heating that occurs to the lipid acyl chains.<sup>155</sup> At temperatures below 278 K the average value of  $\Delta T$  is *ca.* 7 K, and at temperatures above 278 K the average  $\Delta T$  is *ca.* 13 K. These results indicate that we are either detecting a phase transition in the temperature range studied, or that the dissipated transient heat is altering the local environment of the chromophore in such a way that perylene is sensing a change in its location within the bilayer. This explanation is consistent with our finding that perylene changes from a Type II rotor at temperatures below 278 K to a Type III rotor at temperatures above 278 K.

## Conclusion

We have examined the time-resolved fluorescence anisotropy decay behavior of perylene in vesicles comprised of DMPC and cholesterol as a function of both system temperature and chromophore excitation state (Table 6.1). The rotational diffusion constants we have acquired demonstrate that the dynamics of the chromophore are excitation state-dependent (Table 6.2). The state dependence arises from the deposition of excess excitation energy into the surrounding lipid bath. Rotational diffusion measurements allow for estimation of the viscosity of the lipid bilayer in the vicinity of the chromophore. For the bilayers we consider here, which contain both the phosphocholine lipid DMPC and cholesterol, we observe a phase transition in the vicinity of 278 K, based on a distinct change in the reorientation dynamics of perylene at this temperature. We infer from these data a change in the unique axis of rotation for perylene as a function of bilayer temperature. This unexpected finding suggests a substantial change in the chromophore local environment. Such a change was not observed for lipid bilayers comprised solely of DMPC, indicating that cholesterol has a role in this behavior. Using our reorientation data, we estimate the transient temperature change of the lipid local environment due to the dissipation of excitation energy to be *ca.* 7 K for temperatures below 278 K and *ca.* 13 K for temperatures above 278 K. These data suggest that thermal energy is transferred to the surrounding solvent bath (lipid acyl chains) more efficiently at lower temperatures (Table 6.3), consistent with the lipid bilayer existing in a more ordered state below the phase transition.

## CHAPTER 7

### CONCLUSIONS

The ultimate long-term goal of this project is to incorporate functional transmembrane proteins into an artificial lipid bilayer environment for the development of a biomimetic sensor. Planar supported lipid bilayers act as excellent models of the cell membrane, and are attractive platforms for the construction of membrane-based biosensors. However, incorporating transmembrane proteins into supported lipid bilayers while maintaining the proteins' bioactivity, presents a challenge. Transmembrane proteins span the full thickness of the bilayer and require contact with the polar aqueous environment at both terminal ends in order to function properly. In addition, a lipid bilayer fused directly to a solid substrate causes the lipid membrane to lose its fluidity, a property that is crucial for the activity of biological components. This loss of membrane fluidity, and the lack of space for the incorporation of a functional transmembrane protein, led us to consider an alternative lipid bilayer system in the form of unilamellar lipid vesicles. The main advantage of using lipid vesicles over planar bilayers is that both the interior and exterior interfacial regions of the bilayer are in direct contact with the aqueous environment, so in theory, incorporating proteins is possible.

Before attempting to introduce proteins into lipid vesicles, however, it was of the utmost importance for us to investigate the structural organization and dynamic behavior of simple lipid vesicle systems. In order to interrogate our lipid vesicle systems, we used fluorescent molecular probes or chromophores to investigate the interfacial region of the bilayer. Chromophores act as "reporter" molecules, and provide valuable information

regarding the local environment of the probe, such as rotational and translational dynamics, membrane fluidity, and local viscosity. We have designed a series of experiments to examine the effects of global- and molecular-scale perturbations on the organization and fluidity of the lipid vesicle by measuring the motional dynamics of incorporated chromophore molecules. We used low concentrations of chromophores, so as not to further disrupt the bilayer structure due to the presence of the probes.

Chapter 2 discusses our experiments on the hydrogen bonding interactions between lipids with one of two unique headgroup functionalities using a headgroup-tethered chromophore, and how these interactions influence the fluidity of the systems.<sup>154</sup> These lipid systems consisted of either unilamellar vesicles or supported bilayers comprised of phosphocholine (PC), phosphoglycerol (PG), or a mixture of the two lipids. PC lipids are zwitterionic and are believed to experience hydrogen bonding interactions between the phosphate group oxygen atoms of neighboring lipid headgroups,<sup>53-56</sup> while PG lipids are anionic and are thought to form hydrogen bonds between neighboring headgroups and other membrane constituents.<sup>57-60</sup> Our time-resolved fluorescence anisotropy decay measurements show that the rotational diffusion of lipids comprising vesicles is independent of headgroup functionality. However, our fluorescence recovery after pattern photobleaching (FRAPP) measurements on solid-supported lipid bilayers show slower rates of translational diffusion in PG lipid bilayers compared to mixed PC/PG lipid systems, indicating stronger headgroup-headgroup interactions in systems composed primarily of PG. We reconcile these two bodies of data by first considering that translational diffusion measurements sense the motion of the

entire lipid through the bilayer. This movement is mediated by the structure of the bilayer and the strength of the interactions involving the headgroups as well as the acyl chains. It is thus not surprising that a headgroup-tethered chromophore would be sensitive to a portion of the overall molecular motion. Conversely, the rotational motion of tethered chromophores is more directly influenced by the bulk solvent molecules in closest proximity to the chromophores, than by the hydrogen bonding interactions between the headgroups.

In other experiments, we chose to investigate the dynamic behavior of the lipid acyl chain regions of lipid vesicles because these regions are thought to undergo the most structural and organizational changes as a consequence of chemical and thermal perturbations. In Chapter 3, we used steady-state fluorescence techniques to measure the fluorescence emission of pyrene excimers sequestered in the acyl chain regions of 1,2-dimyristoyl-*sn*-phosphatidylcholine (DMPC) lipid vesicles, as a function of ethanol concentration. Pyrene excimer formation is diffusion-limited, and therefore the more fluid the local environment of the probe, the more intense the characteristic pyrene excimer fluorescence emission band (~ 472 nm) becomes. These experiments confirm the dependence of pyrene excimer formation on the bulk ethanol concentration, and consequent fluidity of the bilayer. The steady-state data also show a deviation from the otherwise linear relationship between ethanol concentration and excimer band intensity in the vicinity of 0.6 M ethanol, which points to a structural reorganization of the lipid bilayer.

Building on the steady-state fluorescence experiments discussed in Chapter 3, we next used time-resolved fluorescence anisotropy decay measurements to study the effects

of solution phase ethanol concentration on the rotational motion of the chromophore perylene imbedded in gel and fluid phases of DMPC lipid vesicles. These experiments are presented in Chapter 4. The anisotropy decay data show that ethanol concentration affects the organization of both gel and fluid phase lipid bilayers. In both cases, the rotational diffusion dynamics of perylene molecules incorporated in the bilayer acyl chain region experience a perturbation about their long in-plane rotational axis ( $D_x$ ) for ethanol concentrations in the vicinity of 0.6 M. Taken collectively, the steady-state and dynamic fluorescence data dealing with the effects of ethanol on DMPC lipid vesicles seem to indicate a structural phase transition occurring after *ca.* 0.6 M ethanol has been added to the system, and there is evidence that this transition marks the onset of the interdigitated phase in gel and fluid phase bilayers.

We also chose to examine the time-resolved fluorescence anisotropy decay behavior of perylene in DMPC vesicles as a function of system temperature, lipid phase and the state to which perylene is excited. The specific purpose of these experiments was to study the effect of the deposition of excess excitation energy on the lipid bilayer acyl chain environment in closest proximity to the chromophore. By exciting imbedded perylene to its second excited electronic singlet state ( $S_2$ ) and comparing the recovered fluorescence anisotropy decay(s) (emission from the  $S_0 \leftarrow S_1$  transition) over a range of bulk system temperatures to those obtained for excitation of the  $S_1$  state, the average transient temperature change of the chromophore local environment was estimated to be *ca.* 4 K, with there being a subtle difference in the temperature change for the lipid gel and fluid phases, albeit not outside of the experimental uncertainty. Chapter 5 also

discusses how lipid phase and organization appear to influence the efficiency of thermal energy dissipation. The gel phase is highly ordered and the lipid acyl chains are tightly packed, which promotes vibrational intermolecular energy transfer from the “radiating” chromophore molecule to the surrounding (bath) lipids. Chapter 6 expands on this work by investigating the same excitation energy dissipation from the  $S_2$  state of perylene imbedded in DMPC lipid systems with cholesterol. Our results appear to show a phase transition in the vicinity of 278 K based on a distinct change in the reorientation dynamics of perylene at this temperature – a change that is not observed in pure DMPC lipid systems. We calculate the average transient temperature change to be on the order of 7 K for system temperatures below 278 K, and *ca.* 13 K for temperatures greater than 278 K. Like the results of Chapter 5, these results indicate a more efficient transfer of energy in more ordered systems (*i.e.* the gel phase vs. the fluid phase). It appears that cholesterol plays an important role in regulating the fluidity and phase of model bilayer systems analogous to its behavior in biological cell membranes. Having greater control over the structural and fluid properties of the bilayer will allow us to successfully incorporate biologically-active transmembrane proteins into our bilayer systems.

The results of our experiments have laid the groundwork for a greater understanding of the dynamic behavior of lipid bilayer systems, and have provided us with a means of manipulating the structural properties of simple lipid bilayer systems. Our work with lipid vesicles has demonstrated the importance of understanding the effects and extent of both global- and molecular-scale perturbations on the fluid behavior of lipid bilayers. We believe that by using this knowledge we will be able to incorporate functional transmembrane proteins into these lipid systems, and we expect that our

findings will ultimately lead to the successful development of a transmembrane-incorporated membrane-based biosensor.

## LITERATURE CITED

## Literature Cited

1. Pillman, H. A.; Blanchard, G. J., *The Journal of Physical Chemistry B* **2010**, *114*, 3840.
2. Newman, J. D.; Turner, A. P. F., *Biosensors and Bioelectronics* **2005**, *20*, 2435.
3. Wu, T.-Z., *Biosensors and Bioelectronics* **1999**, *14*, 9.
4. Nikolelis, D. P.; Hianik, T.; Krull, U. J., *Electroanalysis* **1999**, *11*, 7.
5. de Mendoza, D.; Cronan, J. E., *Trends in biochemical sciences* **1983**, *8*, 49.
6. Cooper, R. A., *Journal of Supramolecular Structure* **1978**, *8*, 413.
7. Xu, G.; Wu, Y.; Li, R.; Wang, P.; Yan, W.; Zheng, X., *Chinese Science Bulletin* **2002**, *47*, 1849.
8. Pancrazio, J. J.; Whelan, J. P.; Borkholder, D. A.; Ma, W.; Stenger, D. A., *Annals of Biomedical Engineering* **1999**, *27*, 697.
9. Chaki, N. K.; Vijayamohanan, K., *Biosensors and Bioelectronics* **2002**, *17*, 1.
10. Richter, R. P.; Bérat, R.; Brisson, A. R., *Langmuir* **2006**, *22*, 3497.
11. Groves, J. T.; Dustin, M. L., *Journal of Immunological Methods* **2003**, *278*, 19.
12. Sackmann, E., *Science* **1996**, *271*, 43.
13. Domińska, M.; Blanchard, G. J., *Langmuir* **2009**, *26*, 1043.
14. Wagner, M. L.; Tamm, L. K., *Biophysical Journal* **2000**, *79*, 1400.

15. Tanaka, M.; Sackmann, E., *Nature* **2005**, *437*, 656.
16. Castellana, E. T.; Cremer, P. S., *Surface Science Reports* **2006**, *61*, 429.
17. Lösche, M.; Helm, C.; Mattes, H. D.; Möhwald, H., *Thin Solid Films* **1985**, *133*, 51.
18. Tamm, L. K.; McConnell, H. M., *Biophysical Journal* **1985**, *47*.
19. Brian, A. A.; McConnell, H. M., *Proc. Nat. Acad. Sci. USA* **1984**, *81*, 6159.
20. McConnell, H. M.; Watts, T. H.; Weis, R. M.; Brian, A. A., *Biochimica Et Biophysica Acta* **1986**, *864*.
21. Klee, B.; Duveneck, G. L.; Oroszlan, P.; Ehrat, M.; Widmer, H. M., *Sensors and Actuators B: Chemical* **1995**, *29*, 307.
22. Doherty, G. J.; McMahon, H. T., *Annual Review of Biophysics* **2008**, *37*, 65.
23. Gawrisch, K., The Dynamics of Membrane Lipids. In *The Structure of Biological Membranes*, 2nd ed.; Yeagle, P. L., Ed. CRC Press: New York, 2005.
24. Pabst, G.; Amenitsch, H.; Kharakoz, D. P.; Laggner, P.; Rappolt, M., *Physical Review E* **2004**, *70*, 021908.
25. Koan, M. M.; Blanchard, G. J., *Journal of Physical Chemistry B* **2006**, *110*, 16584.
26. Slavik, J., *Fluorescent Probes in Cellular and Molecular Biology*. CRC Press: Ann Arbor, 1994.
27. Valeur, B., *Molecular Fluorescence*. Wiley-VCH: New York, 2002.

28. Kasha, M., *Discussions of the Faraday Society* **1950**, 14.
29. Acree, W. E.; Tucker, S. A.; Cretella, L. E.; Zvaigzne, A. I.; Street, K. W.; Fetzer, J. C.; Nakasuji, K.; Murata, I., *Applied Spectroscopy* **1990**, *44*, 951.
30. Chen, S.-H.; McGuffin, V. L., *Applied Spectroscopy* **1994**, *48*, 596.
31. Karpovich, D. S.; Blanchard, G. J., *J. Phys. Chem.* **1995**, *99*, 3951.
32. Ray, G. B.; Chakraborty, I.; Moulik, S. P., *J. Colloid Interface Sci.* **2006**, *294*, 248.
33. Waris, R.; Street, K. W.; Acree, W. E.; Fetzer, J. C., *Applied Spectroscopy* **1989**, *43*, 845.
34. Galla, H. J.; Sackmann, E., *Biochimica Et Biophysica Acta* **1974**, *339*, 103.
35. Muentner, J. S.; Deutsch, J. L., *Journal of Chemical Education* **1996**, *73*, 580.
36. Bergmann, W. L.; Dressler, V.; Haest, C. W. M.; Deuticke, B., *Biochimica et Biophysica Acta (BBA) - Biomembranes* **1984**, *772*, 328.
37. Debye, P., *Polar Molecules* Chemical Catalog Co.: New York 1929; p 84.
38. Hu, C. M.; Zwanzig, R., *Journal of Chemical Physics* **1974**, *60*, 4354.
39. Perrin, F., *Journal de Physique et le Radium* **1936**, *7*, 1.
40. Chuang, T. J.; Eisenthal, K. B., *Journal of Chemical Physics* **1972**, *57*, 5094.
41. Garcia, J. J.; Martinez-Ballarín, E.; Millan-Plano, S.; Allue, J. L.; Albendea, C.; Fuentes, L.; Escanero, J. F., *Journal of Trace Elements in Medicine and Biology* **2005**, *19*, 19.

42. Beney, L.; Gervais, P., *Applied Microbiology and Biotechnology* **2001**, *57*, 34.
43. Lapinski, M. M.; Castro-Forero, A.; Greiner, A. J.; Ofoli, R. Y.; Blanchard, G. J., *Langmuir* **2007**, *23*, 11677.
44. Chan, Y. H. M.; Boxer, S. G., *Current Opinion in Chemical Biology* **2007**, *11*, 581.
45. M'Baye, G.; Mely, Y.; Duportail, G.; Klymchenko, A. S., *Biophysical Journal* **2008**, *95*, 1217.
46. Cambrea, L. R.; Haque, F.; Schieler, J. L.; Rochet, J. C.; Hovis, J. S., *Biophysical Journal* **2007**, *93*, 1630.
47. Raguse, B.; Braach-Maksvytis, V.; Cornell, B. A.; King, L. G.; Osman, P. D. J.; Pace, R. J.; Wieczorek, L., *Langmuir* **1998**, *14*, 648.
48. Jadhav, S. R.; Sui, D. X.; Garavito, R. M.; Worden, R. M., *Journal of Colloid and Interface Science* **2008**, *322*, 465.
49. Miersch, S.; Espey, M. G.; Chaube, R.; Akarca, A.; Tweten, R.; Ananvoranich, S.; Mutus, B., *Journal of Biological Chemistry* **2008**, *283*, 18513.
50. Seu, K. J.; Cambrea, L. R.; Everly, R. M.; Hovis, J. S., *Biophysical Journal* **2006**, *91*, 3727.
51. Sakurai, I.; Mizusawa, N.; Ohashi, S.; Kobayashi, M.; Wada, H., *Plant Physiology* **2007**, *144*, 1336.
52. Wada, H.; Murata, N., *Photosynthesis Research* **2007**, *92*, 205.
53. Pandit, S. A.; Bostick, D.; Berkowitz, M. L., *Biophysical Journal* **2003**, *84*, 3743.

54. Pasenkiewicz-Gierula, M.; Takaoka, Y.; Miyagawa, H.; Kitamura, K.; Kusumi, A., *Journal of Physical Chemistry A* **1997**, *101*, 3677.
55. Bockmann, R. A.; Hac, A.; Heimbürg, T.; Grubmüller, H., *Biophysical Journal* **2003**, *85*, 1647.
56. Pasenkiewicz-Gierula, M.; Takaoka, Y.; Miyagawa, H.; Kitamura, K.; Kusumi, A., *Biophysical Journal* **1999**, *76*, 1228.
57. Greenough, K. P.; Blanchard, G. J., *Journal of Physical Chemistry A* **2007**, *111*, 558.
58. Uragami, M.; Miyake, Y.; Tokutake, N.; Zhang, L. H.; Regen, S. L., *Langmuir* **2000**, *16*, 8010.
59. Dicko, A.; Bourque, H.; Pezolet, M., *Chemistry and Physics of Lipids* **1998**, *96*, 125.
60. Zhang, Y. P.; Lewis, R.; McElhaney, R. N., *Biophysical Journal* **1997**, *72*, 779.
61. Hull, M. C.; Cambrea, L. R.; Hovis, J. S., *Analytical Chemistry* **2005**, *77*, 6096.
62. Richter, R. P.; Brisson, A. R., *Biophysical Journal* **2005**, *88*, 3422.
63. Delacruz, J. L.; Blanchard, G. J., *Journal of Physical Chemistry B* **2003**, *107*, 7102.
64. Dewitt, L.; Blanchard, G. J.; Legoff, E.; Benz, M. E.; Liao, J. H.; Kanatzidis, M. G., *Journal of the American Chemical Society* **1993**, *115*, 12158.
65. Gajraj, A.; Ofoli, R. Y., *Langmuir* **2000**, *16*, 4279.
66. Schroeder, R.; London, E.; Brown, D., *Proceedings of the National Academy of Sciences of the United States of America* **1994**, *91*, 12130.

67. Drexhage, K. H., *J. Lumin.* **1970**, 1,2, 693.
68. Girard, C.; Martin, O. J. F.; Dereux, A., *Physical Review Letters* **1995**, 75, 3098.
69. Lukosz, W.; Kunz, R. E., *Opt. Commun.* **1977**, 20, 195.
70. Lukosz, W.; Kunz, R. E., *J. Opt. Soc. Am.* **1978**, 67, 1607.
71. Chattopadhyay, A.; London, E., *Biochimica Et Biophysica Acta* **1988**, 938, 24.
72. Raghuraman, H.; Shrivastava, S.; Chattopadhyay, A., *Biochimica Et Biophysica Acta-Biomembranes* **2007**, 1768, 1258.
73. Chuang, T. J.; Eisenha.Kb, *Journal of Chemical Physics* **1972**, 57, 5094.
74. Lipari, G.; Szabo, A., *Biophysical Journal* **1980**, 30, 489.
75. Szabo, A., *Journal of Chemical Physics* **1984**, 81, 150.
76. Lapinski, M. M.; Blanchard, G. J., *Chemistry and Physics of Lipids* **2008**, 153, 130.
77. Blanchard, G. J., *Journal of Chemical Physics* **1987**, 87, 6802.
78. Shoemaker, S. D.; Vanderlick, T. K., *Biophysical Journal* **2002**, 83, 2007.
79. Smith, L. M.; Weis, R. M.; McConnell, H. M., *Biophysical Journal* **1981**, 36, 73.
80. Starr, T. E.; Thompson, N. L., *Biophysical Chemistry* **2002**, 97, 29.
81. Dickey, A.; Faller, R., *Biophysical Journal* **2008**, 95, 2636.

82. Garret, R. H., Grisham, C.M., *Biochemistry*. 3rd ed.; Thompson Brooks/Cole: Belmont, CA, 2007; p 13.
83. Anderson, T. G.; McConnell, H. M., *Biophysical Journal* **2001**, *81*, 2774.
84. Anderson, T. G.; McConnell, H. M., *Biophysical Journal* **2002**, *83*, 2039.
85. Benvegnu, D. J.; McConnell, H. M., *Journal of Physical Chemistry* **1993**, *97*, 6686.
86. Keller, S. L.; McConnell, H. M., *Physical Review Letters* **1999**, *82*, 1602.
87. Keller, S. L.; Pitcher, W. H. I.; Huestis, W. H.; McConnell, H. M., *Physical Review Letters* **1998**, *81*, 5019.
88. Keller, S. L.; Radhakrishnan, A.; McConnell, H. M., *Journal of Physical Chemistry B* **2000**, *104*, 7522.
89. Lee, K. Y. C.; Klingler, J. F.; McConnell, H. M., *Nature* **1994**, *263*, 655.
90. Radhakrishnan, A.; McConnell, H. M., *Journal of the American Chemical Society* **1999**, *121*, 486.
91. Radhakrishnan, A.; McConnell, H. M., *Journal of Physical Chemistry B* **2002**, *106*, 4755.
92. Subramaniam, S.; McConnell, H. M., *Journal of Physical Chemistry* **1987**, *91*, 1715.
93. Seeman, P., *Pharmacol. Rev.* **1972**, *24*, 583.
94. Slater, J. L.; Huang, C.-H., *Progress in Lipid Research* **1988**, *27*, 325.

95. Vierl, U.; Lobbecke, L.; Nagel, N.; Cevc, G., *Biophysical Journal* **1994**, *67*, 1067.
96. Slater, J. L.; Huang, C.-H., Lipid Bilayer Interdigitation. In *The Structure of Biological Membranes*, Yeagle, P. L., Ed. CRC Press: New York, 2005; p 121.
97. Van Dyke, D. A.; Pryor, B. A.; Smith, P. G.; Topp, M. R., *Journal of Chemical Education* **1998**, *75*, 615.
98. Vanderkooi, J. M.; Callis, J. B., *Biochemistry* **1974**, *13*, 4000.
99. Chong, P. L. G.; Thompson, T. E., *Biophys. J.* **1985**, *47*, 613.
100. Komatsu, H.; Rowe, E. S., *Biochemistry* **1991**, *30*, 2463.
101. Daems, D.; Vandenzegel, M.; Boens, N.; Deschryver, F. C., *European Biophysics Journal with Biophysics Letters* **1985**, *12*, 97.
102. Lianos, P.; Duportail, G., *European Biophysics Journal with Biophysics Letters* **1992**, *21*, 29.
103. Mayer, L. D.; Hope, M. J.; Cullis, P. R., *Biochimica Et Biophysica Acta* **1986**, *858*, 161.
104. Vanderkooi, J. M.; Fischkoff, S.; Andrich, M.; Podo, F.; Owen, C. S., *J. Chem. Phys.* **1975**, *63*, 3661.
105. Dong, D. C.; Winnik, M. A., *Canadian Journal of Chemistry* **1984**, *62*, 2560.
106. Boon, J. M.; McClain, R. L.; Breen, J. J.; Smith, B. D., *J SUPRAMOL CHEM* **2001**, *1*, 17.
107. Bartucci, R.; Pali, T.; Marsh, D., *Biochemistry* **1993**, *32*, 274.

108. Tierney, K. J.; Block, D. E.; Longo, M. L., *Biophysical Journal* **2005**, 89, 2481.
109. Simon, S. A.; McIntosh, T. J., *Biochimica Et Biophysica Acta* **1984**, 773, 169.
110. Lobbecke, L.; Cevc, G., *Biochimica Et Biophysica Acta* **1995**, 1237, 59.
111. Bondar, O. P.; Rowe, E. S., *Biochimica Et Biophysica Acta* **1998**, 1370, 207.
112. Hata, T.; Matsuki, H.; Kaneshina, S., *Biophysical Chemistry* **2000**, 87, 25.
113. McIntosh, T. J.; Lin, H.; Li, S. H.; Huang, C. H., *Biochimica Et Biophysica Acta* **2001**, 1510, 219.
114. Rowe, E. S., *Biochemistry* **1983**, 22, 3299.
115. Vierl, U.; Lobbecke, L.; Nagel, N.; Cevc, G., *Biophys. J.* **1994**, 67, 1067.
116. Zeng, J.; Chong, P. L., *Biophys. J.* **1995**, 68, 567.
117. Zeng, J. W.; Smith, K. E.; Chong, P. L. G., *Biophys. J.* **1993**, 65, 1404.
118. Lee, A., *Current Biology* **2001**, 11, R811.
119. Ikeda, M.; Kihara, A.; Igarashi, Y., *Biological & Pharmaceutical Bulletin* **2006**, 29, 1542.
120. Singer, S. J.; Nicolson, G. L., *Science* **1972**, 175, 720.
121. Harris, R. A.; Burnett, R.; McQuilkin, S.; McClard, A.; Simon, F. R., *Annals of the New York Academy of Sciences* **1987**, 492, 125.

122. Lewis, R. N. A. H.; McElhaney, R. N., The Mesomorphic Phase Behavior of Lipid Bilayers. In *The Structure of Biological Membranes*, Yeagle, P. L., Ed. CRC Press: New York, 2005; Vol. 2nd, p 53.
123. McElhaney, R. N., *Biochimica Et Biophysica Acta* **1984**, 779, 1.
124. McElhaney, R. N., *Crit. Rev. Microbiol.* **1989**, 17, 1.
125. Ryhanen, S. J.; Alakoskela, J.-M. I.; Kinnunen, P. K. J., *Langmuir* **2005**, 21, 5707.
126. Rowe, E. S., *Biochimica Et Biophysica Acta* **1985**, 813, 321.
127. Rowe, E. S., *Biochemistry* **1987**, 26, 46.
128. Simon, S. A.; McIntosh, T. J.; Hines, M. L., The influence of anesthetic. In *Molecular and Cellular Mechanisms of Anaesthesia*, Plenum Press: New York, 1986; p 297.
129. Chen, C. H.; Hoye, K.; Roth, L. G., *Arch. Biochem. Biophys.* **1996**, 333, 401.
130. Tran, R.; Ho, S.; Dea, P., *Biophys. Chem.* **2004**, 110, 39.
131. Yamazaki, M.; Miyazu, M.; Asano, T., *Biochimica Et Biophysica Acta* **1992**, 1106, 94.
132. Li, Q. T.; Kam, W. K., *J. Biochem. Biophys. Methods* **1997**, 35, 11.
133. Zbigniew, F.; Stefan, J., *Molecular Physics Reports* **2001**, 33, 172.
134. Singh, H.; Emberley, J.; Morrow, M., *European Biophysics Journal* **2008**, 37, 783.

135. Marsh, D., *CRC Handbook of Lipid Bilayers*. CRC Press: Boca Raton, FL, 1990.
136. Goldie, S. N.; Blanchard, G. J., *J. Phys. Chem. A* **1999**, *103*, 999.
137. Goldie, S. N.; Blanchard, G. J., *J. Phys. Chem. A* **2001**, *105*, 6785.
138. Jiang, Y.; Blanchard, G. J., *J. Phys. Chem.* **1994**, *98*, 6436.
139. Chuang, T. J.; Eisenhal, K. B., *Journal of Chemical Physics* **1972**, *57*, 5094.
140. Favro, D. L., *Physical Review* **1960**, *119*, 53.
141. Hu, C.-M.; Zwanzig, R., *J. Chem. Phys.* **1974**, *60*, 4354.
142. Hildenbrand, K.; Nicolau, C., *Biochimica Et Biophysica Acta* **1979**, *553*, 365.
143. Debye, P., *Polar Molecules*. In Chemical Catalog Co.: New York, 1929.
144. Zwanzig, R.; Harrison, A. K., *Journal of Chemical Physics* **1985**, *83*, 5861.
145. Jiang, Y.; Blanchard, G. J., *Journal of Physical Chemistry* **1994**, *98*, 6436.
146. Edward, J. T., *Journal of Chemical Education* **1970**, *47*, 261.
147. Frye, L. D.; Edidin, M., *Journal of Cell Science* **1970**, *7*, 319.
148. Cone, R. A., *Nature-New Biology* **1972**, *236*, 39.
149. Poo, M.-m.; Cone, R. A., *Nature* **1974**, *247*, 438.
150. Edidin, M., *Nat Rev Mol Cell Biol* **2003**, *4*, 414.

151. Tocanne, J.-F.; Cézanne, L.; Lopez, A.; Pikhova, B.; Schram, V.; Tournier, J.-F.; Welby, M., *Chemistry and Physics of Lipids* **1994**, *73*, 139.
152. Greenough, K. P.; Blanchard, G. J., *Journal of Physical Chemistry B* **2006**, *110*, 6351.
153. Greenough, K. P.; Blanchard, G. J., *Spectrochimica Acta Part A: Molecular and Biomolecular Spectroscopy* **2009**, *71*, 2050.
154. Greiner, A. J.; Pillman, H. A.; Worden, R. M.; Blanchard, G. J.; Ofoli, R. Y., *Journal of Physical Chemistry B* **2009**, *113*, 13263.
155. Dela Cruz, J. L.; Blanchard, G. J., *Journal of Physical Chemistry A* **2001**, *105*, 9328.
156. Schroder, M., *Cellular and Molecular Life Sciences* **2008**, *65*, 862.
157. Horvath, I.; Multhoff, G.; Sonnleitner, A.; Vigh, L., *Biochim. Biophys. Acta-Biomembr.* **2008**, *1778*, 1653.
158. Edward, J. T., *Journal of Chemical Education* **1970**, *47*, 261.
159. Riddick, J. A., Techniques of Chemistry. In *Organic Solvents*, Wiley: New York, 1986; Vol. II.
160. Crank, J.; Nicolson, P.; Hartree, D. R., *Proceedings of the Cambridge Philosophical Society* **1947**, *43*, 50.
161. Kasha, M., *Faraday Discussions of the Chemical Society* **1950**, *9*, 14.
162. Hambir, S. A.; Jiang, Y.; Blanchard, G. J., *J. Chem. Phys.* **1993**, *98*, 6075.
163. Jiang, Y.; Blanchard, G. J., *J. Phys. Chem.* **1994**, *98*, 9411.

164. Jiang, Y.; Blanchard, G. J., *J. Phys. Chem.* **1994**, *98*, 9417.
165. Jiang, Y.; Blanchard, G. J., *J. Phys. Chem.* **1995**, *99*, 7904.
166. Yeagle, P. L., The Roles of Cholesterol in the Biology of Cells. In *The Structure of Biological Membranes*, 2nd ed.; Yeagle, P. L., Ed. CRC Press: New York, 2005.
167. Burger, K.; Gimpl, G.; Fahrenholz, F., *Cellular and Molecular Life Sciences* **2000**, *57*, 1577.
168. McIntosh, T. J., *Biochimica et Biophysica Acta* **1978**, *513*, 43.
169. Guo, W.; Volker, K.; Huber, T.; Afdhal, N. H.; Beyer, K.; Hamilton, J. A., *Biophysical Journal* **2002**, *83*, 1465.
170. Lindblom, G.; Orädd, G., *Biochimica et Biophysica Acta (BBA) - Biomembranes* **2009**, *1788*, 234.
171. Nicolini, C.; Kraineva, J.; Khurana, M.; Periasamy, N.; Funari, S. S.; Winter, R., *Biochimica et Biophysica Acta (BBA) - Biomembranes* **2006**, *1758*, 248.
172. Oldfield, E.; Chapman, D., *Febs Letters* **1972**, *21*, 303.
173. Nyström, J. H.; Lönnfors, M.; Nyholm, T. K. M., **2010**, *99*, 526.
174. Lewis, R. N. A. H.; McElhaney, R. N., The Mesomorphic Phase Behavior of Lipid Bilayers. In *The Structure of Biological Membranes*, 2nd ed.; Yeagle, P. L., Ed. CRC Press: New York, 2005.
175. Simons, K.; Ikonen, E., *Nature* **1997**, *387*, 569.
176. Simons, K.; Vanmeer, G., *Biochemistry* **1988**, *27*, 6197.

177. Brown, D. A.; London, E., *Biochemical and Biophysical Research Communications* **1997**, *240*, 1.
178. Brown, D. A.; London, E., *Journal of Membrane Biology* **1998**, *164*, 103.
179. Brown, D. A.; Rose, J. K., *Cell* **1992**, *68*, 533.
180. Pillman, H. A.; Blanchard, G. J., *Journal of Physical Chemistry B* **2010**, *114*, in press.
181. Maxfield, F. R.; Tabas, I., *Nature* **2005**, *438*, 612.
182. Simons, K.; Ikonen, E., *Science* **2000**, *290*, 1721.
183. Veatch, S. L.; Keller, S. L., *Physical Review Letters* **2002**, *89*, 268101.
184. Nagle, J. F., *Annual Review of Physical Chemistry* **1980**, *31*, 157.
185. Chong, P. L.-G.; van der Meer, B. W.; Thompson, T. E., *Biochimica et Biophysica Acta (BBA) - Biomembranes* **1985**, *813*, 253.